The Effect of Illumination on the Conformation and Thermodynamics of Conjugated Polymers

A Dissertation Presented for the
Doctor of Philosophy
Degree
The University of Tennessee, Knoxville

Brian Frank Morgan
December 2016

Copyright © 2016 by Brian Frank Morgan
All rights reserved.

ACKNOWLEDGEMENTS

I would like to thank Dr. Mark Dadmun for his guidance over the course of this project, and all the past and present members of the group for their friendship and support. I would like to thank my family and friends for their assistance throughout my time in graduate school. I also appreciate the facilities and funding provided by the University of Tennessee, Oak Ridge National Laboratories, the National Institute of Standards and Technology, and the National Science Foundation.

ABSTRACT

This dissertation explores the effects which illumination has on the structure and conformation of conjugated polymers, both in solution and the bulk. Conjugated polymers are an important class of optoelectronic polymeric materials which make up the active layer of key organic electronic devices such as organic photovoltaics, transistors, and light emitting diodes. Considering the strong link between polymer chain structure and device efficiency in these materials, a comprehensive understanding of certain experimental conditions which may influence this conformation and thusly alter the functionality of the devices predicated upon them is of vital importance.

The first part of this dissertation provides a background to conjugated polymers, their role in common electronic applications, and the known effects of illumination on polymeric materials. The next section outlines an initial exploration of light induced effects on benchmark conjugated polymers in solution elucidated via the use of small angle neutron scattering. The third chapter explores the structural evolution of solution gels formed from conjugated polymers at multiple length scales using small and ultra small angle scattering, as well as quantifying modifications to this structural progression brought on by white light exposure. The fourth and fifth chapters further expand our understanding of the proposed thermodynamic driving forces behind the light induced structural changes in conjugated polymer solutions first through alterations in solvent quality, and then through fine-tuning of incident light wavelength, exposure time, and intensity. Finally, the sixth section studies the self-assembly of conjugated polymer composite thin films cast from a single solution through neutron reflectivity, while additionally monitoring the effects of light exposure during the thermal annealing process upon the final film depth profile.

Ultimately, these works cumulatively provide strong evidence indicating that light exposure is in fact an important parameter with far-reaching implications upon the final structure of organic electronic materials. Overlooking illumination conditions and failing to provide a consistent ambient light environment throughout device fabrication will result in non-uniform chain conformations and layering architectures, inevitably impacting device performance. However, if properly understood and harnessed, these light-induced effects could make possible an entirely novel methodology for in-situ tuning of organic electronic device physical parameters.

TABLE OF CONTENTS

Chapter One Introduction....1
Organic Electronics....2
Optoelectronic Mechanisms in Conjugated Polymers....4
Conjugated Polymer Benchmarks: P3HT and MEH-PPV....7
Stimuli-responsive Light Sensitive Materials and Light Induced Effects on Polymer Structure....10
Chapter Two Illumination of Conjugated Polymer in Solution Alters its Conformation and Thermodynamics....16
Abstract....17
Introduction....18
Experimental....23
Results....24
Discussion....34
Conclusion....43
Acknowledgements....44
Chapter Three Illumination Alters the Structure of Gels Formed from the Optoelectronic Polymer P3HT....45
Abstract....46
Introduction....47
Experimental....51
Results....53
Discussion....66
Conclusion....70
Acknowledgements....71
Chapter Four The Importance of Solvent Quality on the Modification of Conjugated Polymer Conformation and Thermodynamics with Illumination....72
Abstract....73
Introduction....74
Instrumental....75
Results....77
Discussion....93
Conclusion....97
Acknowledgements....98
Chapter Five The Role of Incident Light Intensity, Wavelength, and Exposure Time in the Modification of Conjugated Polymer Structure in Solution....100
Abstract....101
Introduction....102
Instrumental....102
Results....104
Impact of Light Exposure Time on Structural Changes....105
Impact of Light Wavelength on Structural Changes....117
Discussion....123

Conclusion 127
Acknowledgements 129
Chapter Six The Effect of Illumination on the Depth Profile of Thermally Annealed MEH-PPV:dPS Blends 130
Abstract 131
Introduction 131
Instrumental 135
Results 136
Discussion 148
Conclusion 156
Acknowledgments 157
Chapter Seven Conclusions and Future Work 159
Conclusions 160
Illumination of Conjugated Polymer in Solution 160
Illumination of Conjugated Polymer throughout Gelation 162
Illumination of Conjugated Polymer Composite Thin Films during the Thermal Annealing Process 163
Summary 164
Future Work 165
Illumination of Conjugated Polymer in Solution 166
Illumination of Conjugated Polymer Gels 166
Illumination of Conjugated Polymer Composite Thin Films during the Thermal Annealing Process 167
List of References 169
Appendix 179
Vita 181

LIST OF TABLES

Table 2.1: Parameters obtained from the Flexible Cylinder fit for P3HT in deuterated styrene at 60 °C 32
Table 2.2: 1wt% P3HT in d-Styrene sample thickness, light intensity incident to sample, exciton density, and exciton density per polymer chain..... 37
Table 4.1: Reported Solubilities for P3HT in Select Solvents. 78
Table 4.2: Parameters obtained from the Flexible Cylinder fit for P3HT in deuterated styrene at 60 °C. 84
Table 4.3 R_g values from polymer excluded volume model fits to P3HT in d-ODCB. 85
Table 4.4: R_g values from polymer excluded volume model fits to P3HT in d-bromobenzene. 86
Table 4.5: Kuhn length values extracted via global fitting with the fractal flexible cylinder model for the 1wt% samples of MEH-PPV. 92
Table 4.6: Second Virial Coefficients Obtained via Zimm analysis of P3HT in d-styrene, d-ODCB, and d-bromobenzene. 95
Table 5.1: Results for polymer excluded volume model fits to 1 wt% P3HT in d-ODCB. 108
Table 6.1: Parameters obtained from fit to neutron reflectivity data for MEHPPV/dPS films before and after thermal annealing on both bare silicon and PGMA surfaces. 147
Table 6.2: Volume fraction of each component in the layered thin films on bare silicon and PGMA treated samples in both the light and dark. 149
Table 6.3: Total surface energies for relevant experimental materials 153

LIST OF FIGURES

Figure 2.1: Small angle neutron scattering curves of 0.5 wt% P3HT in deuterated styrene at 60°C in both illuminated (red circles) and dark (blue circles) environments. 25
Figure 2.2: Small angle neutron scattering curves of 1 wt% P3HT in deuterated styrene at 60 °C in both illuminated (red circles) and dark (blue circles) environments. 26
Figure 2.3: Small angle neutron scattering curves of 1 wt% Polystyrene in deuterated orthodichlorobenzene at room temperature in both illuminated (red circles) and dark (blue circles) environments 27
Figure 2.4: Flexible Cylinder Fit (black trace) for 1 wt% P3HT in deuterated styrene at 60 °C under illumination 30
Figure 2.5: Small angle neutron scattering curves of 1 wt% MEH-PPV in deuterated THF at room temperature in both illuminated (red circles) and dark (blue circles) environments. 35
Figure 2.6: SANS scattering curve of 1wt% P3HT in d-Styrene. Red data points indicate sample illuminated with 415-590nm light, while blue data points indicate sample illuminated with 610-1200nm light. 39
Figure 3.1: Schematic depiction of proposed P3HT solution gelation mechanism involving aggregate formation from free chains in solution via nanofibrils. .. 49
Figure 3.2: SANS of 17 wt% P3HT gelation under illumination (open circles) and in the dark (closed circles) through a 70-40°C temperature ramp. Color denotes individual temperatures between 40° and 20°C. 54
Figure 3.3: Combination Model (Elliptical Cylinder + Polymer Excluded Volume) fit to 17 wt% P3HT gelation curve in d-ODCB at 34°C in the presence of white light illumination. 57
Figure 3.4: Surface area of the nanofibril face, i.e the cross-section of nanoscale P3HT fibers. This plot shows that the P3HT fibers are consistently larger in the dark than in the light. 58
Figure 3.5: Scale factor obtained from the elliptical cylinder model portion of the fit, a parameter that is directly proportional to the amount of P3HT aggregated in nanofibrils. This data show that the amount of aggregated P3HT remains larger in the dark environment throughout gelation. 59
Figure 3.6: Radius of gyration of P3HT obtained from the excluded volume model, which monitors the size of free P3HT not aggregated in nanofibrils. This structural feature shows that the free chains are larger in the light than the dark, especially at higher temperatures. 60
Figure 3.7: Porod exponent of free P3HT chains obtained via the excluded volume model, a measure of general chain conformation. These results indicate a slightly larger value, and thus more compact polymer chain, in the dark. 61

Figure 3.8: USANS and SANS curves of the 17 wt% P3HT solution in d-ODCB in both the light (red points) and dark (blue) at 24°C. 64
Figure 3.9: R_g obtained from Guinier-Porod power law fit to USANS data for 17 wt% P3HT in d-ODCB. Black points indicate dark sample environment, red points illuminated environment. 65
Figure 4.1: Small angle neutron scattering curves of 1wt% P3HT in d-bromobenzene at 60°C in both illuminated (red circles) and dark (blue circles) environments. 80
Figure 4.2: Small angle neutron scattering curves of 1wt% P3HT in d-ODCB at 60°C in both illuminated (red circles) and dark (blue circles) environments. 81
Figure 4.3: Small angle neutron scattering curves of 1wt% P3HT in d-Styrene at 60°C in both illuminated (red circles) and dark (blue circles) environments. 82
Figure 4.4: Small angle neutron scattering curves of 1wt% MEH-PPV in d-Styrene at room temperature in both illuminated (red circles) and dark (blue circles) environments. 88
Figure 4.5: Small angle neutron scattering curves of 1wt% MEH-PPV in d-THF at room temperature in both illuminated (red circles) and dark (blue circles) environments. 89
Figure 4.6: Small angle neutron scattering curves of 1wt% MEH-PPV in d-cyclohexane at room temperature in both illuminated (red circles) and dark (blue circles) environments. 90
Figure 5.1: Small angle neutron scattering curves of 1 wt% P3HT in d-ODCB at 60°C in dark (blue circles), illuminated (red circles) and an additional dark (green circles) environments. 106
Figure 5.2: Time evolution of the scattering curve at high Q of a 1 wt% solution of P3HT in d-ODCB at 60°C for 0 min (blue traces), 10 min (red traces), 30 min (green traces), and 50 min (yellow traces) white light illumination times. ..110
Figure 5.3: Analysis of 1 wt% P3HT in d-ODCB using the flexible cylinder model over the course of 60 minutes light exposure time with multiple scattering runs of 5 minute duration each. 111
Figure 5.4: Time sensitivity of 1 wt% P3HT in d-styrene at 60°C after 0 hrs (black traces), 1hr (blue traces), 2hr (red traces), 3hr (green traces), and 4hr (yellow traces) of total white light exposure. 112
Figure 5.5: SANS data curves for 1 wt% P3HT in d-styrene in the dark and under total light exposure times ranging from 20 to 300 minutes at 60°C. 114
Figure 5.6: Values for Kuhn length as a function of illumination time (50,000 lux) extracted via the flexible cylinder model for 1 wt% P3HT in d-styrene at 60 °C. 116
Figure 5.7: SANS scattering curve of 1 wt% P3HT in d-styrene at 60°C. Red data points indicate sample illuminated with white light, pink data points indicate sample illuminated with 415-590nm light, blue data points indicate sample illuminated with 610-1200nm light, and black data points indicate sample under no illumination. 119

Figure 5.8: R_g values obtained from the flexible cylinder fit for 1 wt% P3HT at 60°C in d-Styrene under (left to right) no illumination, 610-1200 nm light, 415-590 nm light, and white light illumination. 121
Figure 5.9: R_g values obtained for polymer excluded volume model fit for 1 wt% P3HT at 60°C in d-ODCB under (left to right) no illumination, 610-1200 nm light, 415-590 nm light, and white light illumination.....122
Figure 6.1: Reduced neutron reflectivity data for as-cast 10:90 MEH-PPV:dPS films cast on a bare silicon surface. Blue traces represent "dark" sample, red traces represent "light" sample. 138
Figure 6.2: Reduced neutron reflectivity data for as-cast10:90 MEH-PPV:dPS films cast on a PGMA modified surface. Blue traces represent "dark" sample, red traces represent "light" sample.....139
Figure 6.3: Reduced neutron reflectivity data for 10:90 MEH-PPV:dPS films cast on a bare silicon surface and thermally annealed for 15 minutes at 125°C. Blue traces represent the sample annealed in the dark and red traces represent the sample annealed under illumination. 140
Figure 6.4: Reduced neutron reflectivity data for 10:90 MEH-PPV:dPS films cast on a PGMA modified surface and thermally annealed for 15 minutes at 125°C. Blue traces represent the sample annealed in the dark and red traces represent the sample annealed under illumination.....141
Figure 6.5: Example 2 layer curvefit (black trace) for 10:90 MEH-PPV:dPS film cast on a bare silicon surface and thermally annealed for 15 minutes at 125°C.....143
Figure 6.6: SLD profiles for 10:90 MEH-PPV:dPS films cast onto a bare silicon surface, where the distance from interface is defined from the polymer-air interface. Broken traces indicate as-cast samples (blue for dark, red for light) and solid traces indicate samples annealed for 15 minutes at 125°C (blue for dark, red for light).....144
Figure 6.7: SLD profiles for 10:90 MEH-PPV:dPS films cast onto a PGMA treated surface, where the distance from interface is defined from the polymer-air interface. Broken traces indicate as-cast samples (blue for dark, red for light) and solid traces indicate samples annealed for 15 minutes at 125°C (blue for dark, red for light).....145
Figure 6.8: Volume fraction profile of MEH-PPV in the 10:90 MEH-PPV:dPS blend cast on HF stripped silicon, where Z is defined as the distance from the polymer-air interface. Broken traces indicate as-cast samples (blue for dark, red for light) and solid traces indicate samples annealed for 15 minutes at 125°C (blue for dark, red for light).....150
Figure 6.9: Volume fraction profile of MEH-PPV in the 10:90 MEH-PPV:dPS blend cast on a PGMA coated silicon wafer, where Z is defined as the distance from the polymer-air interface. Broken traces indicate as-cast samples (blue for dark, red for light) and solid traces indicate samples annealed for 15 minutes at 125°C (blue for dark, red for light). 151

Figure 0.1: Molecular structure of benchmark conjugated polymers poly[2-methoxy-5-(2-ethylhexyloxy)-1,4-phenylenevinylene] (left), and poly(3-hexylthiophene-2,5-diyl) (right). 180

CHAPTER ONE
INTRODUCTION

Organic Electronics

The role of polymeric materials in the field of functional electronics has long been primarily a supporting one. This is due in large part to one of the fundamental characteristics of most commonly used and industrially relevant polymers: their insulating nature. Endowed by their atomic composition of non-conducting organic materials, this consistent facet of polymeric standards such as polystyrene and polypropylene has led to their incorporation primarily as buffer materials and occasionally as dielectrics, as with poly(methylmethacrylate). However, the 1970's saw the introduction of an entirely new class of polymers ideally suited for use as the primary semiconducting active layer. These conjugated polymeric materials were defined by the presence of alternating double and single bonds over their primary chain backbone, allowing rapid transport of electrons across the length of the chain via the mesomerization made possible by the overlap of p_z π-orbitals. Electron delocalization over monomeric repeat units results in current flow through individual polymer chains and persists on a macro scale when these polymers are placed in bulk as the active layer of electronic devices.

Harnessing these effects has led to the development of an entire field of organic electronic devices predicated on replacing traditional conducting and semiconducting materials with functionalized polymers and polymer composites. Utilization of these novel organic materials has culminated in devices which possess powerful advantages in weight and flexibility over their traditional

counterparts, fostering development of an entirely novel paradigm for consumer and industrial electronics through growth of portable and application-flexible devices. Especially notable fields include organic light emitting diodes (OLEDs), organic photovoltaics (OPVs), organic thin film transistors (OTFTs), and specialized chemical sensors. All rely on the fundamental mechanism by which charge carrier pairs, also known as electron hole pairs or excitons, are generated, transported, and terminated within the material. In OLEDs the injected charge carrier recombines to give off a luminescence which results in the net effect of a tunable light source, while OPVs generate excitons via incident light absorbance and ultimately separate them at a phase interface to generate a net electrical current. The direct band gap of many prominent conjugated polymers provides another crucial strength of these materials in light sensitive devices, as it encourages efficient absorption of photons from the visible spectrum and thus facilitates vigorous generation of excitons. Ultimately the design of efficient and effective organic electronic devices revolves around properly synthesizing and characterizing the relevant conjugated polymers and incorporating them into active layers in such a way to as to maximize properties directly related to final device efficiencies, such as exciton dissociation lengths and bulk heterojunction morphologies. Continued work in this field is crucial towards better understanding the conformational structures and active layer morphologies at play, as this information has repeatedly driven overall progress industry wide and allowed the

continued improvements in organic electronic device design necessary to keep the field relevant in today's technological environment.

Optoelectronic Mechanisms in Conjugated Polymers

As stated previously, the device functionality afforded by the class of optoelectronic conjugated polymers is primarily rooted in their ability to generate and transport electronic excited states. These excited states are generated via unique pathways depending on the specific device architecture in question, whether it be absorption of a photon from incident light of a suitable wavelength with OPVs or injection of discreet electrical charge as in the case of OLEDs. Regardless, upon this energy stimulus an electron belonging to the conjugated polymer highest occupied molecular orbital, or HOMO, becomes electronically excited, causing its promotion out of the HOMO band, leaving that level partially empty. The now positively charged monomer exerts an attractive Coulombic force, signaling the formation of the electron-hole excited state commonly referred to as the exciton.[1] Due to the fact that the bandgap of many light-sensitive semiconducting conjugated polymers lies well within the range associated with visible light, i.e. usually 1-4 eV, these materials excel at efficiently creating healthy amounts of these excited states. This quality is further evidenced by the relatively high photoluminescent efficiencies (Φ_{exc}) of these materials, indicating a favorable ratio of photons ultimately converted into useful charge carriers.[2,3,4]

However, exciton formation represents only the initial step in the useful lifetimes of excitons, as they must then effectively migrate to the appropriate material interface within the device for particle recombination or dissociation and thus serve their ultimate purpose. If the integrity of the electron hole pair is prematurely compromised before it becomes properly located in the ideal phase, the carrier and overall device efficiency suffers. Considering that excitons possess average lifetimes on the order of single nanoseconds in conjugated materials, these charge carriers typically can only travel 5-20 nanometers before they expire, understandably leading to one of the leading causes of efficiency loss in organic devices.[5,6] A substantial portion of the difficulty inherent to excitons propagating in a polymer phase is the intrinsic lack of pure crystallinity, as though the excitons can coherently translate down a given polymer chain very quickly, these chains possess a finite length.[7] Thus to propagate over the distances necessary to reach device interfaces, the excitons must physically "hop" between chains in an incoherent form of motion predicated on very inefficient inter-chain charge transport mechanisms.[8] Many conjugated polymers are semi-crystalline in nature, and better facilitate this inter-chain transfer process by π-stacking the conjugated backbones to form regions where excitons can transfer between chains in the z dimension with a significantly lower energy barrier.[9,10] Maximizing semi-crystalline domains in these materials is often prioritized for this reason as a means of boosting device efficiencies.[11] For conjugated polymer based photovoltaic devices, decreasing the necessary

distance required for the exciton to travel to a termination interface represents another means of efficiency improvement. Maximizing the surface area of the phase interface between donor and acceptor materials in many devices accomplishes this by ensuring that a suitable termination location is accessible to a substantial portion of generated excited species. As a result, promotion and target design of concepts such as the bulk heterojunction have resulted in significantly boosted exciton dissociation ratios and subsequently boosted total generated current.[12,13]

From this discussion it should begin to become clear how vital proper knowledge of conjugated polymer chain conformation and multi-size domain structure becomes when addressing increased functionality of organic electronic devices. There exists clear, unmistakable links between local polymer structure and the micro-scale device architectures constructed from them, and the resultant electronic structure and charge transport characteristics which ultimately define overall device efficiency.[10,13,14,15] Additionally, due to the inherent morphological complexities involved in these systems, it becomes economically difficult or even impossible to effectively synthesize structures for an exact targeted structural function, meaning that a majority of the work done in the field revolves around analyzing and optimizing architectures obtainable via already established fabrication techniques. As a result, proper characterization and quantitative analysis of the structure factors which dominate most of the

industrially relevant organic electronic systems has become of paramount importance.

Conjugated Polymer Benchmarks: P3HT and MEH-PPV

Due in large part to the relatively recent explosive growth in the optoelectronic polymer field, it currently stands awash in novel and potentially exciting yet often industrially untested molecular prototypes. To avoid getting bogged down in this academic sea of new polymers a strong majority of characterization work conducted throughout the field is focused on a handful of benchmark materials chosen for their consistency and representative nature, as well as general resiliency in typical working environments. For these reasons, one of the most commonly studied conjugated polymers is the ubiquitous polythiophene poly(3-hexylthiophene-2,5-diyl). Polythiophenes were popularized in the 1990s after it was discovered that doping the materials would initiate electrical conductivity, while the chemical incompatibility between the conjugated polythiophene backbone and alkyl side chains resulted in the buildup of a layered self-assembled structure in which π-stacked polythiophene backbones alternate with layers of more or less ordered alkyl side chains.[16,17,18] These materials displayed initial power conversion efficiencies (PCEs) ranging from 2-5%, and exhibited excellent solubility in many common and industrially relevant organic solvents due to their alkyl side chain groups.[19,20] Amongst this group P3HT quickly emerged as the preeminent model system due to a combination of its

facile processability, large charge carrier mobilities (10^{-2}–10^{-3} cm^2 $V.s^{-1}$) and environmental stability.[21] As has been stated before, since form drives function within an organic electronic device, the conformation of P3HT within devices and in processable solution has been of extensive interest. Typically, P3HT is incorporated into a device relevant architecture via a convenient and economic solvent-based deposition method such as spin coating, drop casting, or inkjet printing.[22,23] Upon gradual solvent withdrawal the P3HT chains shift conformation from a semi-flexible cylinder form and systematically aggregate to form higher order lamellar structures.[15] Having achieved this level of order in a very highly concentrated solution or bulk layer, P3HT has been shown to possess three characteristic length scales pertaining to its structural self-arrangement: a lamellar period of about 1.5-2 nm, a length scale on the order of tens of angstroms related to the π-stacking period of the thiophene backbones, and a larger order length scale describing the alteration between amorphous and semi-crystalline domains of the P3HT dispersion.[24] These characteristic length scales have repeatedly demonstrated a strong responsiveness to methodological stimuli thus allowing manipulation via variation in a huge array of parameters such as molecular weights, polydispersities, regioregularities, solvent environments, material additives, additional device components, processing conditions, and casting methods throughout a typical fabrication process, allowing immense control over final morphologies and thus offering relatively accessible control over device relevant parameters.[25,26,27,28,29,30]

Another conjugated polymer commonly found in experimental organic devices is poly[2-methoxy-5-(2-ethylhexyloxy)-1,4-phenylenevinylene], referred to as MEH-PPV. A derivative of poly(p-phenylene vinylene) (PPV), MEH-PPV has been of special interest in the optoelectronic materials field due to its wide range of conformational effects easily elicited by a range of common organic solvents, as well as its tendency to form large aggregates in solution which persist into device active layers, directly leading to large observed boosts in charge carrier mobilities.[31,32] These aggregates are formed by the agglomeration of rigid MEH-PPV chains into exceptionally large and extensive fractal networks, where chain proximity and conjugated ring stacking greatly facilitate the flow of excitons.[33] Again one of the experimental strengths of this material is the ease with which its structure can be controlled via solvent choice, offering designers the tools to elicit desired structural features by manipulating the solvent mixture. For instance, while solvated in chlorobenzene the MEH-PPV chains exhibit a rigid rod-like conformation prone to promoting large amounts of aggregation and thus larger fractal structures, while a THF environment results in more tightly coiled chains resistant to aggregation, and an increasingly unfavorable solvent such as cyclohexane leads to extensive chain collapse and little to no large length scale network formation.[34] As a result of this ability to generate tunable aggregates conducive to exciton mobilities, MEH-PPV has been incorporated into a wide range of relatively high efficiency organic electronic devices, most notably in OPVs and OLEDs.[35,36,37,38] However though these fractal aggregates

are certainly integral to device functionality, their massive size with molecular weights often on the order of tens or hundreds of millions makes solvent dissolution and precise structural characterization often decidedly problematic. Thus careful experimental design predicated around ideal concentration environments and properly separated material phases is required to achieve the data collection necessary to properly characterize systems based on this material. With the proper steps taken, MEH-PPV becomes a powerful tool for probing generic structural effects visited upon conjugated polymers by many common environmental stimuli or industrial fabrication effects, proving repeatedly to be a powerful benchmark for the class of conjugated optoelectronic polymers.

Stimuli-responsive Light Sensitive Materials and Light Induced Effects on Polymer Structure

Another broad class of commercially relevant polymeric materials includes the field of stimuli responsive materials. These polymers are defined as materials that can respond to stimuli such as pH, light, temperature, ionic strength, electric or magnetic field variations by changing their own properties such as size, surface area, solubility, permeability, shape, mechanical, and optical properties, among others.[39] Polymers are uniquely suited to this role due to their high versatility and ability to dramatically alter their intrinsic properties as a function of small environmental changes. Many of the interesting properties of these responsive polymers arise from a transition in solubility or conformation of the

macromolecule in the presence of a solvent. In this manner, transitions at the molecular level can be amplified to result in a change in nanoscale structure and materials properties.[40] One such example is the well studied field of pH-responsive polymers or polymer nanocomposites. These materials are designed to bind drug compounds within their network structure, keeping them isolated from the surrounding environment. However upon a shift in the pH of their surroundings, the basic or acidic functional groups attached to the polymer backbone interact differently with their solvent, causing a swelling or collapse of the entire polymer chain, thus releasing the drug compounds which they encapsulate.[41,42] Temperature sensitive polymers operate under a similar mechanism, where change in temperature past a certain low or high critical solution temperature induces a volume phase transition brought on by changes in hydrogen bonding preferences between polymer-polymer and polymer-solvent interactions.[43] These examples typify the stimuli-responsive mechanism behind most polymers employed in this field, where an external stimulus causes an abrupt shift in polymer chain size and conformation by altering its thermodynamic stability and interactions with its relevant solvent. Another commonly considered stimuli source is light, especially relevant considering its relative ease of application and manipulation both in pre-processing and in-situ. Light-responsiveness has been extensively harnessed for decades in polymer-based systems through the use of methods such as UV curing, which can employ incident UV light to trigger crosslinking between monomer and oligimer units,

allowing for measured control over the extent and rate of final hardening, elasticity, or toughness in the bulk material.[44,45] A wide array of more recent and novel mechanisms have been developed for targeted functions made possible by light sensitive polymer materials, such as light-controlled drug delivery composites which effectively encapsulate the medicinal compounds in-vivo until located in the desired area of the body, after which exposure to UV or visible light radiation initiates a rupture of the polymer capsule and subsequent release of the enclosed agents.[46,47] Incorporating light responsive functionalities such as azobenzene into polymer chains has opened up the door to tunable in-situ control over mechanical properties, as careful light exposure can reproducibly and sometimes reversibly induce transformations such as plasticization or directional bending in bulk materials.[48,49] However all these previously mentioned examples induce these light-sensitive effects through the doping of polymer samples with appropriately reactive agents such as initiators or specialized dyes, or require careful synthesis to embed light sensitive functionalities into a polymer chain which otherwise would remain unaffected by a light source. As a result, polymer mixtures, blends, or co-polymers must be employed with several chemically distinct components: the constituents which provide the actual device or material properties integral to primary functionality such as conductivity or structural toughness, and an additional component added in an amount ideally large enough to elicit light-induced effects upon the entire system, but yet small enough to avoid compromising primary material function. Clearly, developing

stimuli-responsive methodologies for an impetus such as light which could broadly elicit effects over a wide range of otherwise unmodified functional materials would have many powerful upsides including simplification of polymer system design and large decreases in synthesis and implementation cost.

The field of conjugated optoelectronic polymers immediately comes to mind as a suitable candidate for light-induced stimuli-responsive control of physical parameters, considering many conjugated benchmark materials serve as active layer photovoltaic components which excel at absorbing visible light in order to generate excitons. As has been stated previously, great effort has been taken over past decades to determine the ideal structural architectures and length scales conducive to facilitating exciton generation and transport, and subsequently to develop experimental and industrial methods for consistently producing these desired morphologies in the relevant organic electronic devices. Unfortunately, nowhere near this level of experimental data exists for light induced effects on conjugated polymer chain conformation, i.e. potential changes in physical parameters of the chain brought on by the presence of an excited species such as an exciton on the polymer backbone. Molecular dynamics simulations revolving around the presence of lowest order excitations on the backbone of PPV oligomers predict a distinct change in local chain rigidity between electronic ground and excited states.[50] Due to the delocalization of these excited states over several monomer repeat units, the entire chain experiences a marked increase in rigidity as a global energy minimum emerges

in this planarized state. Further experimental work has tentatively corroborated these hypothesis, finding alterations in conjugated polymer film properties upon light illumination. Most notable is the work of Reiter et al. and their dewetting experiments involving blended thick films of MEH-PPV and polystyrene conducted both in the presence and absence of simple white light illumination.[51] By monitoring the rates at which the MEHPPV/PS films dewetted off of the silicon substrate after deposition as a function time in these distinct illumination environments, the authors observed a consistent and reversible relationship between dewetting rate and illumination environment. As the films dewetted significantly more slowly from the temperature controlled substrate in the presence of light, it was determined that illumination was effectively increasing the relative viscosity of the blend. Given that radiation outside MEH-PPVs absorbance band had no similar effect, the authors concluded that the presence of excited states on the polymer chain backbone created from absorbed photons contributed to a planarization of the backbone and thus led to the increased chain rigidity demonstrated by the increased film viscosity. Considering that the rigidity transition was seen to occur on an easily controllable timescale of roughly 30 minutes to an hour, and that the alterations were both non-destructive and completely reversible upon withdrawal of the light source, it appears to be an ideal candidate for further exploration as a stimuli-responsive structure control methodology. In fact further work applying this effect has demonstrated an ability to alter a number of fundamental optoelectronic properties of conjugated polymer

films such as photoluminescence simply via an uncomplicated illumination pre-treatment process.[52] Thus this light induced control over conjugated polymer physical properties on the local and macro length scales presents a promising method for a type of tunable and reversible control mechanism for polymer morphology which ideally can be further developed and applied into device fabrication methodologies, thus potentially allowing unprecedented in-situ manipulations of active layer assembly.

CHAPTER TWO

ILLUMINATION OF CONJUGATED POLYMER IN SOLUTION ALTERS ITS CONFORMATION AND THERMODYNAMICS

Abstract

The importance of chain structure in conjugated polymer-based material active layers and its relation to device efficiencies in OPVs, organic field transistors, OLEDs, and other devices has been well established. However the influence that the absorbance of the light inherent to these devices might have on the conjugated polymer structure is not well understood. Herein, we employ small angle neutron scattering to investigate structural changes occurring in solutions of poly(3-hexylthiophene-2,5-diyl) with exposure to white light. Results indicate significant decrease in both Kuhn length (b) and radius of gyration (R_g) of the polymer upon illumination, coupled with a drop in the second virial coefficient (A_2). We explain this phenomenon through a chain collapse model, proposing that the interaction of light with the polymer backbone alters its thermodynamic interactions with and solubility in the surrounding solvent. The presence of such an effect, which we observe in several conjugated polymers, introduces the possibility of a powerful, non-destructive, and tunable method for controlling polymer conformation in solution. This in turn opens a path to develop a broad range of new light-responsive materials, in that a variety of conjugated polymers could be used as the stimuli-responsive material. Additional implications include the identification of the importance of illumination in the reproducible fabrication of organic electronic active layers from conjugated polymer inks.

Introduction

Conjugated polymers are promising functional materials utilized in devices such as organic light emitting diodes (OLEDs), organic semiconductors, chemical sensors, and organic photovoltaics (OPVs). Their use in these applications has led to expanded interest in the properties and dynamics of these polymers. A crucial aspect of the performance in these devices is the ordering and packing of the conjugated polymer in the solid state in the active layer. For instance, organic semiconductors and transistors rely on maximized charge transport and mobility control, accomplished through carefully controlled and optimized molecular packing and crystallinity.[53] In most cases, the conjugated polymer self-assembles into aggregates or fibrils in solution prior to film deposition, or during the film deposition itself, which directly impacts the morphology and performance of the conjugated polymer based active layer.[54,55,56]

Recent studies have mostly paid special attention to examining and controlling chain conformation and morphology of these conjugated polymer in the solid state active layers, as it is closely tied to the optoelectronic properties and performance of these devices.[57,58,59,60] For instance, in the case of photovoltaics, an incident photon creates electron-hole pairs (excitons) which must migrate to an appropriate interface to dissociate before recombination occurs in create free charge carriers. Thus, improving the performance characteristics of the active layer by control of the active layer morphology has been extensively studied.[61,15] Similarly, for devices such as OLEDs, electrons are

injected into a conjugated polymer layer whereupon excitons are formed, which recombine to emit a photon. Control of the morphology in these materials focuses on designing the polymer phases that encourage charge transport in the device while minimizing quenching effects, often through processing and fabrication methods which encourage mixing of interfaces and avoid undesirable side effects such as ink clotting.[62,63]

Even though the importance of the morphology of the polymer in the active layer is well studied, the importance of the conformation of the conjugated polymer in solution prior to deposition is often overlooked. If the polymer film is deposited from a modest to poor solvent, the conjugated polymer may have already self-assembled into larger fibrils or aggregates that will dominate the active layer morphology. Thus, the conformation of the polymer chain in solution prior to deposition, and its assembly during deposition, can dramatically impact the final morphology and performance of the conjugated polymer based active layer.

Thus, while extensive work has been completed to examine the role of the conjugated polymer structure and mixing behavior in optimizing exciton formation and stability in organic electronic devices, the physical effects of the presence of the exciton on the conformation of the polymer chain itself have received much less attention. Moreover, recent work with conjugated polymers has shown compelling evidence of light-induced effects on its physical properties. Reiter et al examined the dewetting behavior of poly[2-methoxy-5-(2-ethylhexyloxy)-1,4-

phenylenevinylene] (MEH-PPV)/polystyrene blend films, and found that the rate of dewetting of the films dramatically slowed down when exposed to white light relative to when the films dewet in the dark. The authors attribute this to an increased viscosity of the films that are exposed to white light, ostensibly due to the planarization of the MEH-PPV.[51] In related studies, Botiz et al examined similar polymer blend films and observed increases of up to 40% in the photoluminescent intensity of films that were treated with white light.[52] Both phenomena were attributed to the planarization of the MEH-PPV chain upon exposure to light due to the formation of excitons on the chain, a condition that has been shown to significantly alter photophysical properties.[64] Additionally, simulations demonstrate that the formation of excitons will force a planarization of poly(phenylene vinylene) (PPV) chains, thus increasing chain rigidity and stiffness due to the delocalization of the exciton over several monomer units.[50] However, the underlying structural factors that govern the change in dewetting with illumination remain unclear, as establishing an experimental methodology which both effectively probes the appropriate length scales while simultaneously allowing for alternating states of strong illumination and total darkness is non-trivial. This paper addresses this problem using small angle neutron scattering to examine the conformation of select conjugated polymers in solution when in both the presence and absence of white light.

Harnessing photo-induced conformational changes of a single conjugated polymer itself would be a powerful tool, both in the specific field of organic

electronics and in the design of novel stimuli responsive materials. Device fabrication methodology remains a crucial focus of OPV and OLED development, as the time and expense required to optimize these processes dictates in large part the commercial viability of organic electronic devices. Incorporating a step where the conformation of the polymer can be manipulated as the device is fabricated would allow homogenous, non-destructive control of the device morphology and could offer previously unattainable tunability of performance. More broadly, the presence of a strong, reproducible, photophysical response in conjugated polymer systems will have far reaching implications and applications. Photoresponsive, smart macromolecules which respond to stimuli are of significant interest, as they provide a molecular level mechanism to direct a desired conformation change that can enable a targeted response, such as biological sensors or drug delivery agents.[65,66] In many cases, this molecular response is not inherent to the polymer molecule itself, but rather is the response of a photochromic derivative that is embedded in or attached to the chain, such as azobenzene or spiropyran, which isomerize in response to light exposure.[67,68,69] For instance, exposure of azobenzene containing polymer films to light can prompt local, controllable and reversible plasticization of the surface.[49] Similarly, previous studies have shown that exposure of select regions of an azobenzene functionalized polymer film to a polarized laser produces non-thermally driven formation of stable but reversible "surface relief structures."

Moreover, the functional groups that are currently available for such light-responsive molecular motors are limited to a small number of photo-chromic molecules, many of which have been known for decades.[70,71] Therefore, there is a clear need for new photosensitive molecules whose molecular level conformation can be tuned by exposure to light. Correlation of the local electronic and structural changes that occur in a conjugated polymer when exposed to light will therefore provide a thorough understanding of the fundamental processes that hierarchically guide the change in macroscopic behavior of conjugated polymer systems as a result of photon absorption. This information, in turn, provides a fundamental understanding of the mechanism by which photon absorption by conjugated polymers alters its macroscopic physical properties in order to provide guidelines by which this exciting phenomenon can be controlled and exploited to realize new light-responsive materials.

The experimental evidence that light exposure modulates the dynamics and structure of a conjugated polymer in solution provide the foundation to develop a broad range of new light-responsive materials, in that a variety of conjugated polymers could be used as the stimuli-responsive material. This increase of potential materials will surely expand the applications that can be controlled and patterned by light exposure, which offers the opportunity to realize new applications that can be controlled by illumination and dramatically extends the practicality of light-responsive materials.

Experimental

The conjugated photoactive polymer poly(3-hexylthiophene-2,5-diyl) was purchased from Rieke Metals. This polymer has a regioregularity > 98% and a molecular weight < 50,000, per the manufacturer. This material was used without further purification, where it was dissolved in deuterated (d8) styrene purchased from Polymer Source, which was pre-filtered with 0.45μ sieves. To prevent localized gelation, the samples were kept at 60°C throughout the scattering experiments by a thermally controlled sample holder. Poly[2-methoxy-5-(2-ethylhexyloxy)-1,4-phenylenevinylene] (MEH-PPV) was purchased from Sigma Aldrich. This polymer is reported by the manufacturer to have a number average molecular weight (M_n) between 150,000 and 250,000. Deuterated tetrahydrofuran (d8) was purchased from Sigma Aldrich in sealed ampoules and used as received.

The small angle neutron scattering experiments were completed in quartz solution cells, where the sample cells were wrapped in 0.1 mm thick aluminum foil to create the dark environment. The illuminated environment was realized by exposing the quartz cells to an optical illuminator consisting of a 125-watt halogen bulb, which provides 50,000 lux at 5cm. Aluminum was used to inhibit light from entering the sample, as aluminum is nearly transparent to neutrons. Regardless, special care was taken during the analysis to be certain that the presence of the aluminum was accounted for in the reduction of the raw data to absolute units. For instance, the empty cell scattering of the dark sample

consisted of an empty cell wrapped in aluminum and the transmission of the ‘dark’ sample was determined separately from that of the light sample (i.e. with and without the aluminum wrapping, respectively)

The small angle neutron scattering experiments (SANS) were conducted at the National Institute of Standards and Technology's Center for Neutron Research using the NG3 beamline. Three separate detector distances of 0.3, 4, and 13 meters with a wavelength of 6 Å allowed a Q range of 0.0034 to 0.3363 $Å^{-1}$, where $Q = 4\pi/\lambda\sin(\theta/2)$, λ is the neutron wavelength, and θ is the scattering angle. Additional SANS experiments were performed at the High Flux Isotope Reactor at Oak Ridge National Laboratory on the CG-2 GP SANS beamline, employing detector distances of 18.5, 2, and 0.3 meters. The raw data was reduced using NCNR macros and corrected for empty cell (with and without aluminum) scattering, dark current, and detector sensitivity. Absolute coherent scattering was obtained through the elimination of contributions from background incoherent scattering and thermal fluctuations.

Results

The conformation of the conjugated polymers in solution were monitored using small angle neutron scattering by collecting the SANS scattering curve of the sample in complete darkness followed subsequently by an identical experiment where the sample is fully illuminated. Figures 2.1 -2. 2 show the resultant SANS curves for the 0.5 and 1 weight percent P3HT in deuterated

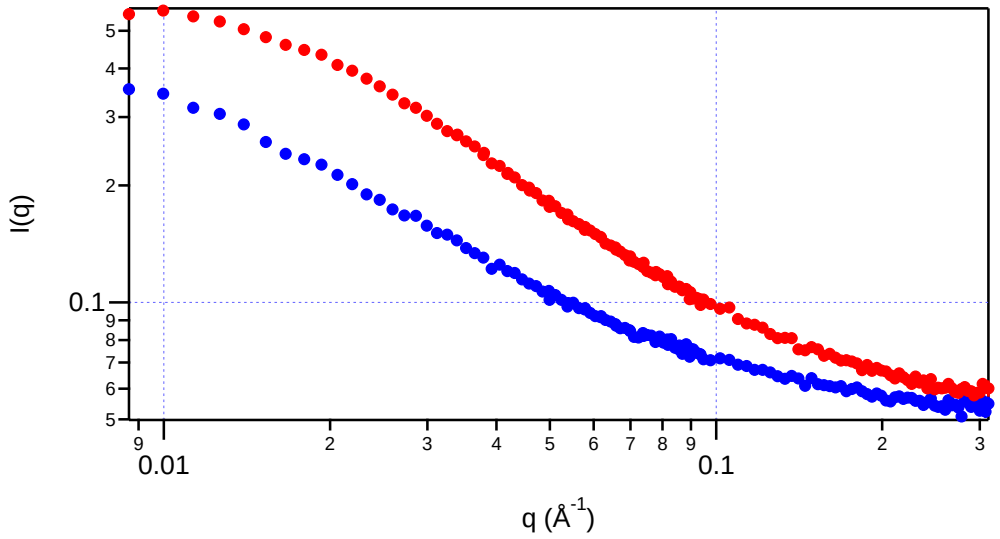


Figure 2.1: Small angle neutron scattering curves of 0.5 wt% P3HT in deuterated styrene at 60°C in both illuminated (red circles) and dark (blue circles) environments.

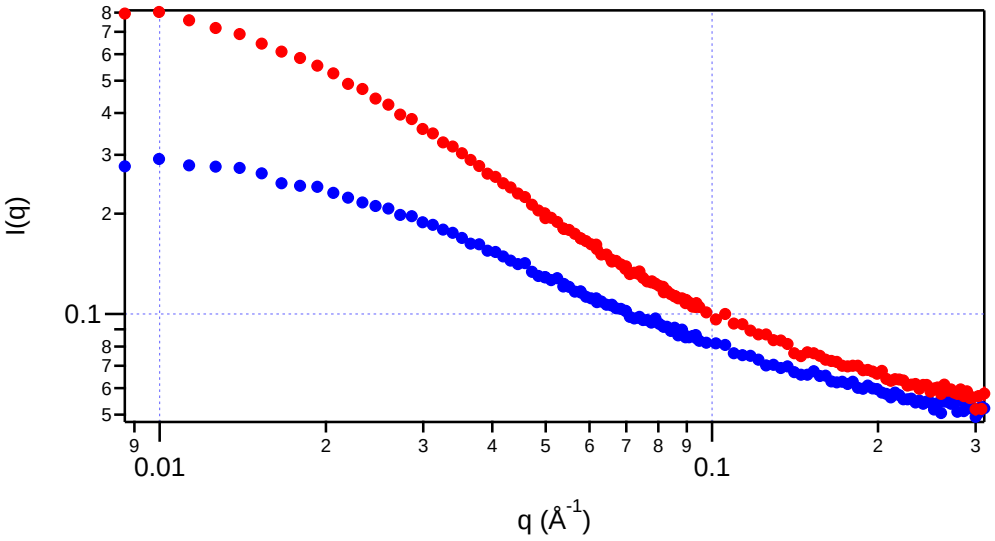


Figure 2.2: Small angle neutron scattering curves of 1 wt% P3HT in deuterated styrene at 60 °C in both illuminated (red circles) and dark (blue circles) environments.

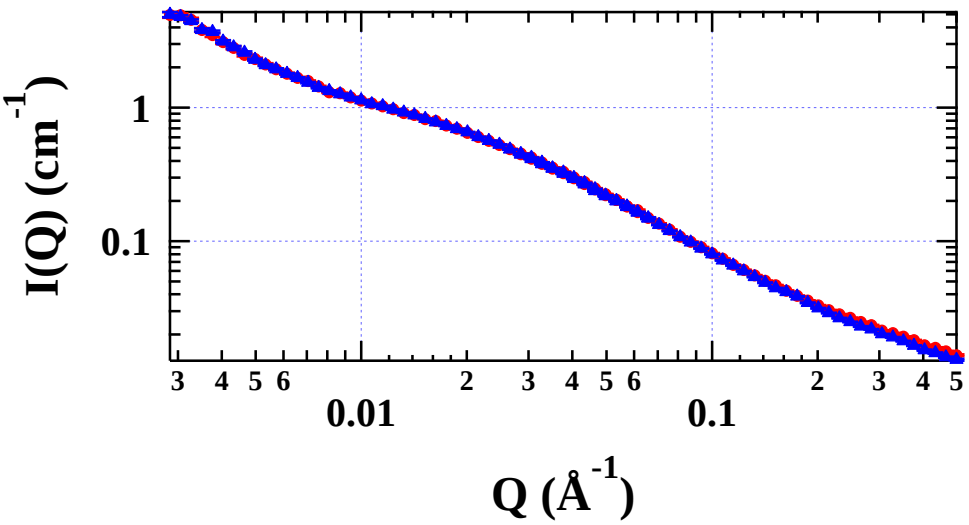


Figure 2.3: Small angle neutron scattering curves of 1 wt% Polystyrene in deuterated orthodichlorobenzene at room temperature in both illuminated (red circles) and dark (blue circles) environments

styrene at 60 °C for both conditions, respectively. The scattering from the samples that is illuminated (the “light” sample) show consistently stronger scattering intensity relative to the samples that are enclosed in aluminum foil (the “dark” sample), with this effect especially pronounced at increasingly lower Q values. Clearly, the data show that the conformation of the conjugated polymer in solution is altered when it is exposed to light.

To verify that these results are not an artifact of the experimental procedure or that the data reduction does not accurately account for the presence of the aluminum, the small angle neutron scattering curves of a 1 wt% solution of 140,000 MW polystyrene in deuterated ortho-dicholorobenzene was also measured when illuminated and when wrapped in aluminum foil. These results are presented Figure 2.3, where in stark contrast to the P3HT sample, the scattering curves of the polystyrene sample are identical in both the ‘light’ and ‘dark’ conditions, as would be expected. These results, therefore, verify that the observed variation in the scattering patterns of the P3HT sample is a consequence of the change in the conformation of the conjugated polymer when it is exposed to light, and is not the results of ancillary effects such as scattering contributions from the aluminum foil or a temperature elevation due to the optical illuminator.

The SANS curves of the P3HT solutions were fit to the flexible cylinder model of Pedersen and Schurtenberger.[72,73] This model provides the form factor of a semi-flexible Gaussian chain with a non-negligible circular cross-section

which accounts for excluded volume interactions within the random walk. The scattering Length Density (SLD) of P3HT and deuterated styrene were determined to be 6.76×10^{-7} and 5.2×10^{-6} Å^{-2}, respectively, using the NCNR SLD Calculator[74] and fit using NCNR SANS analysis macros in Igor Pro.[75] Figure 2.4 shows the result of this fit, including the residuals, for the scattering of the 1wt% P3HT solution under illumination. Excellent agreement is observed for the entire Q-range for all fits, especially for the lower concentrations. The flexible cylinder model provides a measure of the chain contour length (L) and Kuhn length (b) of the polymer chain, where b is equivalent to twice the persistence length (l_p) of the chain. Because the persistence length is defined as the distance over which correlations to the original bond direction are lost, it is an indicator of chain stiffness and provides a measurable quantity to monitor any changes to chain stiffness that may occur due to the presence of excitons on the chain in the illuminated sample.

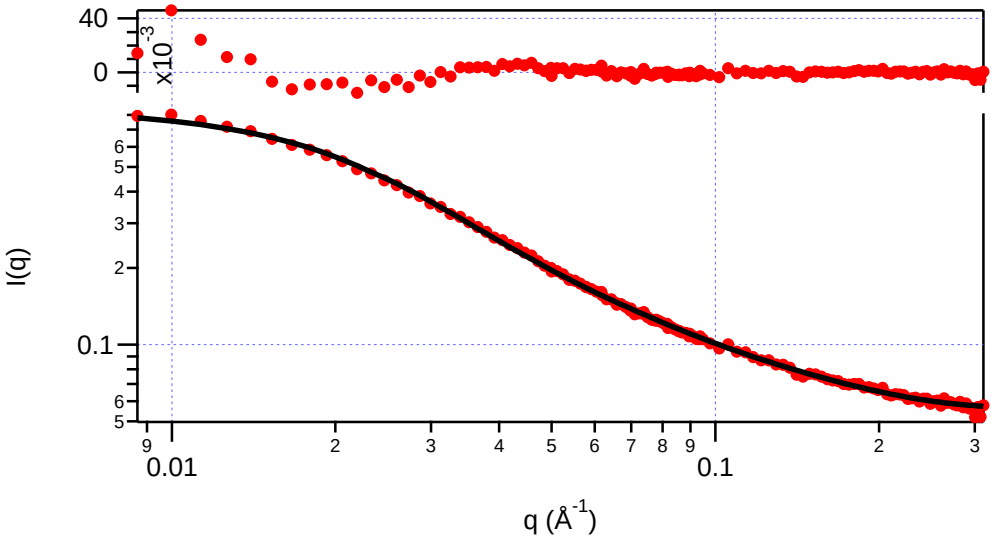


Figure 2.4: Flexible Cylinder Fit (black trace) for 1 wt% P3HT in deuterated styrene at 60 °C under illumination

Table 2.1 lists the Kuhn lengths and radii of gyration (R_g) of the P3HT molecule that are obtained from this analysis for several solution concentrations in both light and dark environments. The radius of gyration of the polymer chains is determined from the parameters that are obtained with the flexible cylinder model fit using the relationship $R_g^2 = \alpha(n_b^2)bL/6$. In this equation, α is a function of the number of Kuhn segments per chain, n_b the number of Kuhn segments per chain, b the Kuhn length itself, and L the contour length of the polymer chain.

To complement the fits of the lowest concentrations to the flexible cylinder model, the scattering from the P3HT solutions with a series of concentrations (0.5 – 2.0 wt%) was also measured and analyzed in a Zimm plot to provide a self-consistent check of the data analysis. The Zimm plot provides the θ = 0 and Q = 0 extrapolations to deliver an independent measure for the polymer chain radius of gyration as well as the second virial coefficient of the solutions. This analysis indicates that the R_g of the P3HT in the dark and light, respectively, are 94.6 ± 0.9 and 61.0 ± 6.2 Å. The second virial coefficient, which provides a measure of the polymer-solvent interactions, are -0.085 and -0.046 (±0.007) for the samples in light and dark conditions, respectively. Both Zimm plots also converge to indicate a molecular weight of the polymer chain that is ~28,000 g/mol, well within the expected values based on the manufacturers information.

Table 2.1: Parameters obtained from the Flexible Cylinder fit for P3HT in deuterated styrene at 60 °C

Sample	**Kuhn Length (Å)**	**R_g (Å)**
0.5 wt% "dark"	125 ± 3	93 ± 6
0.5 wt% "light"	65 ± 2	63 ± 5
1.0 wt% "dark"	114 ± 2	103 ± 3
1.0 wt% "light"	48 ± 1	70 ± 1

In order to explore whether these light-induced conformational effects are unique to P3HT or more generally applicable to a wider range of conjugated polymers, we have completed similar small angle neutron scattering experiments on solutions of MEH-PPV in deuterated THF in the presence or absence of incident light. The results of this scattering experiment are presented in Figure 2.5, showing the SANS curves of a 1 wt% sample at room temperature in both the presence and absence of light. On first inspection, it may appear that the changes in these samples are not as pronounced as in the P3HT samples, but it must be emphasized that the scattering is on a log scale and the maximum scattering intensity is almost an order of magnitude greater in Figure 2.5 than Figure 2.4. Thus, these results do show that the scattering of the sample that is exposed to light differs, well outside error, from that of the sample that is in the dark. Moreover, the larger scattering intensity signifies that the polymer chains are not individually dispersed, but are likely aggregated. Thus, this data is fit to the fractal flexible cylinder model, a model that accounts for a sample that is comprised of flexible cylinders that aggregate into fractal entities.[76] This experiment was completed for a series of concentration and solvents, and that data is currently being analyzed. Interestingly, MEH-PPV that is dissolved in deuterated THF show significantly greater difference in the 'light' and 'dark' samples than similar samples dissolved in deuterated styrene, a substantially better MEH-PPV solvent. Analyzing the data by the Zimm plot consistently result in negative intercepts in the $\theta=0$ and $Q=0$ lines, which is consistent with

significant aggregation. Regardless of these details, the data in Figure 2.5 clearly show that there exist measurable differences in the scattering, and therefore structure, of these MEH-PPV samples when the sample is illuminated or not. Thus, a light induced conformational change appears to be a generic effect that is common to a range of conjugated optoelectronic polymers.

Discussion

The data presented here indicates the exposure of conjugated polymers in solution alters the structure of the polymer in solution. However, the molecular level mechanism that is responsible for this effect is less clear. As noted above, previous studies have hypothesized that the formation of excitons or polarons on the conjugated polymer backbone will increase chain rigidity to explain changes in physical properties.[77]

As a first step, a cursory investigation of excited species density can test the validity of the interpretation that these effects are driven by the presence of excitons. Thus, through a combination of P3HT spectroscopy data, sample-specific light intensity measurement, and additional neutron experiments we seek to quantify the number of excitons present on a given conjugated polymer chain. To estimate the exciton density on the polymer chains in our experiments, we turn to a photo-luminescent spectroscopy based analysis. Conjugated polymers have been studied extensively via fluorescence spectroscopy and associated methods both in solution and films.[78]

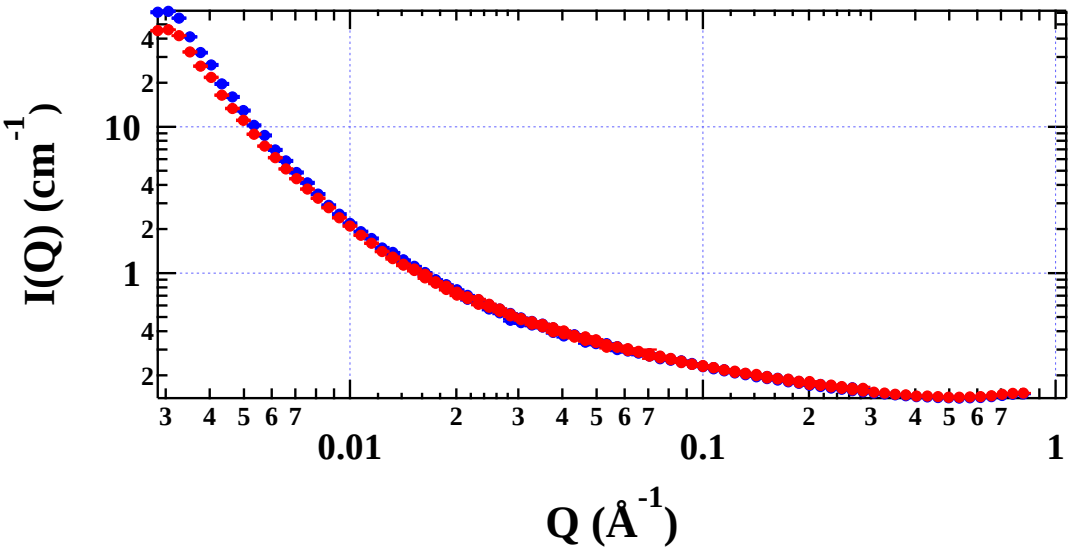


Figure 2.5: Small angle neutron scattering curves of 1 wt% MEH-PPV in deuterated THF at room temperature in both illuminated (red circles) and dark (blue circles) environments.

As discussed previously, incident photons can be absorbed by the polymer chain, resulting in a variety of excited states such as excitons, the radiative decay of which can be analyzed to quantify the number of excited species present for a given volume.[79,80] The following equation gives this excited state density, as a number of excited states for a given sample volume, N_{exc}:

$$N_{exc} = \frac{\Phi_{exc} F}{L}$$

where Φ_{exc} is the quantum yield, F the absorbed laser fluence, and L the sample thickness.[81] As P3HT is utilized throughout the conjugated polymer community as a benchmark standard, its photoluminescent properties have been well established, including a fluorescence quantum yield of 33%.[82,83] Given this information in addition to the illumination light intensities incident to our samples, sample thickness, and P3HT absorbance values over the respective wavelengths, we can estimate excited state densities in our samples.[7] Table 2.2 gives values of the number of excited states per cubic centimeter per second (N_{exc}) and number of excited states per polymer chain per second ($N_{exc\text{-}chain}$) for our original "light" sample, as well as the two wavelength dependant samples described below. To further interrogate the impact of the number of excitons on the structural changes of the P3HT chain in solution, we have monitored the change in polymer chain structure when the samples are illuminated in narrow wavelength bands.

Table 2.2: 1wt% P3HT in d-Styrene sample thickness, light intensity incident to sample, exciton density, and exciton density per polymer chain.

Sample	**Thickness (cm)**	**Light Intensity (lux)**	**Light Intensity (μmol/m^{2}s)**	**N_{exc} (cm^{-3}s^{-1})**	**$N_{exc\text{-}chain}$ (s^{-1})**
Light	0.2	50000	1000	4.4×10^{16}	2.0
415-590	0.2	6300	126	6.3×10^{15}	0.28
610-1200	0.2	2000	40	6.2×10^{13}	2.9×10^{-4}

Figure 2.6 displays the SANS scattering data of a 1wt% P3HT solution in d-Styrene that has been exposed to incident light both inside a wavelength band where P3HT strongly absorbs (415-590nm) and in a wavelength band with very little P3HT absorbance (610-1200nm).[3,4]

The qualitative trends in these scattering curves mirror the response of the P3HT solution to conditions with or without illumination (i.e. light/dark), though the magnitude of the differences between the scattering curves are reduced. Fitting this data to the flexible cylinder model shows that the Kuhn lengths of P3HT under these conditions are 85±1 Å and 95±1 Å for the 415-590 nm and 610-1200 nm samples, respectively. A moderation of the structural changes due to light exposure is certainly partly due to the much reduced intensity of the incident light due to the lower transmission of the filters used in these experiments, as well as the fact that the 415-590nm filter does not accommodate the entire P3HT absorbance region. Regardless, these results are consistent with a change in P3HT structure that is driven by the presence of excitons, even with much reduced incident light intensities.

Moreover, the correlation of these changes to the estimated exciton density is also consistent with our interpretation. The excited state density is several orders of magnitude greater in the fully illuminated sample than that in the sample exposed only to light outside the optimal P3HT absorbance region.

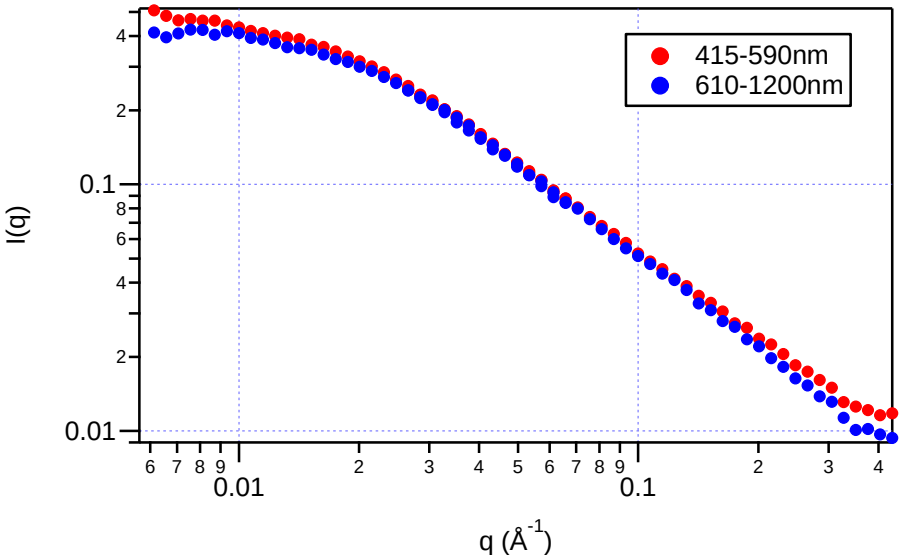


Figure 2.6: SANS scattering curve of 1wt% P3HT in d-Styrene. Red data points indicate sample illuminated with 415-590nm light, while blue data points indicate sample illuminated with 610-1200nm light.

Calculating the exciton density per chain assuming chain MW of 28,000 yields multiple excitons per chain per second under white light illumination while the N_{exc} of the sample that is exposed to the 415-590 nm wavelength band drops by an order of magnitude and that of the sample exposed to the 610-1200 nm wavelength band contains far fewer excitons per chain.

Clearly there exist substantial differences in exciton density based on illumination level and absorbance, and the magnitude of the observed changes in the polymer structural characteristics scale with the amount of total illumination. It is also important to note that the structural changes we observe in all samples are not instantaneous, but rather materialize over illumination times on the order of minutes or hours, where the exact timescale is still under investigation. Therefore, it becomes necessary to consider the number of charges present on a chain over the entirety of these intervals, leading to the density of excited states that approach hundreds or thousands per chain over the timescale of the structural transition. Considering these large total net differences in exciton density between illuminated and non or slightly illuminated samples, this analysis shows that the number of excitons present throughout the P3HT sample over the neutron analysis time window are sufficient to elicit the conformational changes observed in our experiments, and thus consistent with our interpretation that these changes are driven by the presence of the excitons.

Moreover, the results of this SANS experiment do not coincide with the hypothesis that the formation of excitons or polarons on the conjugated polymer

backbone increase chain rigidity. The results reported in Table 2.1 clearly show that the Kuhn length actually *decreases* in the P3HT when it is exposed to light. Therefore, if there is not an increase in the rigidity of the polymer with illumination, there must be another mechanism to explain the structural changes of the conjugated polymer with light absorption. For guidance, we can look to the underlying mechanisms of other light responsive materials.[84] The most studied photo-sensitive molecules fall into three categories, those that undergo a.) photo-isomerization, such as azobenzene or spiropyran,[85] b.) photo-induced ionic dissociation,[42] or c.) photo-reactive molecules such as cinnamates.[86] Inspecting the underlying mechanism that drives each of these changes, none appear to fit the conjugated polymer system that is studied here; the conjugated polymer does not undergo an isomerization, nor a reaction. The closest analogy is that of the photo-induced ionization, though the formation of the exciton is not equivalent to forming an ion pair. However, the mechanism by which the ionic dissociation physically responds is due to the increased electrostatic repulsion between the photo-generated charges. A corresponding change in the conjugated polymer would be the planarization of the conjugated polymer due to geometric deformations of the vibrational mode strongly coupled to the relaxation of the initial photoexcitation on the excited state surface.[50] A mechanism that is not often invoked in the mechanisms for the change in structure of photoresponsive molecules is the change in the solubility of the photo-stimulated structure relative to that of the ground state material.

Thus, we consider whether the change in solubility of the conjugated polymer when it is photo-excited can explain our results. A range of studies have shown that varying solvent quality in conjugated polymer solutions through methods such as solvent choice, solvent evaporation, and addition of poor solvents, can have powerful effects on final polymer morphology in deposited films.[54,87,11,88] Moreover, the results of this study clearly show that the thermodynamics of the conjugated polymer solution are altered when the solution is exposed to light. The second virial coefficients (A_2) obtained from the Zimm plot, -0.085 and -0.046 (±0.007) for the samples in light and dark conditions, respectively, clearly show that the solvent quality of the deuterated styrene decreases for P3HT upon exposure to light as evidenced by the more negative A_2. This is also consistent with a decrease in the R_g of the polymer when illuminated relative to that of the polymer in the dark, where a polymer chain collapse in the poorer solvent is expected. Thus, we interpret these results to indicate that the exposure of a conjugated polymer to light deteriorates the thermodynamic interaction between the polymer and solvent, resulting in a contraction of the polymer chain. It appears that the presence of excitons on the polymer backbone alter the thermodynamic interaction between the polymer and the surrounding solvent. The decrease in solubility leads to the formation of more P3HT-P3HT interactions, driving the polymer to contract to a more compact conformation. Thus, it appears that the change in the thermodynamic interaction between polymer chain and solvent dominates the photo-stimulated alteration of

the polymer conformation in solution, offering a novel mechanism to control the structure of conjugated polymer in solution. Ramifications of this discovery include the development of new opportunities for a broad range of novel light-sensitive materials and the fact that the morphology, and therefore the performance, of conjugated polymers in organic electronic devices will be altered by exposure to light during the fabrication process. This latter implication strongly suggests that the illumination conditions of the ink before and during film deposition must be considered in the reproducible fabrication of organic electronic device fabrication.

Conclusion

Small angle neutron scattering experiments that monitor the conformation of P3HT in deuterated styrene indicate significant changes in the structure and conformation of the polymer in solution due to its exposure to light. Careful data reduction and analysis indicates significant changes in the Kuhn length, radius of gyration and thermodynamic interaction between the polymer and solvent upon exposure to white light. Interestingly, the Kuhn length and radius gyration of the polymer chain *decrease* when exposed to light. This result is counter to an increase in the rigidity of the conjugated polymer in the presence of the exciton, a mechanism that has been put forward in previous studies.

We propose that the formation of the electron-hole pair on the conjugated polymer alters the polymer-solvent interactions and thus the solubility of the

conjugated polymer in solution. This decrease in solubility with exposure to light drives the polymer chain to contract, leading to a de-swelling of the polymer chain. Preliminary results show similar behavior by the conjugated polymer MEH-PPV under similar conditions, pointing towards the presence of a generic effect. The identification of such an effect opens the door to a wide range of applications revolving around the ability to passively control chain structure through simple illumination, such as in-situ processing methods or localized morphology control. Crucially, these results identify the illumination history as an important parameter that can alter the morphology of conjugated polymer inks, and can thus impact the reproducible fabrication of organic electronic device active layers. Further understanding and quantification of the underlying fundamental processes will be key in fully harnessing its full potential.

Acknowledgements

The authors gratefully acknowledge the National Science Foundation (DMR-1409034) for support of this project. We also acknowledge the support of the National Institute of Standards and Technology, U.S. Department of Commerce, in providing the SANS facilities used in this work, where these facilities are supported in part by the National Science Foundation under Agreement No. DMR-0944772. Additional SANS facilities provided by Oak Ridge National Laboratory, U.S. Department of Energy.

CHAPTER THREE

ILLUMINATION ALTERS THE STRUCTURE OF GELS FORMED FROM THE OPTOELECTRONIC POLYMER P3HT

Abstract

Studying the gelation process of conjugated optoelectronic polymers has often been employed as a means of better understanding the final morphology and assembly in active layers of organic electronic devices due to the correlation between the experimentally observed sol-gel transition and many common solution based fabrication techniques. The nature of the percolated network structures formed through the molecular assembly that occurs during this gelation directly affects device performance in conjugated polymer based active layers. Thus, precise knowledge of the evolution of structures during gelation provides crucial information that is needed to rationally improve device performance by directing the assembly during processing. Additionally, observing the effects of environmental factors such as ambient light exposure upon the gelation process will direct efforts towards improving universally overlooked facets of the typical fabrication procedure. Thus, we have conducted a series of ultra small angle and small angle neutron scattering experiments to probe the temperature-driven gelation process of the conjugated photoactive polymer poly(3-hexylthiophene-2,5-diyl) (P3HT) in both the presence and absence of white light. Analysis of the resultant scattering data shows that the gelation process consists of the creation and steady growth of cylindrical aggregates formed by the agglomeration of free chain P3HT. Furthermore, clear differences in the gel structure and assembly between illuminated and non-illuminated gels are observed across multiple length scales, pointing towards an optically-induced

variation in the gelation process. Our results indicate that simple white light exposure sharply retards the growth of conjugated polymer microstructures, which clearly suggests that ignoring illumination conditions throughout organic electronic fabrication processes risks producing inconsistent and non-reproducible active layer architectures and ultimately endangers dependable device performance.

Introduction

One of the most crucial production processes associated with commonly used optoelectronic conjugated polymers is polymer gelation, the process by which a 3-D polymer rich network percolates in a phase that lies somewhere between liquid and solid.[54] Knowledge of the gelation process assists in the development of certain electronic inks and printed films; processes which seek to avoid large-scale gelation due to its tendency to form blockages and inhomogeneities within the desired system.[29] But more importantly for broader purposes, studying the gelation process allows insight into the pathway of aggregate formation in optoelectronic polymers, as it acts as a form of polymeric self-assembly conducive to the formation of stable structure networks that are effective charge carriers.[55] Gaining insight into the specific details of the self-assembly process can allow substantial structural control of the final film through variations in polymer concentration, solvent identity, and gelation impetus;

amongst other experimental variables.[56,89] One of the more common manifestations of these effects occurs during typical organic electronics device fabrication techniques such as spin-coating. Over the relatively brief timescale of spin-coating, a polymer film is created through the quick removal of solvent via fluid motion and evaporation.[27] Due to the rapid loss of the favorable solvent environment, an accelerated formation of aggregates occurs until kinetically frozen by sufficient solvent withdrawal. The gelation mechanisms (such as nanofibril formation and macro-aggregation) observed in solution systems drive this process as well, albeit in modified form on a different timescale. Thus, a fundamental understanding of solution gelation mechanisms carries over to the formation of bulk films by specific processing methods and consequently can aid the design of tunable electronics fabrication methods in order to produce desired morphologies and architectures.[90,91,20]

There exists a wide range of proposed pathways through which some of the more common conjugated polymers aggregate during the gelation process including percolation[92] and phase separation.[93] Specifically for poly(3-hexylthiophene-2,5-diyl), an optoelectronic benchmark polymer, a multi-step physical gelation process is often assumed, as illustrated in Figure 3.1.

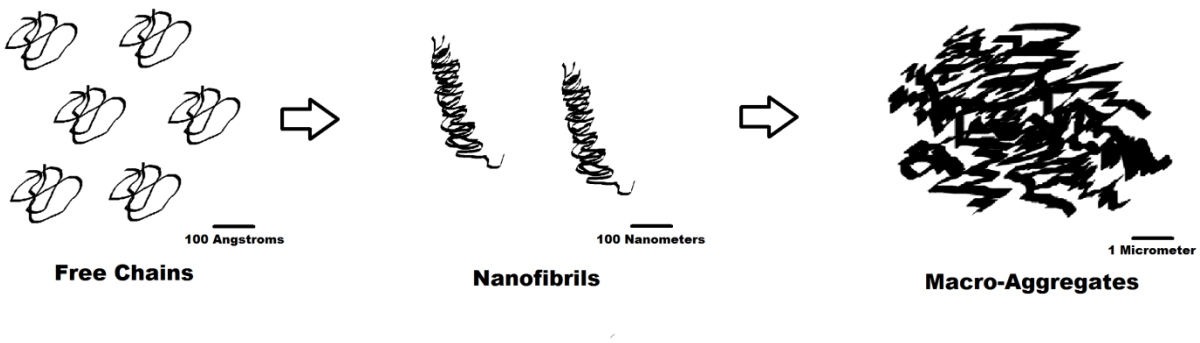


Figure 3.1: Schematic depiction of proposed P3HT solution gelation mechanism involving aggregate formation from free chains in solution via nanofibrils.

During the initial stages of applied system stress, such as decreased temperature or solvent quality, strong inter- and intra-chain π-stacking interactions cause aggregation of individual P3HT chains into small bundles known as nanowhiskers or nanofibrils.[94] These nanostructures themselves further aggregate into clusters to begin the onset of gelation, ultimately forming a viscoelastic 3-D network, which percolates throughout the sample. Though these rough physical outlines of the P3HT gelation process are generally well known, the exact quantitative nature of the structures formed as they evolve throughout the stimuli ramp is mostly unclear. In this work, we present a quantitative and qualitative analysis of structure factors of the gelling of P3HT in a favorable solvent monitored closely step-by-step throughout a temperature ramp, and these scattering data are analyzed to quantitatively monitor the crucial structural parameters as they evolve.

Though much attention across the field of optoelectronic polymers has been focused on optimizing morphological environments in order to induce favorable device efficiencies, the question of whether or not the process which provides the driving force behind the device mechanisms, i.e. the formation of excitons, may itself be influencing polymer chain conformation has remained somewhat of an afterthought. Current preliminary experiments hint towards the validity of this postulate, potentially opening the door to a wide range of opportunities to control polymer morphology before and during device processing, through selective illumination of sensitive active layers. Thus, in

addition to monitoring structural changes throughout gelation, this chapter seeks to expand our understanding to the impact of the presence of light on the self-assembly of conjugated polymer chains in concentrated solution by monitoring the effect of in-situ white light illumination on the structures that form during the gelation process. Moreover, the degree to which this illumination influences the structural growth of the gel network is also monitored, as these characteristics will ultimately impact the foundation of subsequent active layer device morphologies.

Experimental

Gelation samples were created using poly(3-hexylthiophene-2,5-diyl) purchased from Rieke Metals with a regioregularity > 98% and a molecular weight < 50,000, per the manufacturer. The polymer material was dissolved in deuterated 1,2 ortho-dichlorobenzene (ODCB) to give a sample consisting of 17% P3HT by weight (275 mg/mL). Samples were elevated to 70°C to ensure complete dispersion of the polymer in the solvent. All experimental sequences were conducted using a temperature ramp which employed thermostat heating controls to move in set temperature increments through gelation to its completion at room temperature. Starting at 40°C, scattering data were collected at temperatures every 2°C down to 20°C, with a 15 minute thermal equilibration allowed between each data collection period. Following a gelation sequence, the

samples were again returned to 70°C and maintained there until re-use as part of a subsequent run with a change in illumination conditions.

Small angle neutron scattering (SANS) experiments were conducted at the CG-2 GPSANS beamline of the High Flux Isotope Reactor (HFIR) at Oak Ridge National Laboratory. Scattering was collected at a single sample-detector distance using a neutron wavelength of 6 Å, allowing a Q range ranging from 0.003 to 0.5 $Å^{-1}$, where $Q = 4\pi/\lambda \sin(\theta/2)$ with λ being the neutron wavelength and θ the scattering angle. Raw data was reduced using SPICE ORNL reduction protocol macros in Igor Pro.[75] Samples were mounted in 2 mm wide glass banjo cells holding approximately 0.4 g of P3HT solution.

Ultra small angle neutron scattering (USANS) experiments were performed at the National Institute of Standards and Technology in Gaithersburg, Maryland on the BT-5 beamline. Using six buffers and an initial neutron wavelength of 10 Å allowed for collection of scattering data down to $3.5x10^{-5}$ $Å^{-1}$. Raw data was reduced using the NIST NCNR reduction and desmearing macro suite in Igor Pro. Curve fitting analysis of both the USANS and SANS data was performed using NCNR analysis macros in Igor Pro as well as the DANSE SasView software project.

To achieve proper light/dark environments, a consistent methodology was adhered to. "Dark" trials were conducted by wrapping the sample cells in 0.1 mm aluminum foil, effectively blocking out all incident photons while remaining transparent to neutrons. Removing the foil and illuminating the sample at a 5 cm

distance with an optical illuminator consisting of a 125 watt halogen bulb providing 50,000 lux created the "light" conditions for the appropriate trial runs. Analyzing a solution of 1wt% polystyrene under the above experimental conditions provides a control sample and verifies that the changes in scattering data are due to the presence of the illumination, and not an experimental artifact. Representative data for this control experiment is available in a previous chapter,[95] confirming that both the "light" and "dark" curves overlap well throughout the entire Q range, as expected. As a result, the methodology utilized in these experiments to collect neutron scattering of conjugated polymer solutions under illuminated and non-illuminated conditions appears valid and free from error associated with thermal effects or scattering artifacts that are due to the presence of aluminum.

Results

Small angle neutron scattering data was collected for the 17 wt% P3HT sample at each temperature along a thermal ramp starting at 70°C to ensure full polymer dispersion in the solvent, and then continuing from 40°C to 20°C in 2°C increments. The process was conducted first without ambient light, and immediately repeated under illumination, employing identical thermal histories for both trials. The resultant data curves are shown in Figure 3.2, wherein filled data points correspond to experimental trials conducted in the dark, and open data points indicate trials performed under white light illumination.

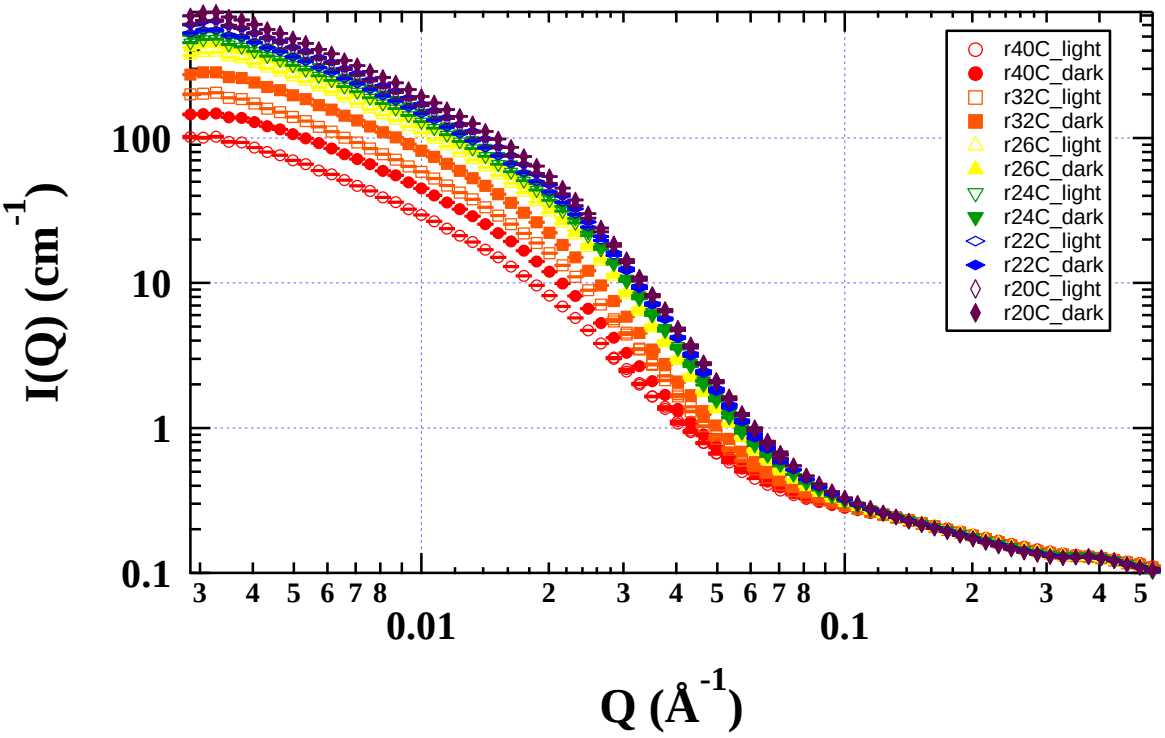


Figure 3.2: SANS of 17 wt% P3HT gelation under illumination (open circles) and in the dark (closed circles) through a 70-40°C temperature ramp. Color denotes individual temperatures between 40° and 20°C.

Overall the samples produce powerful scattering curves indicative of large aggregates formed at these high concentration conditions. Increased scattering intensity is seen as temperature decreases, an intuitive trend considering the rapid growth of the strongly scattering P3HT aggregates as gelation progresses. Large differences in absolute intensity are observed in the low Q regions between light and dark samples for all temperatures, with the dark samples consistently exhibiting much stronger scattering.

These differences in absolute intensity range from 5-20% for most samples, up to an increase of over 40% for the lowest Q region of the higher temperature samples. However for Q> 0.1$Å^{-1}$ all intensity differences have dissipated and universal overlap for all temperatures is observed, indicating little change in local chain structure of the samples throughout the gelation process.

The complexity of the hierarchical structures that exist during the P3HT gelation process requires a multiscale model to properly fit the data. P3HT nanofibril aggregates are modeled using an elliptical cylinder or parallelepiped form factor which assumes an oval or rectangular aggregate cross section, respectively.[96,97,28] Fitting to this model allows extraction of two-dimensional parameters related to the surface area of the nanofibril face, the scattering length density of the aggregate, which is proportional to its composition, and a scale factor, which is proportional to the volume fraction of aggregates. In order to account for the presence of "free" P3HT chains not yet aggregated in solution, a polymer excluded volume model is included via linear addition. This allows the

structural size and shape of the individual un-aggregated chains to be monitored throughout gelation by monitoring its radius of gyration and Porod exponent.

The combination model approach has been shown to accurately fit the P3HT system under similar gelation conditions over a wide Q range encompassing all relevant SANS data.[30] The total combined model is described by:

$$I(q) = \phi_{P3HT}\phi_{ECM}(\Delta\rho_{ECM})^2 P_{ECM}(q) + \phi_{P3HT}(1 - \phi_{ECM})(\Delta\rho_{PEV})^2 P_{PEV}(q)$$

where ϕ_{P3HT} describes the total volume fraction of P3HT in the solution, ϕ_{ECM} is the volume fraction of aggregated P3HT present and modeled as an elliptical cylinder model, P_{PEV} is the free chain excluded volume form factor for P3HT, P_{ECM} describes the elliptical cylinder form factor for the aggregates, and $\Delta\rho_{ECM}$ and $\Delta\rho_{PEV}$ are the scattering length density contrast between P3HT aggregates and the solvent and between the free P3HT chains and the solvent, respectively. Figure 3.3 shows an example fit of the data to the combined ECM/PEV model for a given single temperature. Data fit well across the entire Q range using this model for the range of temperatures studied, including the crossover region between models. Through a fitting methodology based on systematically holding known parameters constant, a variety of structural parameters of the gelling sample are then extracted in both illuminated and dark environments. Figures 3.4-3.7 illustrate the evolution of select parameters during the gelation process in both the light and dark.

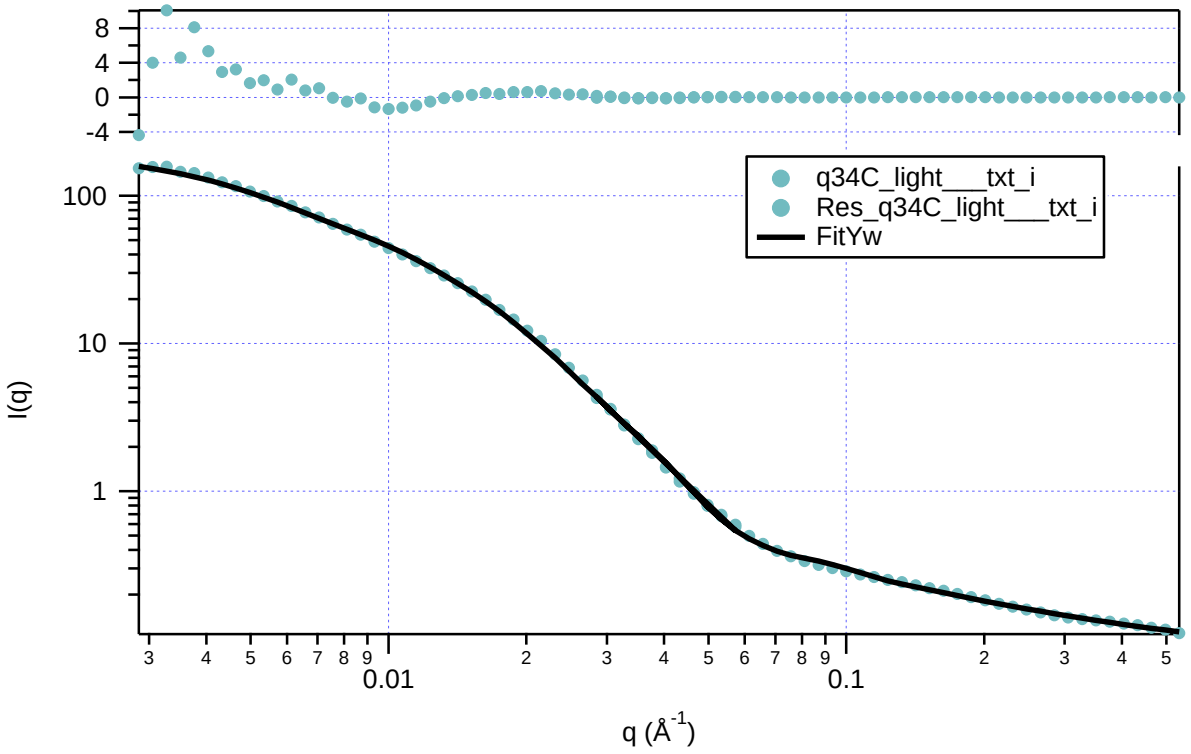


Figure 3.3: Combination Model (Elliptical Cylinder + Polymer Excluded Volume) fit to 17 wt% P3HT gelation curve in d-ODCB at 34°C in the presence of white light illumination.

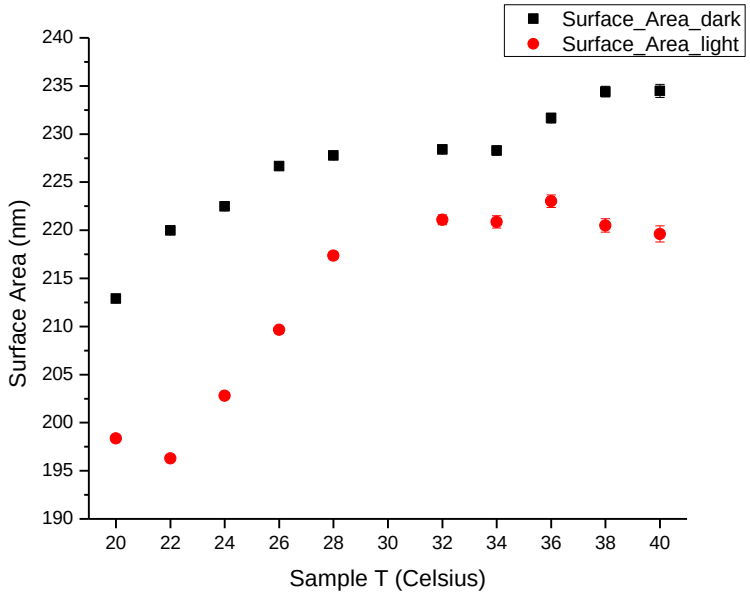


Figure 3.4: Surface area of the nanofibril face, i.e the cross-section of nanoscale P3HT fibers. This plot shows that the P3HT fibers are consistently larger in the dark than in the light.

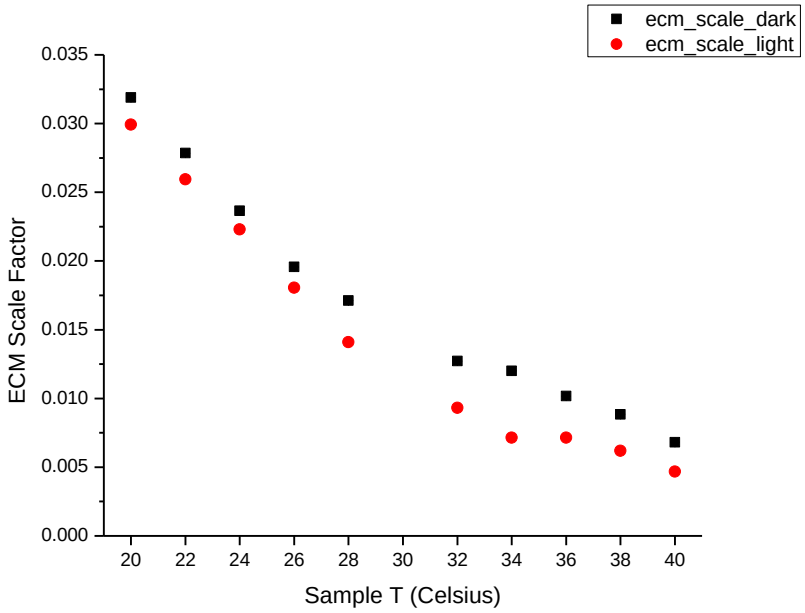


Figure 3.5: Scale factor obtained from the elliptical cylinder model portion of the fit, a parameter that is directly proportional to the amount of P3HT aggregated in nanofibrils. This data show that the amount of aggregated P3HT remains larger in the dark environment throughout gelation.

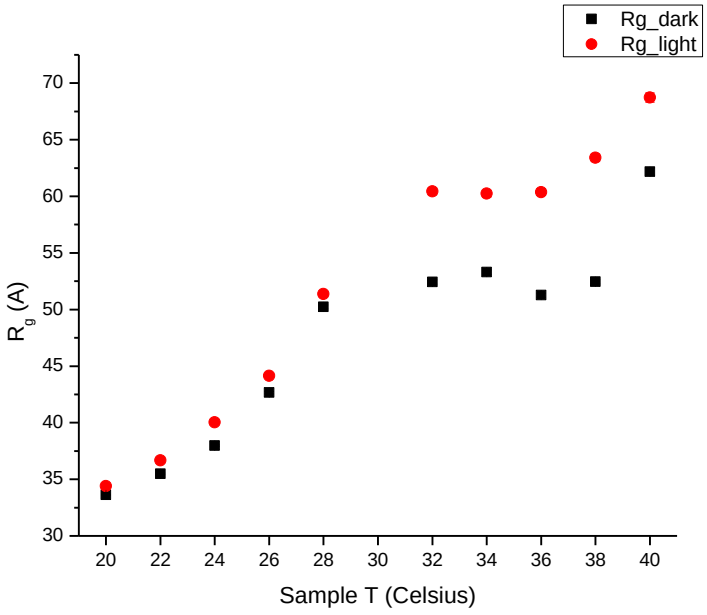


Figure 3.6: Radius of gyration of P3HT obtained from the excluded volume model, which monitors the size of free P3HT not aggregated in nanofibrils. This structural feature shows that the free chains are larger in the light than the dark, especially at higher temperatures.

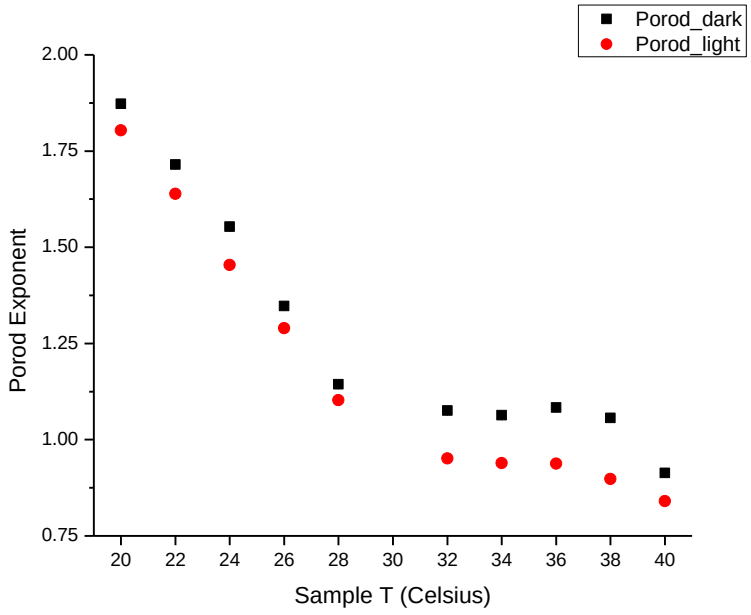


Figure 3.7: Porod exponent of free P3HT chains obtained via the excluded volume model, a measure of general chain conformation. These results indicate a slightly larger value, and thus more compact polymer chain, in the dark.

Figure 3.4 gives values for the cross sectional area of the P3HT nanofibrils described by the elliptical cylinder model, essentially describing the cross-sectional area of the nanofibril faces. Our data show this parameter is consistently smaller in the light than in the dark. Figure 3.5 displays the elliptical cylinder model scale factor, which is directly proportional to the amount of P3HT that exists in the aggregated nanofibrils, as opposed to existing in a free chain form. This value remains consistently larger in the dark than in the light throughout gelation. Use of the polymer excluded volume model gives the radius of gyration for free chains, and is shown in Figure 3.6, with the illuminated chains appearing larger than the non-illuminated chains, especially at higher temperatures. Finally, Figure 3.7 reports the Porod exponent values obtained from the excluded volume model for the free chains, a parameter related to the conformation of the polymer chain, with a value of 1 indicating a classic rigid rod while a value of 2 denotes a Gaussian coil. As gelation progresses, all values increase from a rigid rod-like state towards a more Gaussian conformation, with the illuminated sample values consistently somewhat smaller throughout. As with the raw data, these quantitative analyses show that there exist clear differences between light and dark samples in all structural parameters through the gelation process.

Though SANS analysis provides a great deal of insight into the nanometer level structure of the P3HT gelation process, in order to probe larger length scales of the full aggregates, expanding the Q range through USANS becomes

necessary. Replicating exactly the experimental methodology of the above SANS setup, USANS measurements were conducted on an identical 17wt% P3HT in d-ODCB sample using the same temperature ramp protocol in the presence and absence of illumination. Example USANS data curves are plotted with their respective SANS curves from these experiments in Figure 3.8.

Like the SANS data, the USANS curves show significant difference in absolute intensity between light and dark, a discrepancy which intensifies towards the end of gelation at lower temperatures. The data was fit using a Guinier-Porod Power law model, a general approach to determine the size and dimensionality of multi-scale scattering objects.[98] Using this model, the radii of gyration of the large macro-aggregates were obtained, with the results shown in Figure 3.9. Intuitively, the overall aggregate size grows with decreasing temperature as increasingly more nanofibrils interact to form larger bundles as solvent quality decreases. Additionally, towards the end of gelation a very strong dependence of the R_g on the illumination environment develops, indicating that light exposure influences the local structure enough to alter the larger structure of the gel as the gelation progresses.

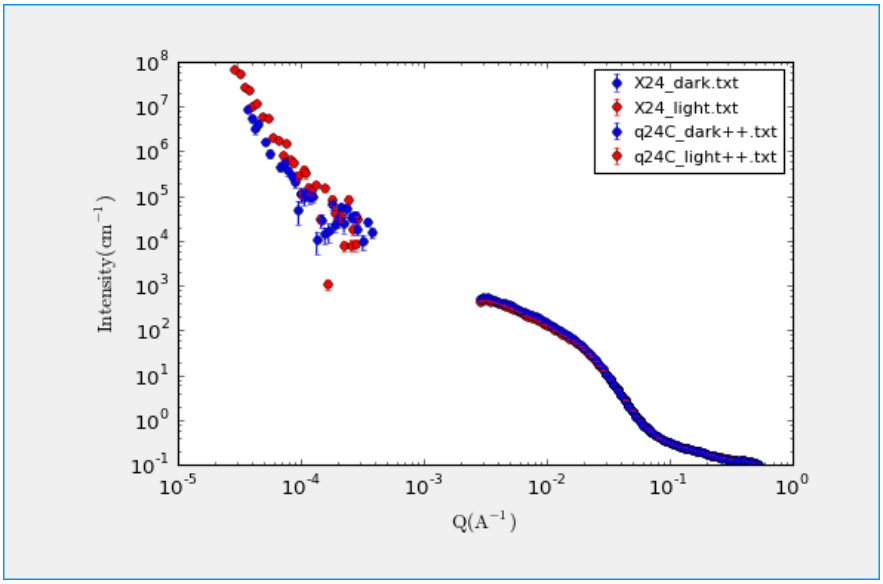


Figure 3.8: USANS and SANS curves of the 17 wt% P3HT solution in d-ODCB in both the light (red points) and dark (blue) at 24°C.

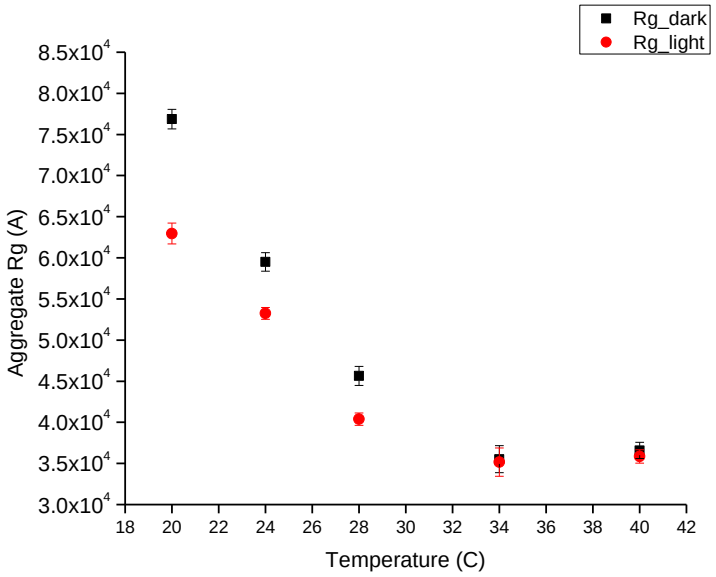


Figure 3.9: R_g obtained from Guinier-Porod power law fit to USANS data for 17 wt% P3HT in d-ODCB. Black points indicate dark sample environment, red points illuminated environment.

Discussion

Analysis of the small and ultra small angle neutron scattering for a high concentration solution of an optoelectronic polymer offers special insight into the evolution of the structure of the forming gel as well as solution information during the gelling process. In particular, this analysis offers insight into the effect of white light illumination on the assembly of the conjugated polymers into the gel. Determining the size of the aggregated P3HT whiskers is crucial to understanding the structure-performance relationship in P3HT based active layers, as the size and shape of these P3HT semi-crystalline domains that emerge from these nanostructures has been shown to directly impact exciton dissociation and device efficiencies.[99,22]

Analysis of SANS data monitors the cross-sectional surface area of the assembling fibrils. The data in Figure 3.4 shows fairly small changes in this cross-sectional area of the nanofibrils throughout gelation (~10%), indicating that once they are formed, the nanofibrils maintain a relatively uniform cross-sectional size and undergo further π-stacking to grow in length. Nanofibrils formed in the light show consistently smaller cross-sectional surface areas than their counterparts formed in the dark. This alteration in the assembly process is consistent with a change in the local chain structure or thermodynamic interaction between the polymer and solvent,[95] which is initiated by light exposure and hinders aggregation. Figure 3.5 gives the scaling factor for the fit of the scattering data to the model, which is proportional to the amount of P3HT that

has aggregated in solution. Intuitively, this increases with a decrease in temperature as decreasing solvent quality forces greater polymer-polymer interaction. Additionally, as in the case of nanofibril surface area, the "light" samples are much less aggregated than the samples that are formed in the dark, which is also consistent with a reduced extent of aggregation in the samples that are exposed to white light.

The combined ECM/PEV model also allows us to monitor the size and shape of the un-aggregated P3HT chains. Figure 3.6 shows that decreasing temperature results a decrease in the R_g of these free chains, a trend which becomes even more pronounced below 30°C. This effect is what would be expected for a thermodynamically driven chain collapse due to decreasing solvent quality with decreasing temperature. The values for the free chain Porod exponent, shown in Figure 3.7, corroborate this model as well, as the exponent increases as gelation progresses, indicative of conversion from a semi-rigid rod conformation to a more compact state resembling a Gaussian coil. The impact of illumination is also present in the free chain characteristics, with white light illuminated samples boasting both larger radii of gyration and lower Porod exponents. Both parameters suggest that light exposure hinders the collapse of the free chains in solution, leading to a more expanded chain conformation that is less inclined to aggregate.

Figure 3.9 displays the analysis of the USANS data with a power law model documenting the R_g of the aggregated P3HT bundles on the length scale

of hundreds to thousands of nanometers. The sizes of these aggregates remain relatively constant through the higher temperatures, but as with the SANS data, these aggregates begin to grow as the temperature drops below 30°C. Interestingly, the state of illumination dramatically impacts the final aggregate size, showing differences with illumination as aggregate growth accelerates below 30°C. The non-illuminated samples produce significantly larger gelled macro-aggregates for all of these temperatures, culminating in a final aggregate radius that is over 20% larger than samples that are produced in the light. This trend is consistent with the SANS data, which showed that smaller nanofibrils are formed in samples under illumination.

Clearly illumination conditions have a profound effect on the aggregated structures of P3HT that are formed by a thermally driven gelation process. The presence of white light stunts the growth of P3HT nanofibril chains, which appears to be a direct result of the change in conformation of the individual free chains from which the nanofibril aggregates form. The free chains in the light-exposed P3HT solution are much less compact than identical solutions that are allowed to assemble in the dark. This larger radius of gyration appears to interfere with the required stacking that drives fibril formation. As a result, the cross-sectional area of the whisker aggregates that initially form remain distinctly smaller when the sample is illuminated. Predictably the macro-aggregate clusters that are composed of these smaller building blocks grow to smaller sizes than those that assemble in the dark. All structural parameters are consistent with this

interpretation, including smaller R_g values as determined by USANS and the volume fraction of aggregated P3HT chains elucidated via SANS.

Therefore, these results clearly demonstrate that the presence of incident light will dramatically affect the assembly and gelation of P3HT in concentrated solution. Moreover, illumination will also have a direct impact on the production of device active layers that utilize P3HT as the hole transport component, as the gelation process dictates the morphology and charge transport pathways in the P3HT in such devices.[94,30] Therefore, because the morphologies that are generated through gel formation carry over to the final device architecture, the illumination conditions under which device fabrication occurs should not be overlooked. The results of this experimental program show that inconsistent illumination histories among otherwise identical samples can lead to large variations in size and amount of assembled gel structures. However, as this phenomenon is further studied and controlled it could also allow for protocols that offer pathways to targeted morphologies, including those that can be localized to areas of interest throughout a device by patterned illumination. Such an approach would provide a powerful in-situ means to impart hierarchical morphologies to the desired areas within active layers, while avoiding any damage or chemical alteration of the system in question.

Conclusion

Thermally driven gelation of the conjugated optoelectronic polymer P3HT has been monitored in-situ through a temperature ramp with both small and ultra small angle neutron scattering to monitor the change in the assembly process due to the presence or absence of illumination. Data analysis clearly indicates formation of cylindrical nanofibril aggregates which themselves further self-assemble into macro-aggregates, a process that occurs quickly with decreasing temperature. Careful analysis of the resultant scattering patterns demonstrates that the presence of illumination on the gelling solution results in a decrease in the driving force for gelation, smaller nanofibrils, and a lower volume fraction of gelled P3HT. This behavior is obvious across multiple length scales and leads to ultimately smaller P3HT microstructures than the non-illuminated counterparts. These results, therefore, indicate for the first time that careful control of the illumination conditions during P3HT active layer based device fabrication is crucial to maintain reliability and reproducibility in their production and performance. Additionally, while failure to effectively monitor and control illumination environment during device fabrication may ultimately yield undesirable and inconsistent architectures, morphologies and performance, proper harnessing of these optoelectronic structural effects through carefully controlled illumination methodologies could conversely open the door to a new field of localized morphology control and active layer structural manipulation geared towards further optimizing organic electronic device performance.

Acknowledgements

The authors gratefully acknowledge the National Science Foundation (DMR-1409034) for support of this project. We also acknowledge the support of the National Institute of Standards and Technology, U.S. Department of Commerce, in providing the USANS facilities used in this work, where these facilities are supported in part by the National Science Foundation under Agreement No. DMR-0944772. The SANS experiments of this research was completed at ORNL's High Flux Isotope Reactor, which was sponsored by the Scientific User Facilities Division, Office of Basic Energy Sciences, US Department of Energy.

CHAPTER FOUR

THE IMPORTANCE OF SOLVENT QUALITY ON THE MODIFICATION OF CONJUGATED POLYMER CONFORMATION AND THERMODYNAMICS WITH ILLUMINATION

Abstract

Device efficiency in key organic electronic devices such as OPVs, organic field transistors, and OLEDs has long been known to be closely tied to the conformation of the conjugated polymer chains which make up the active layers. Our previous results have indicated that the often overlooked yet ubiquitous experimental condition of simple light exposure can have a profound effect on the structure of these optoelectronic materials in solution, an effect we attribute to an alteration in the thermodynamic interactions of the polymer with the surrounding solvent. In order to advance our understanding of this phenomenon, we have further studied the modulation of these illumination dependent structural changes on key conjugated polymers as a function of solvent quality over a wide range of polymer solubilities. Analysis of this data indicates that use of poorer conjugated polymer solvents ultimately results in larger absolute alterations to polymer conformation. This discovery opens the door to controlling final device morphology through careful manipulation of solvent composition during solution based device casting techniques, moving our efforts closer to the development of a powerful, non-destructive, and tunable method for light-driven control of polymer conformation in novel light-responsive organic materials.

Introduction

The last two chapters have indicated substantial changes in polymer chain structure upon light exposure in both solution (0.5-3 wt%) and sol-gel (~17wt%) environments with the common conjugated polymer standard poly(3-hexylthiophene-2,5-diyl) (P3HT). Specifically, for the samples solvated at lower concentrations in deuterated styrene, a dramatic drop in both Kuhn length (b) and radius of gyration (R_g) is observed upon sufficient light exposure. Further analysis indicates that illumination of the sample results in a lowering of the second virial coefficient. Thus, the data points towards a decrease in polymer chain size under illumination, along with a significant deterioration of the polymer-solvent interaction parameter.

Our interpretation has some analogy to a typical thermodynamic chain-to-globule collapse of a polymer chain, where the addition of an array of excited species to the P3HT backbone via light exposure provides sufficient thermodynamic "push" to cause P3HT chain contraction, a response facilitated by P3HT's already limited solubility in styrene. This comparison is grounded in the fundamental concept of chain collapse understood in polymer science and solution dynamics, under which atactic chain molecules will collapse to a denser structure if the net attraction between components becomes sufficiently large.

The study of such chain collapse processes is quite broad and encompasses a wide range of polymer types and collapse stimuli, such as solvent loading ratios and temperature ramps.[100,101,102] Of particular interest are

the class of ionic polyacrylamide polymers and co-polymers which exhibit controllable collapse behavior upon inclusion of charge on the polymer through ionic side group functionality.[103,104] By considering the individually temporary, but net persistent, effect of the electrostatic disturbances created by the presence of light-induced excited species such as excitons on the conjugated polymer backbone, a similar explanation for the observed structural changes emerges. Thus, this chapter seeks to further explore the underlying driving forces for these illumination induced conformational changes occurring within a wider range of solvent quality and concentration environments.

Instrumental

The conjugated optoelectronic polymer poly(3-hexylthiophene-2,5-diyl) was purchased from Osilla Chemicals, with a described regioregularity of 94% and a molecular weight of ~30,000. This material was used without further purification, where it was dissolved in one of three pre-filtered solvents: deuterated (d8) styrene purchased from Polymer Source, deuterated 1,2-ortho-dichlorobenzene (d-ODCB) purchased from Sigma-Aldrich, or deuterated bromobenzene via Sigma-Aldrich. To prevent localized gelation, the samples were kept at 60°C throughout the scattering experiments by a thermally controlled sample holder. Additionally, poly[2-methoxy-5-(2-ethylhexyloxy)-1,4-phenylenevinylene] (MEH-PPV) was purchased from Sigma Aldrich with a manufacturer reported number average molecular weight (M_n) between 150,000

and 250,000. Deuterated tetrahydrofuran (d8) and deuterated cyclohexane (d12) were purchased from Sigma Aldrich in sealed ampoules and used as received. In order to establish an experimental environment for the small angle neutron experiments free of ambient light, the quartz solution cells were wrapped in 0.1 mm thick aluminum foil for the duration of the "dark" data collection periods. For the sample runs involving fully illuminated conditions, the quartz cells were exposed to light provided by an optical illuminator housing a 125-watt halogen bulb, which provides 50,000 lux at 5cm exposure distance. Aluminum was specifically chosen to inhibit light from entering the sample given its near total transparency to neutrons. Nevertheless, data reduction procedures considered both the quartz cell and the aluminum wrapping during background subtraction, ensuring that the presence of the foil has no effect upon the final scattering curves.

Most small angle neutron scattering experiments (SANS) were conducted at the Oak Ridge National Laboratories (ORNL) at the High Flux Isotope Reactor (HFIR) using the General Purpose SANS (CG-2) beamline. Three separate detector distances of 0.3, 2, and 12.5 meters with a wavelength of 6 Å allowed a Q range of 0.0034 to 0.3363 $Å^{-1}$, where $Q = 4\pi/\lambda\sin(\theta/2)$, λ is the neutron wavelength, and θ is the scattering angle. Additional SANS experiments were conducted at the National Institute of Standards and Technology's Center for Neutron Research using the NGB30 beamline using detector distances of 0.3, 4, and 13 meters with a wavelength of 6 Å.[105] The raw data was reduced using

NCNR macros and corrected for empty cell (with and without aluminum) scattering, dark current, and detector sensitivity.[106] Absolute coherent scattering was obtained through the elimination of contributions from background incoherent scattering and thermal fluctuations.

Results

In order to study the effects of light on the structure of conjugated polymer samples in solution, we have conducted mirrored scattering experiments for each prepared solution: once under direct illumination and then again while completely isolated from ambient light via aluminum foil. We will refer to these samples as “light” and “dark” respectively throughout the text. Additionally, we have applied this methodology to a non-conductive polymer sample in order to confirm that the effects we observe are not conflated with environmental, experimental, or methodological contributions. Data plots for these controls are available in a previous publication.[95] As the raw data curves for these experiments overlap completely, this eliminates concerns that thermal effects or the presence of aluminum foil influence our results. Experimental P3HT samples were created in an array of solvents of varying P3HT solubility over a range of polymer concentrations from 0.5 - 2 wt%. These solvents have P3HT solubilities listed in Table 4.1, which in order of decreasing P3HT solubility are: deuterated bromobenzene, deuterated ortho-dichlorobenzene, and deuterated

Table 4.1: Reported Solubilities for P3HT in Select Solvents.

Solvent	**P3HT Solubility (mg/ml)**
Deuterated bromobenzene	84.1
Deuterated ortho-dichlorobenzene	30.0
Deuterated styrene	1.2

styrene.[107,108,109] SANS data for these three solvents are shown in Figures 4.1-4.3, where blue traces indicate “dark” data while red traces refer to “light” data.

Bromobenzene is the best solvent for P3HT of the three, and Figure 4.1 shows significant overlap for the light and dark data across all Q values, indicating minimal differences in structure at all length scales. Figure 4.2 presents the results for P3HT in the relatively moderate solvent d-ODCB and reveals discrepancy between the light and dark data at high Q values, pointing towards a change in the local structure of the chain upon light exposure. Finally, Figure 4.3 contains data for the least favorable of the P3HT solvents, deuterated styrene. Large differences in intensity are observed across the entire Q range, indicating light induced structural alterations across all length scales. Clearly the raw data trends indicate that decreasing solvent quality leads to increased magnitude of structural changes, while increasing solvent quality seems to mask or moderate these light induced effects. In order to quantify the exact nature of structural changes occurring, we employ several data analysis techniques. Our previously established approach to analyze the complete Q range of P3HT in solution involves applying Pedersen and Schurtenberger's Flexible Cylinder Model, which provides the form factor of a semi-flexible Gaussian chain with a non-negligible circular cross-section which accounts for excluded volume interactions within the random walk.[72,73]

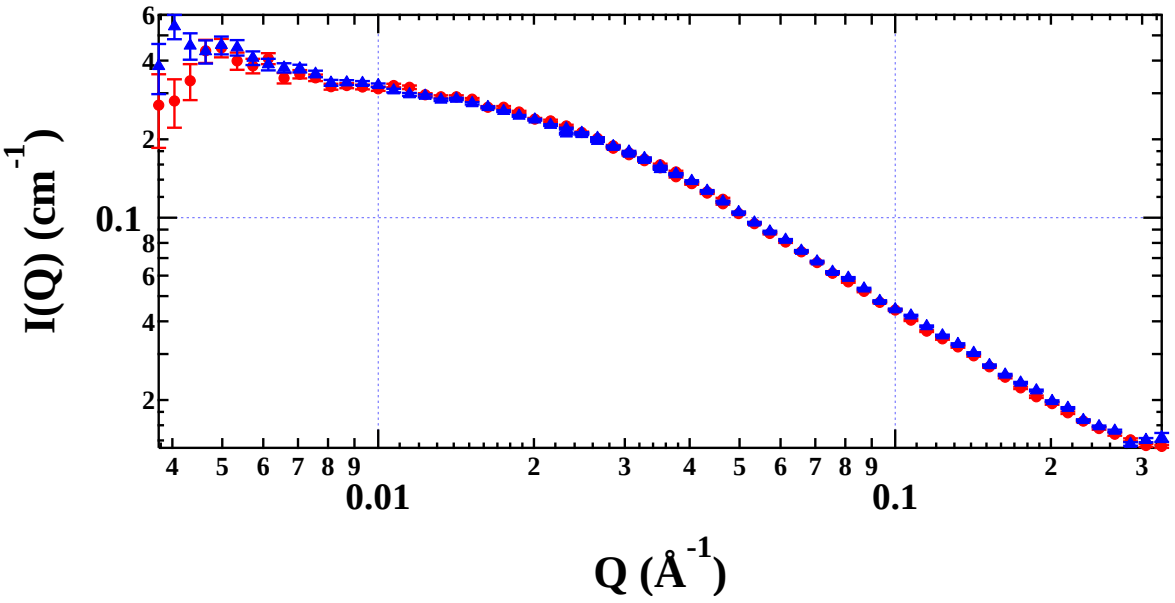


Figure 4.1: Small angle neutron scattering curves of 1wt% P3HT in d-bromobenzene at 60°C in both illuminated (red circles) and dark (blue circles) environments.

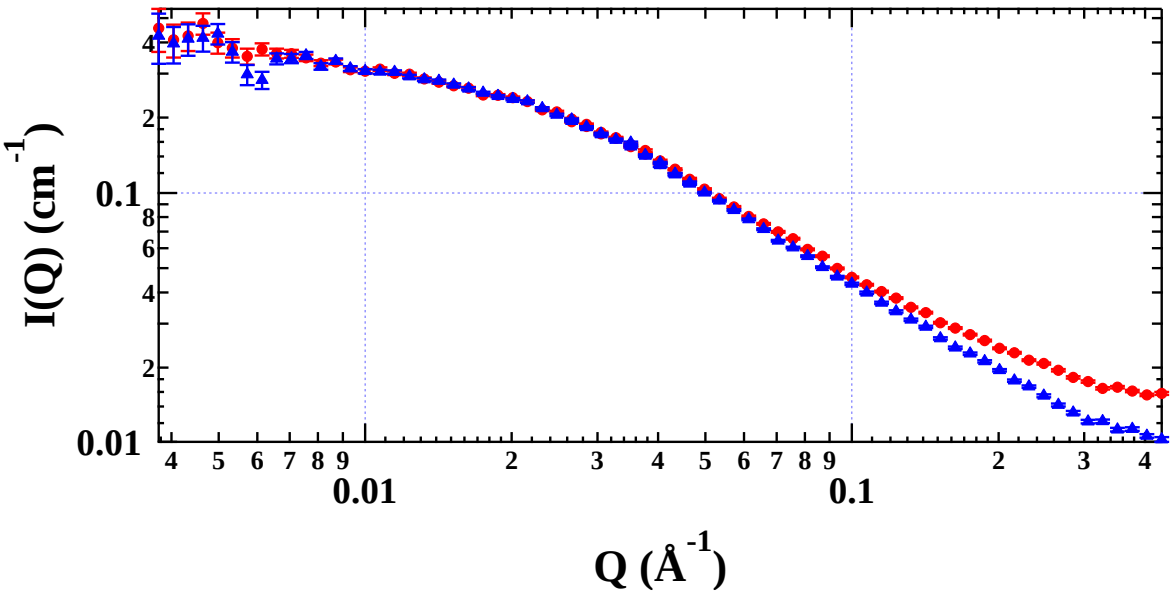


Figure 4.2: Small angle neutron scattering curves of 1wt% P3HT in d-ODCB at 60°C in both illuminated (red circles) and dark (blue circles) environments.

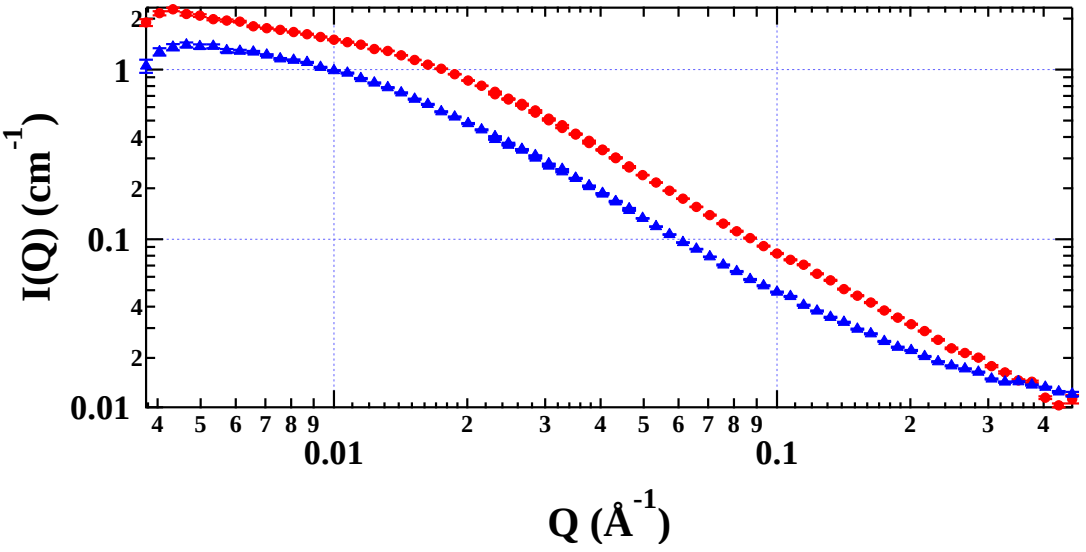


Figure 4.3: Small angle neutron scattering curves of 1wt% P3HT in d-Styrene at 60°C in both illuminated (red circles) and dark (blue circles) environments.

Assuming proper knowledge of each component's scattering length density (SLD), successful fitting to this model provides the contour and Kuhn lengths of the polymer chain, measurements of total chain size and chain rigidity, respectively.

Employing the flexible cylinder model allows us to compare the structural parameters of the P3HT in each solvent in light and dark conditions. Given the clear differences between the raw data of light and dark P3HT samples in d-styrene, the structural information obtained unsurprisingly shows substantial change between light and dark states, as summarized in Table 4.2.

However, for the more moderate solvent d-ODCB, analyzing the local changes with the flexible cylinder model fails to adequately capture the local changes clearly occurring at small length scales. In order to effectively quantify these changes, analysis at high Q was emphasized by fitting the data to the polymer excluded volume model, a fundamental expression of a semi-flexible polymer coil with considerations for excluded volume effects.[110] Fitting the d-ODCB data with the excluded volume model provides the radii of gyration (R_g), shown in Table 4.3 for a range of P3HT concentrations in both light and dark environments. As expected from the raw data plots, the magnitude of light-dark structural changes are reduced from that of the d-styrene samples, however the general trend remains. Analysis of the d-bromobenzene samples unsurprisingly reveal an even smaller magnitude of structural changes initiated by light exposure, as shown in Table 4.4.

Table 4.2: Parameters obtained from the Flexible Cylinder fit for P3HT in deuterated styrene at 60 °C.

Sample	**"Dark" R_g (Å)**	**"Light" R_g (Å)**
1 wt%	117 ± 3	77 ± 3
0.5 wt%	140 ± 4	67 ± 4

Table 4.3 R_g values from polymer excluded volume model fits to P3HT in d-ODCB.

Sample	**"Dark" R_g (Å)**	**"Light" R_g (Å)**
1 wt% P3HT	37 ±5	37 ±5
0.5 wt% P3HT	56 ±5	50 ±5
0.1 wt% P3HT	57 ±5	42 ±5

Table 4.4: R_g values from polymer excluded volume model fits to P3HT in d-bromobenzene.

Sample	**"Dark" R_g (Å)**	**"Light" R_g (Å)**
1 wt% P3HT	42 ± 4	41 ± 3
0.5 wt% P3HT	39 ± 4	37 ± 3
0.1 wt% P3HT	42 ± 4	42 ± 3

Taking data from these three solvents, it appears that the increased favorability of the polymer-solvent interaction suppresses any photon-induced conformational effects of the polymer chains.

In order to broaden our understanding of the light driven changes in conjugated polymer systems as well as the role which solvent quality plays in the moderation of these effects, we have conducted a series of similarly inspired experiments incorporating another conjugated polymer benchmark, poly[2-methoxy-5-(2-ethylhexyloxy)-1,4-phenylenevinylene], commonly referred to as MEH-PPV. This polymer has been studied in solution in both the favorable solvents deuterated styrene and deuterated THF, as well as the definitively unfavorable solvent deuterated cyclohexane. The scattering data of MEH-PPV in these solvents collected in both light and dark environments are displayed for select polymer concentrations in Figures 4.4-4.6. A cursory investigation of this scattering data reveals a similar trend to that of the P3HT data, where the most favorable solvent environment, deuterated styrene in this case, displays little difference in light and dark data traces as seen in Figure 4.4. The d-THF sample, a less favorable solvent than d-styrene but still a widespread standard for MEH-PPV solutions, shows overlap of the scattering data across most of the observed Q range, with the exception of the lowest Q data points where consistent deviation is seen for all concentrations.

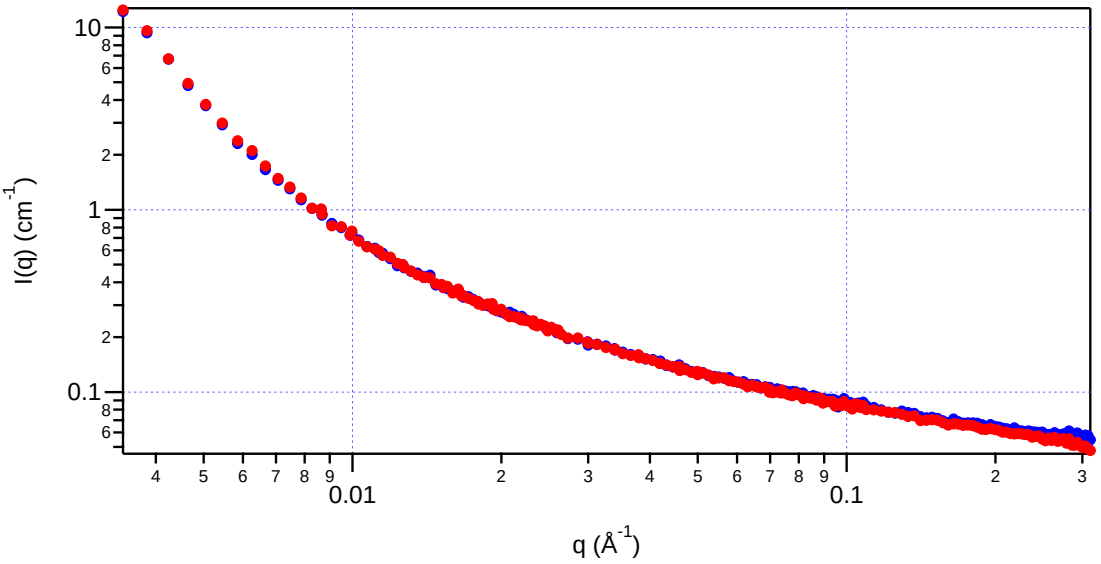


Figure 4.4: Small angle neutron scattering curves of 1wt% MEH-PPV in d-Styrene at room temperature in both illuminated (red circles) and dark (blue circles) environments.

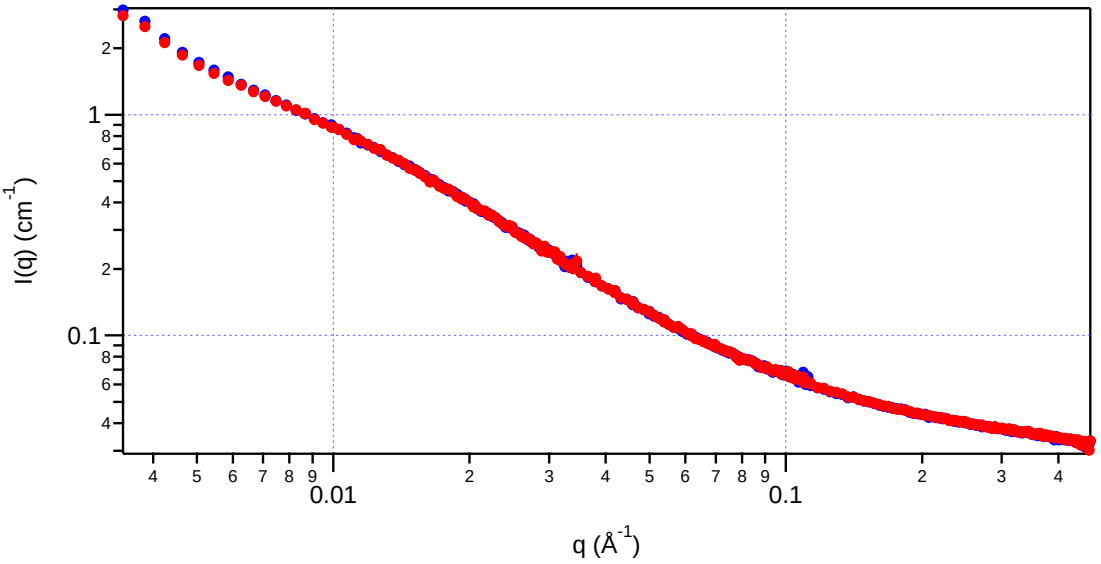


Figure 4.5: Small angle neutron scattering curves of 1wt% MEH-PPV in d-THF at room temperature in both illuminated (red circles) and dark (blue circles) environments.

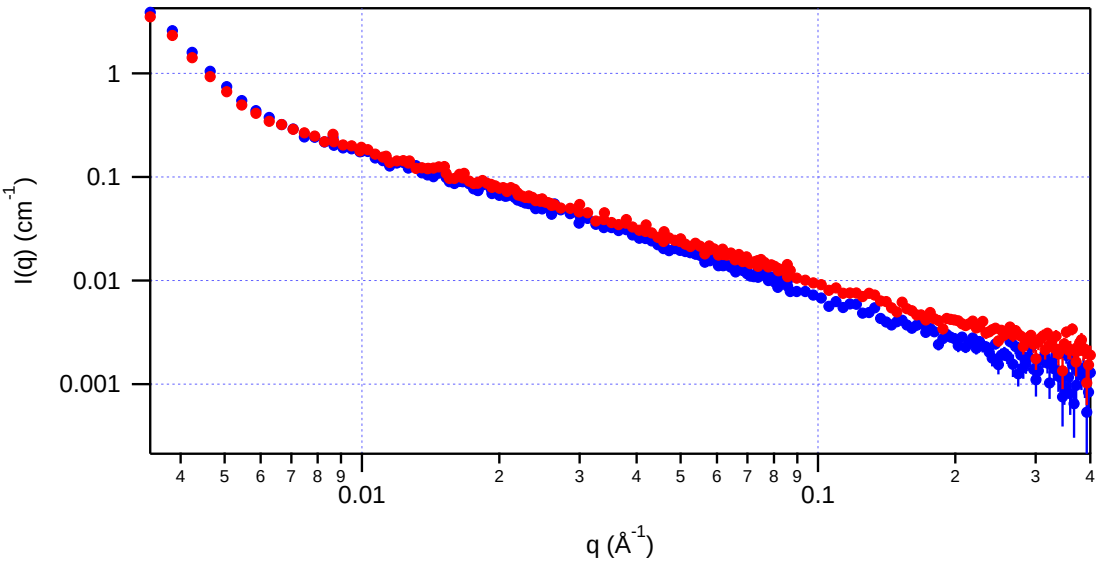


Figure 4.6: Small angle neutron scattering curves of 1wt% MEH-PPV in d-cyclohexane at room temperature in both illuminated (red circles) and dark (blue circles) environments.

The 1wt% sample data is presented as an example in Figure 4.5. However, it is again the poorest solvent that elicits the largest differences between the light and dark scattering patterns. In the case of MEH-PPV, this is the d-cyclohexane sample shown in Figure 4.6. The direction of the shift in high Q scattering is of particular interest, as it directly mimics the direction of the intensity shift with illumination observed in the P3HT d-ODCB samples.

Given that high molecular weight PPV polymers in solution have been shown to form very large fractal aggregates,[111,112] fitting the resultant raw data is best accomplished through the use of a modified version of the previously used flexible cylinder model, specifically the fractal flexible cylinder model with polydispersity of length, which takes into account this large length scale aggregate formation of the semi-flexible conjugated polymer chains as well as effects related to polydispersity.[76,113] Table 4.5 lists the Kuhn length values extracted via global fitting of the 1wt% samples of MEH-PPV in d-THF and d-cyclohexane with the fractal flexible cylinder model. As suggested by a qualitative examination of the raw data, the model fits indicate that the MEH-PPV samples exhibit the same general behavior as the previously studied P3HT samples; specifically in the poorest solvent environments the polymer chain experiences the largest overall structural transformations initiated by white light exposure while the more friendly solvents effectively mask any light induced structural effects.

Table 4.5: Kuhn length values extracted via global fitting with the fractal flexible cylinder model for the 1wt% samples of MEH-PPV.

Solvent	**“Dark” Kuhn Length (Å)**	**“Light” Kuhn Length (Å)**
d-THF	44 ± 1	44 ± 1
d-cylohexane	51 ± 2	37 ± 2

In addition, this data confirms the generic nature of the light induced conformational effects, which clearly pertain to the broad field of conjugated materials rather than only to a single case polymer example.

Discussion

Through careful experimental design and pertinent SANS fitting analysis, the role of light in the alteration of conjugated polymer structure has been carefully monitored as a function of solvent quality resulting in a wide range of polymer-solvent quality conditions. Such experimental design allows further investigation pertaining to our initial hypothesis based around thermodynamically driven chain collapse induced by alterations to the polymer-solvent interaction parameter due to the presence of excited species on the conjugated polymer backbone. Our earlier work that focused on the conjugated polymer P3HT is furthered by experiments in a series of increasingly favorable solvent environments: deuterated styrene, deuterated ortho-dichlorobenzene, and deuterated bromobenzene, with documented P3HT solubility values listed in Table 4.1. The sharp contrast in solvent favorability apparent here becomes crucial in interpreting the neutron scattering results for each solvent environment upon light illumination. The d-styrene samples unsurprisingly display the same behavior as previous experiments, namely a sharp decrease in R_g between dark and fully illuminated environments. Illumination of P3HT in d-ODCB, a very common benchmark solvent for P3HT due to its solvating properties for both the

conjugated polymer and common device co-components, produces a significantly moderated structural change in the solution compared to the poorer d-styrene samples. The excellent P3HT solvent, d-bromobenzene, further continues this trend in our data, with no substantial changes to polymer structure observed upon illumination of these samples.

Approaching this data set through the lens of solution thermodynamics again provides a clarification of the phenomenon. As mentioned before, a Zimm analysis of the scattering data has repeatedly shown a decrease in the second virial coefficient, a measure of polymer-solvent interaction favorability, upon light exposure. In order to establish the second virial coefficient of P3HT in each solvent relevant to this experiment, we have plotted the SANS data curves in a single Zimm plot for polymer concentrations 0.25, 0.5, and 1wt% in each of the three solvents. The second Virial coefficients of these solutions under ambient conditions from these analyses are listed in Table 4.6.

These values, which qualitatively agree with the documented P3HT solubility values, quantitatively describe the decreasing favorability of the solvent environment for P3HT present in each sample employed in this experiment. Looking over the data as a function of initial polymer solvent favorability, it becomes clear that the poorest P3HT solvent environments result in the largest absolute observed changes in structure, while conversely the most favorable solvent environments mitigate or eliminate any changes to polymer conformation.

Table 4.6: Second Virial Coefficients Obtained via Zimm analysis of P3HT in d-styrene, d-ODCB, and d-bromobenzene.

Solvent	**P3HT Solubility (mg/ml)**	**Second Virial Coefficient**
d-styrene	1.2	-0.05
d-ODCB	30.0	0.45
d-bromobenzene	84.1	0.52

.

Thus it appears that the thermodynamic “push” afforded by the exposure of the sample to white light is limited in absolute scope over a given time frame and illumination intensity and its ultimate structural effects vary as a function of solvent quality. Samples such as P3HT in d-bromobenzene or MEH-PPV in d-THF, which begin in an especially good solvent environment, enjoy a strong polymer-solvent relationship which cannot be overcome by the thermodynamic change afforded by light exposure and subsequent exciton creation. However, samples such as P3HT in d-styrene or MEH-PPV in d-cyclohexane can be powerfully affected across broad length scales due to the respective polymer's already tenuous relationship with the solvent. So by choosing a solvent of appropriately high quality, the polymer can essentially be ‘shielded’ from the influence of the light exposure on polymer conformation, while alternatively choosing a poorer solvent results in the largest magnitude variation in polymer structure. This powerful relationship between solvent quality and the magnitude of light-induced conformational changes provides additional confirmation of the thermodynamic nature of the light exposure phenomenon which we have previously proposed[95] and offers an exciting new tool in manipulating conjugated polymer conformation in solution.

Towards this end, the definitive importance of solvent quality upon observed light induced polymer conformational changes opens up the door to a myriad of possible device fabrication manipulations. Selecting solvents based on their thermodynamic suitability for the given conjugated polymer will allow for

control over the size of structural changes observed and therefore ultimately the domain sizes present within the bulk material of the final active layer. Previous work by our group has demonstrated that light induced changes occurring during the solution fabrication process can be expressed within the final gels formed.[114] Thus, carefully adjusting solvent quality before commencement of common solution-based fabrication methods such as spin-coating or inkjet printing methods can result in generation of a powerful, tunable, and non-intrusive control of final device morphology. A wide range of continued functional possibilities exist for active, inexpensive, and non-destructive alteration of polymer morphology with simple modifications to the nature of the illumination environment under which most organic electronic devices are commonly fabricated.

Conclusion

The effect of solvent quality on the impact of illumination on the conformation of conjugated polymers in solution has been studied through a series of small angle neutron scattering experiments in a variety of solvents with a range of solvent quality for P3HT and MEH-PPV. Proper analysis of the collected data provides confirmation of earlier observed results, which point towards white light absorbance by conjugated polymers effectively deteriorating the polymer-solvent interaction parameter, leading to strong alterations in chain

conformation. Specifically, this work focuses on the effects of varying solvent quality for several conjugated polymers under illumination, and finds that the absolute magnitude of structural changes which occur appear highly reliant on the suitability of the chosen solvent for the conjugated polymer, with poorer solvents resulting in larger shifts in polymer conformation upon light exposure. This effect appears to be generic and applicable to several key members of the class of optoelectronic conjugated polymers. Given that conjugated polymer solution behavior and conformation are therefore in part a function of solvent quality, this data offers an array of possibilities for controlling and moderating the conformational changes induced in a conjugated polymer sample, and subsequently directing the formation of active layer morphologies. With this ability, selective device fabrication methods through non-destructive and unobtrusive light illumination methodologies could eventually become an inexpensive and easily applicable industrial tool.

Acknowledgements

The authors gratefully acknowledge the National Science Foundation (DMR-1409034) for support of this project. The SANS experiments of this research were completed at ORNL's High Flux Isotope Reactor, which was sponsored by the Scientific User Facilities Division, Office of Basic Energy Sciences, US Department of Energy. We also acknowledge the support of the National Institute of Standards and Technology, U.S. Department of Commerce,

in providing additional SANS facilities used in this work, where these facilities are supported in part by the National Science Foundation under Agreement No. DMR-0944772.

CHAPTER FIVE

THE ROLE OF INCIDENT LIGHT INTENSITY, WAVELENGTH, AND EXPOSURE TIME IN THE MODIFICATION OF CONJUGATED POLYMER STRUCTURE IN SOLUTION

Abstract

Our recent investigations indicate that simple white light exposure holds intriguing potential to alter the structure of conjugated polymer chains. To provide further insight into how to rationally control this process, we have employed small angle neutron scattering to investigate structural changes occurring in solutions of poly(3-hexylthiophene-2,5-diyl) upon exposure to white light. Our previous results indicate significant change in the structure of the polymer upon illumination, an effect we attribute to an alteration in the thermodynamic interactions of the polymer with the surrounding solvent. This chapter provides additional information to further refine our understanding of this phenomenon by studying the relationship between the magnitude of exciton creation and subsequent structural changes through a series of exposure time, light intensity, and wavelength sensitive experiments. The results demonstrate a clear and consistent relationship between the number of absorbable photons available to the conjugated polymer chain and more powerful alterations in polymer structural parameters, indicating that net exciton generation provides the fundamental driving force for this phenomenon. This points towards the feasibility of employing light exposure protocols as a powerful unobtrusive in-situ method for precise tailoring of optoelectronic active layers over a wide range of organic electronic device fabrication procedures.

Introduction

This chapter seeks to study the methods by which the light-based effects on polymer structure demonstrated in previous chapters can be more finely controlled and tuned by way of exposure time and wavelength sensitivity, essentially studying the relationship between total net P3HT absorbable photons, the levels of structural alteration initiated by their absorbance and the subsequent generation of excitons on the polymer backbone. Together our previous work has shown that structural shifts of the conjugated polymer with illumination are not instantaneous, but rather require a given period of exposure time before full transition is achieved. By varying the amount, type, and total time of light exposure applied to a range of conjugated polymer samples, a more complete understanding of these light driven conformational effects can be attained. Moreover, this information is required to enable its future use in manipulating active layer morphologies, with the goal of developing a non-intrusive in-situ methodology for controlling device structure and ultimately boosting device performance.

Instrumental

Poly(3-hexylthiophene-2,5-diyl) was purchased from Osilla Chemicals with a regioregularity of 94% and a molecular weight of ~30,000, per the manufacturer. This material was used as received, and was dissolved in either

deuterated (d8) styrene purchased from Polymer Source, or 1,2-ortho-dichlorobenzene (d4) (ODCB) purchased from Sigma-Aldrich. The samples were kept at 60°C throughout the scattering experiments by a thermally controlled sample holder in order to prevent localized aggregation or gelation.

Samples for use in the small angle neutron scattering experiments were assembled within 2mm quartz solution cells. These sample cells were then either wrapped in 0.1 mm thick aluminum foil to create the dark environment or exposed to illumination provided by an optical illuminator consisting of a 125-watt halogen bulb, generating 50,000 lux at a 5 cm distance at maximum intensity. Aluminum was chosen as a barrier for light exposure due to its near total transparency to neutrons. Regardless, special care was taken during the analysis to be certain that the presence of the aluminum was accounted for in the reduction of the raw data to absolute units. These methods involved, amongst others, separate determination of sample transmittance and empty cell scattering for the light and dark samples.

The small angle neutron scattering experiments (SANS) were conducted on instruments located at both Oak Ridge National Laboratories (ORNL) and the National Institute of Standards and Technology (NIST). ORNL experiments took place at the High Flux Isotope Reactor (HFIR) using the General Purpose SANS (CG-2) beamline. Employing three separate detector distances of 0.3, 2, and 12.5 meters with a wavelength of 6 Å allowed a Q range of 0.0034 to 0.3363 $Å^{-1}$, where $Q = 4\pi/\lambda\sin(\theta/2)$, λ is the neutron wavelength, and θ is the scattering

angle. NIST scattering data was collected at the Center for Neutron Research (NCNR) using the NGB 30 beamline using detector distances of 0.3, 4, and 13 meters with a wavelength of 6 Å.[105] The raw data was reduced using NCNR macros and corrected for empty cell (with and without aluminum) scattering, dark current, and detector sensitivity.[106] Elimination of contributions from background incoherent scattering and thermal fluctuations allowed acquisition of absolute coherent scattering.

Results

In order to study the effects of light on the structure of conjugated polymer samples in solution, we have developed a procedure to conduct mirrored scattering experiments for each prepared solution: once under direct illumination and then again while completely isolated from ambient light via aluminum foil. We will refer to samples analyzed under these conditions as "light" and "dark" respectively throughout the text. In order to establish a control baseline we have applied this methodology to a non-conductive polymer sample in order to confirm that the effects we observe are not conflated with environmental, experimental, or methodological contributions, with the pertinent SANS data plots available in our previous publications.[95] As the data curves overlap completely, this eliminates concerns that thermal effects or the presence of aluminum foil influence our results.

Impact of Light Exposure Time on Structural Changes

Our past experiments have described in detail the structural changes which occur in a conjugated polymer before and after it has been exposed to a light source, however the rate of these changes and the permanence of their nature have yet to be fully investigated. Towards this end the following experiments are designed to expand our understanding of this phenomenon by examining the structure of the P3HT polymer chain over a wider range of light exposure time sequences and intensities. Firstly, SANS experiments were designed to study the permanence and reversibility of the illumination-induced structural effects by monitoring the change in structure of the P3HT chain after an illuminated sample is returned to a completely dark environment. Figure 5.1 displays an example of this experiment in the favorable P3HT solvent d-ODCB at 1 wt% polymer loading, where data is collected first after the sample had been kept in the dark for over 8 hours, then while exposed to illumination for 1 hour at 9,000 lux, and then measured again after resting in the dark for 4 hours. The scattering data show that there is a significant shift in scattering intensity at high Q as the sample cycles between dark (blue trace), light (red trace), and dark again (green trace); a transition indicative of a change in local polymer chain structure brought on by the exposure to illumination. These experiments have been conducted in both the dark to light and light to dark sequences, with no noticeable discrepancy between the two methodologies.

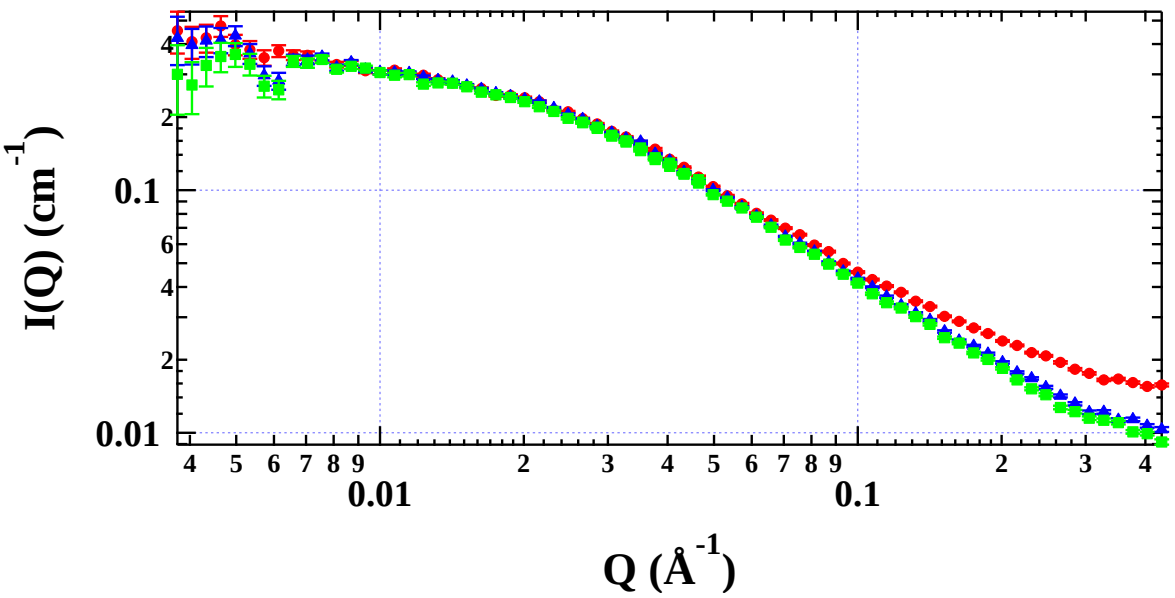


Figure 5.1: Small angle neutron scattering curves of 1 wt% P3HT in d-ODCB at 60°C in dark (blue circles), illuminated (red circles) and an additional dark (green circles) environments.

The overlap between the scattering patterns of the two dark samples indicates that these light-induced changes to structure of the P3HT chain quickly subsides upon removal of the light source and returns to an environment free of photons This effect persists through all studied concentrations of P3HT in this solvent.

Fitting the raw data with the polymer excluded volume model allows quantitative analysis of the structural changes occurring at the local length scales where the most obvious structural changes occur. This analysis provides the radius of gyration (R_g) of the conjugated polymer chain throughout the illumination sequence, where Table 5.1 presents the results for these fits. This analysis confirms the decrease in polymer size that occurs with illumination, as well as the chain's reflex back to its original size once illumination is removed.

To determine the time dependent nature of the change in chain structure with illumination, the exact timescale over which the transitions occur must be more closely observed. In order to quantify the exact time period required for these illumination driven effects to drive polymer structure to an equilibrium state, we have conducted a series of SANS experiments for several select samples. Beginning with a standard "dark" scattering experiment, illumination at 9,000 lux is applied and consecutive scattering curves are obtained over sequential time intervals, resulting in a representation of time evolution of the structural changes that occur with illumination.

Table 5.1: Results for polymer excluded volume model fits to 1 wt% P3HT in d-ODCB.

Sample	**R_g(Å)**
1 wt% P3HT in d-ODCB "Dark"	59 ±1
1 wt% P3HT in d-ODCB "Light"	58 ±1
1 wt% P3HT in d-ODCB "Dark 2"	59 ±1

An example of the data obtained from this experiment is presented in Figure 5.2, which provides the raw data set for a 1 wt% solution of P3HT in d-ODCB. This data focuses on the high Q region where the local structural changes of P3HT are consistently observed in this solvent. As in the earlier experiments, a characteristic increase in scattering at high Q data is observed with increasing illumination time. Moreover, the timescale of these changes and its equilibration is consistent with the results presented in Figure 5.1. Analysis of this data using the excluded volume model yields the change in the R_g of the polymer chain with illumination time as shown in Figure 5.3. These results show a gradual decrease in the R_g of P3HT, evolving to a polymer chain size that is consistent with our previous studies of the change in the structure of P3HT in d-ODCB with illumination. These results show that the size of the polymer chain stabilizes after about half an hour of total light exposure. This data indicates that the light-driven P3HT structural changes are not instantaneous and instead require prolonged exposure time in order to allow for proper absorption and creation of the required number of excitons to realize maximum structural effects. To understand the impact of solvent quality on the time evolution of these structural changes, Figure 5.4 shows the SANS curves for the change in the structure of a 1 wt% solution of P3HT in d-styrene, a much less favorable solvent for P3HT. This sample is illuminated under a moderate intensity of roughly 9,000 lux over the course of several hours.

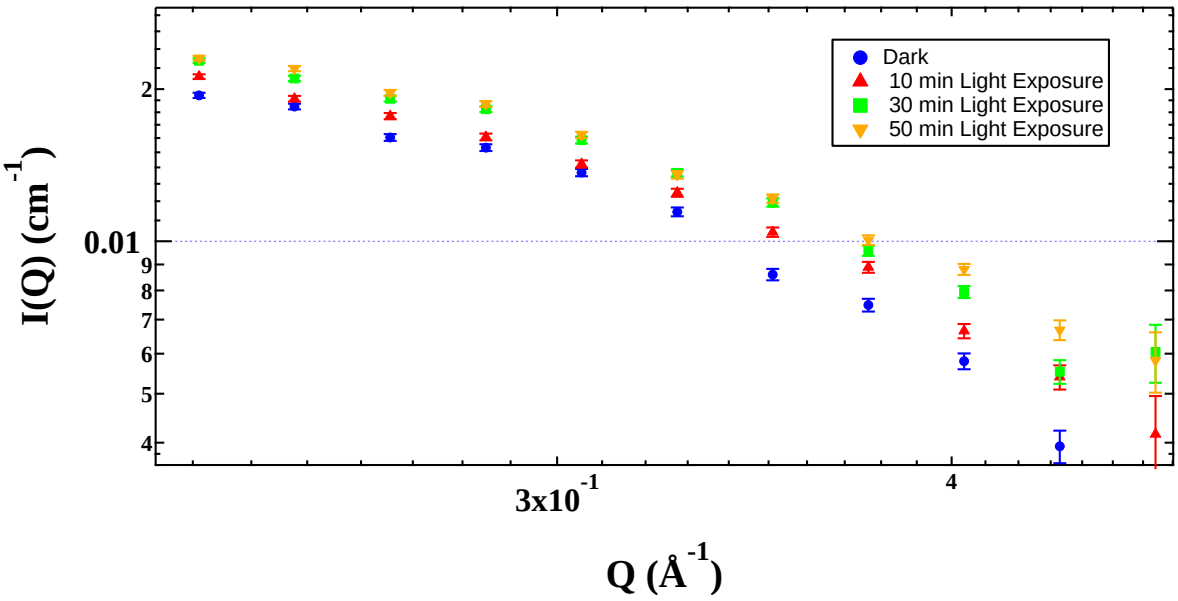


Figure 5.2: Time evolution of the scattering curve at high Q of a 1 wt% solution of P3HT in d-ODCB at 60°C for 0 min (blue traces), 10 min (red traces), 30 min (green traces), and 50 min (yellow traces) white light illumination times.

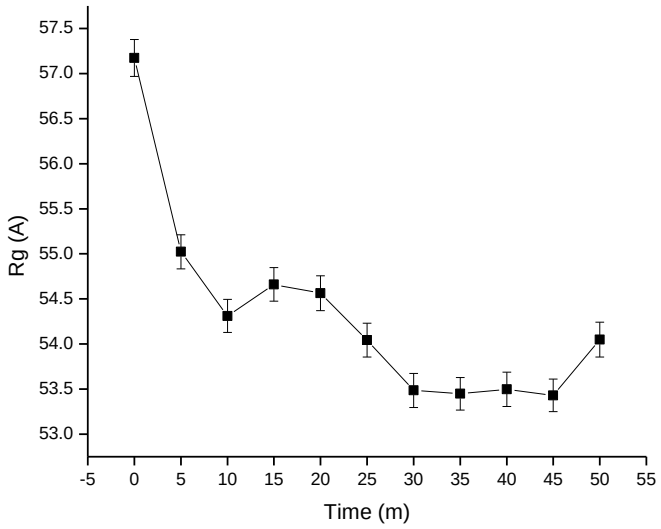


Figure 5.3: Analysis of 1 wt% P3HT in d-ODCB using the flexible cylinder model over the course of 60 minutes light exposure time with multiple scattering runs of 5 minute duration each.

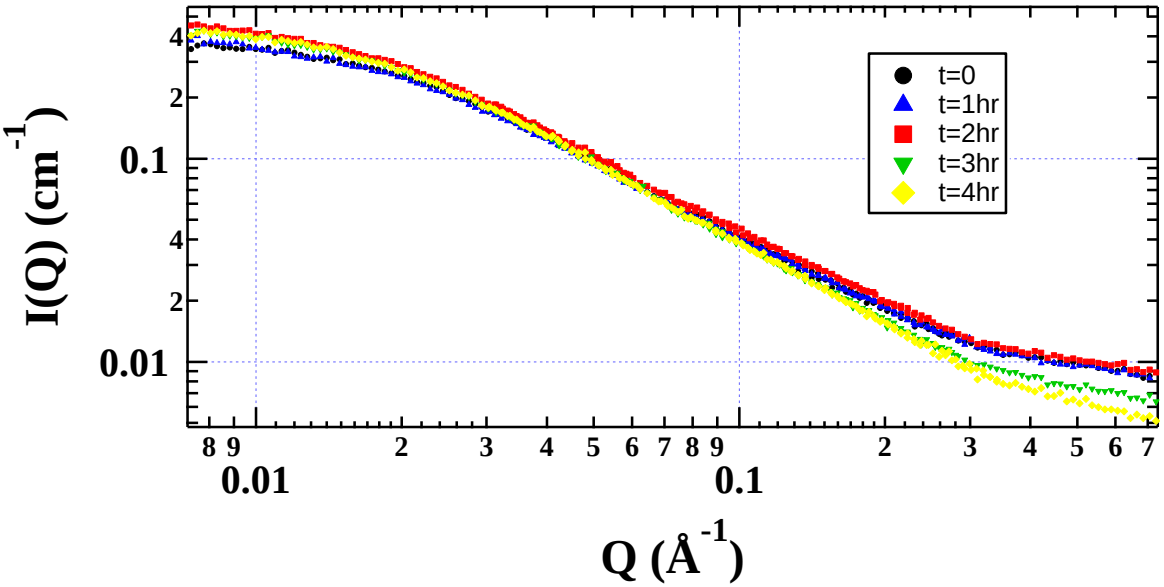


Figure 5.4: Time sensitivity of 1 wt% P3HT in d-styrene at 60°C after 0 hrs (black traces), 1hr (blue traces), 2hr (red traces), 3hr (green traces), and 4hr (yellow traces) of total white light exposure.

From the raw data. it is readily apparent that the timescale for P3HT structural transformations in this solvent occur on a much longer timescale than the structural changes of P3HT in d-ODCB. After illumination is applied, a gradual increase in intensity is observed for the low Q data, while the high Q data instead decreases moderately. This may be indicative of complex structural shifts occurring at different length scales, or may actually be a result of structural differences emerging during the finite timescale of the experiment. Regardless, this data indicates that the structure of the P3HT chain continues to evolve in this less favorable solvent over a substantially longer time period than the previously observed d-ODCB solvent system. Clearly, the timescales of the structural changes are a function of the solvent quality and vary substantially from one environment to another. This may indicate that different polymer-solvent systems require different levels of generated exciton density to create the required thermodynamic environment to observe structural changes to the polymer chain.

Additionally, our understanding of the time dependence of the illumination induced structural changes can be further refined by running a similar experiment over a narrower Q range and altering the illumination intensity to the maximum available with our illuminator, 50,000 lux. Figure 5.5 contains the time resolved scattering data for a 1 wt% P3HT in d-styrene sample measured in 10 separate runs over the course of 300 minutes of total light exposure time.

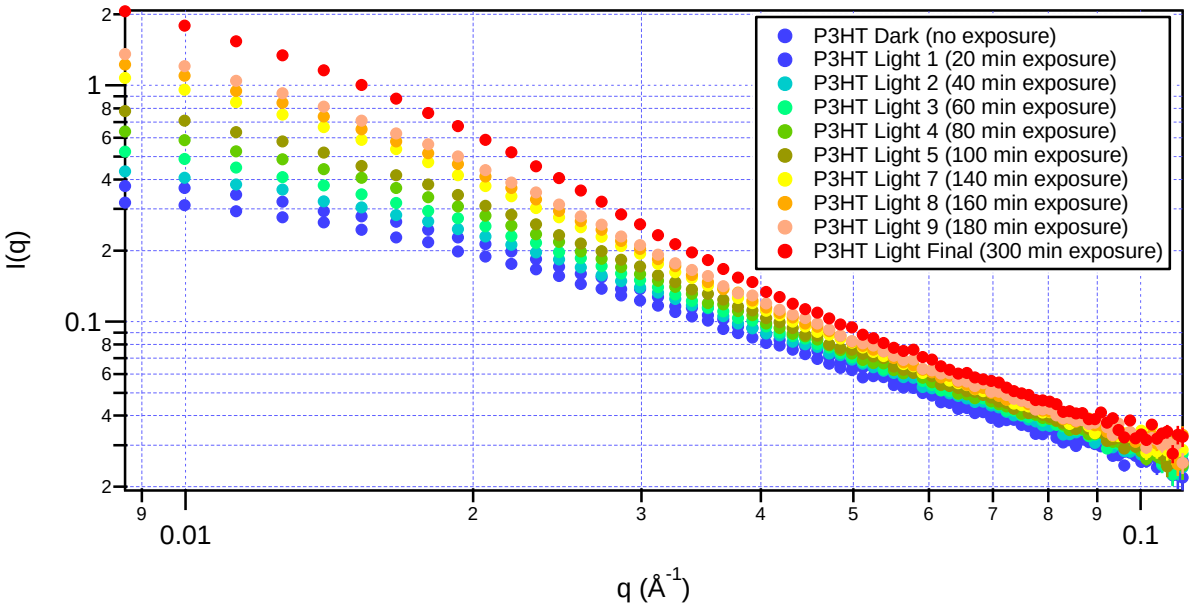


Figure 5.5: SANS data curves for 1 wt% P3HT in d-styrene in the dark and under total light exposure times ranging from 20 to 300 minutes at 60°C.

For this moderate-Q region of the scattering range the effect of increasing illumination intensity is quite pronounced, as the raw data plots for the samples evolve much more quickly and substantially with illumination than the sample that was illuminated at the lower intensity of 9,000 lux. Figure 5.6 presents the Kuhn length of the P3HTas a function of illumination time as determined from fitting the data in Figure 5.5 to a flexible cylinder model, quantifying the changes in polymer structure with illumination time. Clearly, the decrease in structural size, though ultimately more pronounced, takes a substantially longer illumination time to reach equilibrium compared to the P3HT in d-ODCB samples. Whereas the size changes in d-ODCB equilibrate in 60 minutes, the d-styrene sample has yet to begin its most substantial decrease in Kuhn length by this time, instead requiring roughly two hours to reach a steady state. However, though they clearly require a more extended light exposure window in order to materialize, the overall magnitude of the changes observed is substantially larger, equating to a 70% decrease in Kuhn length as opposed to the roughly 10% drop in R_g for d-ODCB. Additionally, this d-styrene data equilibrates after about two hours under high intensity illumination, in sharp contrast to the d-styrene sample which received much lower intensity illumination that had not yet ceased its evolution after four hours of continuous illumination. Both of these examples illustrate the key role which solvent quality and illumination intensity play in determining the magnitude and timescale of structural changes of conjugated polymer chains elicited by light exposure.

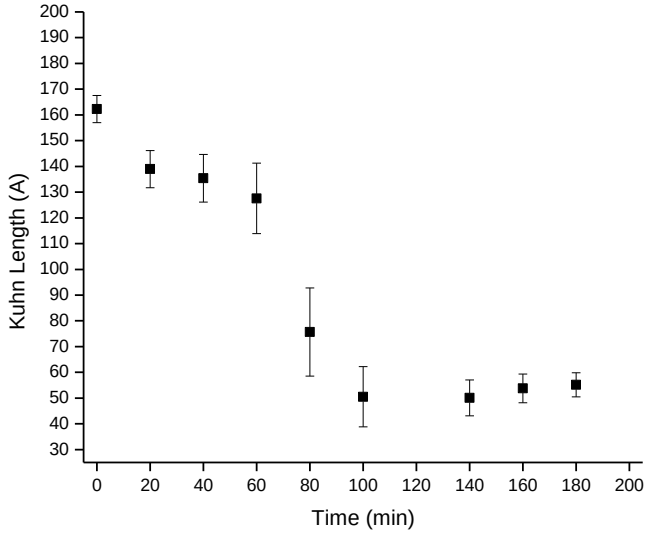


Figure 5.6: Values for Kuhn length as a function of illumination time (50,000 lux) extracted via the flexible cylinder model for 1 wt% P3HT in d-styrene at 60 °C.

Impact of Light Wavelength on Structural Changes

Investigating the structural changes in P3HT upon exposure to wavelength controlled incident light, rather than full spectrum white light exposure employed above, provides additional insight into the mechanisms behind the light-driven effects. In a typical solution state, P3HT absorbs across a wide spectrum from roughly 300-600 nm, with a maximum absorbance around ~450 nm.[3,82] Given this information, and taking into account the close relationship between photon absorption and the subsequent exciton generation, utilizing filters to limit the wavelength of the light that illuminates the P3HT sample provides a mechanism to more precisely link observed structural effects in the light-absorbing polymers directly to generated exciton density.

To accomplish this goal experimentally, the change in the structure of the P3HT polymer chain is studied when it is illuminated by wavelengths that are within the strongly absorbing range and comparing that an identical sample that is illuminated by light with wavelengths outside the primary absorbing region. If the observed structural effects are indeed predicated on photon absorption and exciton generation, then the sample exposed to illumination from the highly absorbing portion of the P3HT absorption spectrum should exhibit a significantly stronger and/or quicker change in chain structure than changes observed in the sample that is exposed to wavelengths that P3HT does not absorb as strongly. A series of optical bandgap filters provide a means of controlling the wavelengths of light incident to the sample provided all background light is properly blocked as

well. By passing the generated white light of the optical illuminator through selected filters onto the conjugated polymer sample, experiments that document the impact of the wavelength of light on the observed structural changes can be completed. Figure 5.7 shows the raw data from an experiment conducted in this fashion with 1 wt% P3HT in d-styrene, where the sample was exposed to light with wavelengths within the strongest absorbing region for P3HT using a 415-590 nm bandgap filter, a sample that exposed to light with wavelengths 610-1200 nm, where P3HT absorbs poorly. The scattering curves of the P3HT solution in the dark and under white light illumination are also plotted in this Figure.

The curves representing the entirely dark sample (black traces) and the fully illuminated sample (red traces) appear very similar to those found in previously conducted experiments, while the scattering curves representing the sample exposed to the light that is strongly absorbed by P3HT (415-590 nm; pink traces) and the sample exposed to light in the poorly absorbing region of the P3HT absorption spectrum (610-1200 nm; blue traces) fall in between. Interestingly, the sample exposed to the more strongly absorbing portion of the spectrum exhibits a scattering curve that is higher intensity than the scattering of the sample that is exposed to the wavelengths that P3HT does not absorb as strongly, indicating that the larger amount of absorbable photons elicits a more substantial shift in structure.

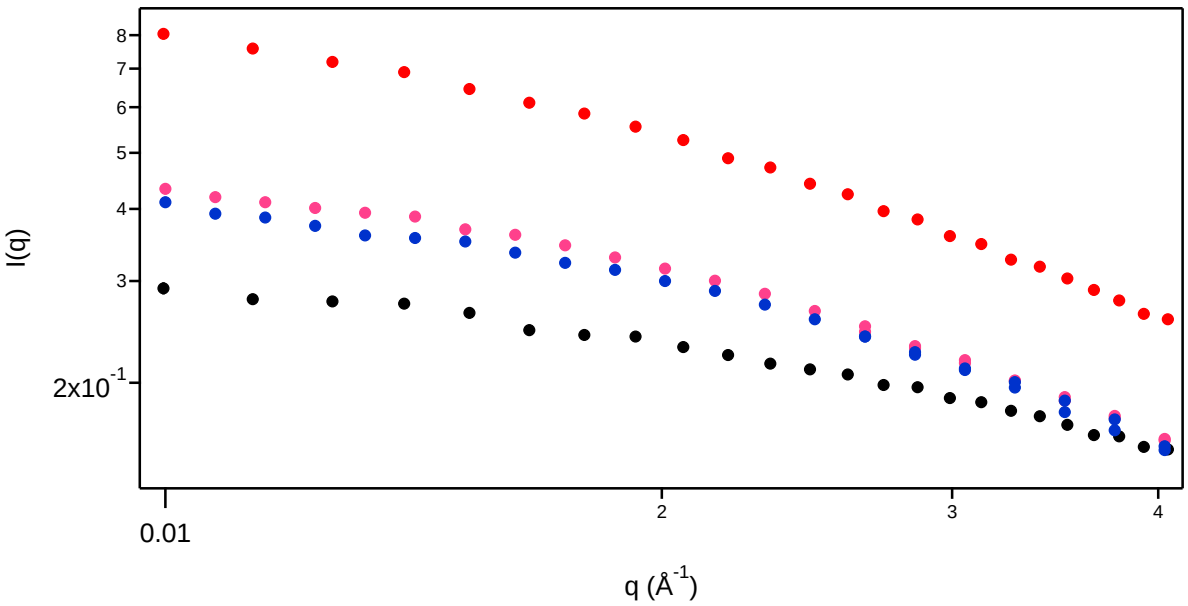


Figure 5.7: SANS scattering curve of 1 wt% P3HT in d-styrene at 60°C. Red data points indicate sample illuminated with white light, pink data points indicate sample illuminated with 415-590nm light, blue data points indicate sample illuminated with 610-1200nm light, and black data points indicate sample under no illumination.

Analysis and curve fitting of these data curves with the flexible cylinder model quantitatively confirms this relationship, where Figure 5.8 plots the radius of gyration of the P3HT chain under the various illumination conditions.
The samples exposed to the un-attenuated illumination source predictably give the largest changes in polymer chain R_g, while the sample that is illuminated by the 415-590 nm wavelength light experiences a less substantial though still pronounced shift in R_g. Finally, the sample that is exposed to light with 610-1200 nm wavelengths retains an R_g that is closer to that of the polymer in the dark, decreasing only slightly. These results indicate that by limiting the number of absorbable photons available to the photoactive polymer chains, the extent of the structural changes induced by light exposure can be modulated.

The sensitivity of the structural changes to exposure of light with different wavelengths has also been performed for the more favorable solvent systems as well. Similar to the time sensitive experiments, the scattering curves of P3HT in d-ODCB have been obtained for samples exposed to unfiltered white light, to 610-1200 nm light outside the prime P3HT absorbance band, to 415-590 nm light inside the strong P3HT absorbance region, and in complete darkness. These scattering curves have been analyzed with the excluded volume model at high Q to quantify local changes in chain structure. Figure 5.9 displays the R_g data for this analysis for the P3HT in ODCB sample for the various illumination conditions.

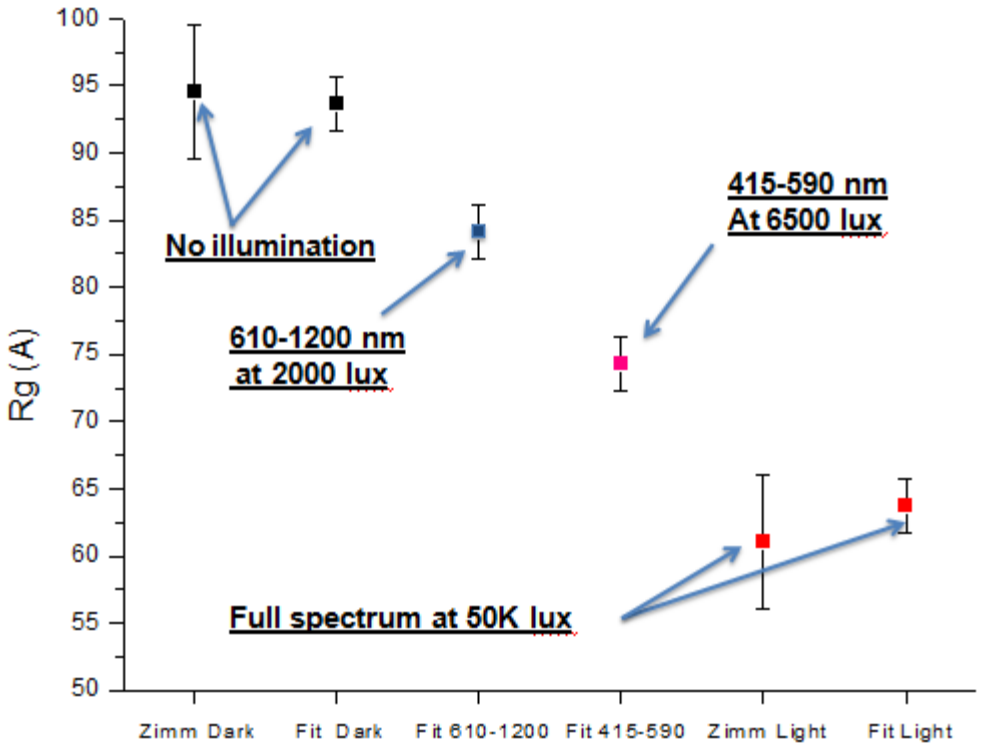


Figure 5.8: R_g values obtained from the flexible cylinder fit for 1 wt% P3HT at 60°C in d-Styrene under (left to right) no illumination, 610-1200 nm light, 415-590 nm light, and white light illumination.

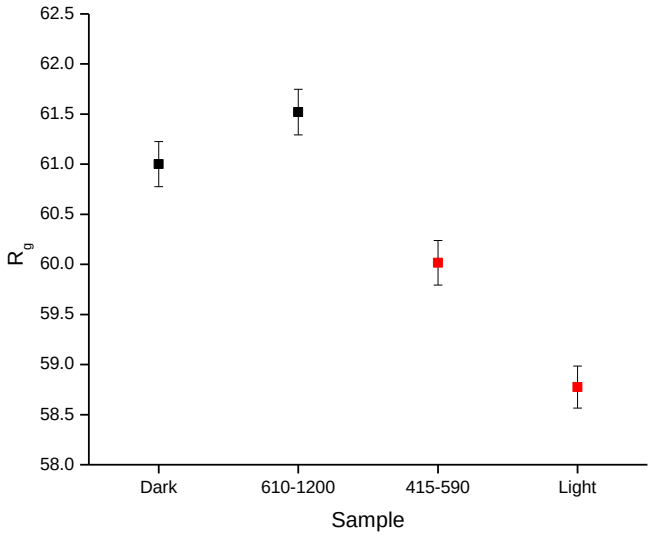


Figure 5.9: R_g values obtained for polymer excluded volume model fit for 1 wt% P3HT at 60°C in d-ODCB under (left to right) no illumination, 610-1200 nm light, 415-590 nm light, and white light illumination.

As with the samples in d-styrene, increasing photon absorption by P3HT causes a decrease in polymer R_g. Clearly, the data from several solvent environments indicates that controlling the intensity and wavelength of incident light allows for the manipulation of the size of the polymer in solution, where maximizing the absolute intensity of P3HT absorbable light provides a straightforward method to significantly control the structural transformation.

Discussion

The results of these neutron scattering experiments provide further insight into the alteration of the structure of conjugated polymers in solution by illumination. In these studies, the impact of illumination intensity, exposure time, and wavelength of light on the alteration of conjugated polymer structure in solution is monitored. This work builds off of our initial investigations that tied the significant changes observed in conjugated polymer structure upon light exposure to a thermodynamically driven chain collapse induced by alteration of the polymer-solvent interaction parameter due to the presence of excited species on the conjugated polymer backbone.[95] The data shown here provides additional insight into the relationship between total absorbable photons available to the photoresponsive polymer and the magnitude of the subsequent alterations to polymer chain structure.

Our previous work indicates that the number of excitons on a given polymer chain number in the single digits under full white light illumination.[95]

Given that these P3HT chains have a molecular weight of ~30,000 g/mol, a couple excitons may seem intuitively insufficient to elicit the large scale conformational shifts which we consistently observe. However, the time sensitive studies reported here further our understanding of the nature of the relationship between light exposure, exciton density, and subsequent conformation effects. Inspection of the results of time evolution of structure in P3HT in d-styrene and d-ODCB reveals that a certain amount of exposure time for a given illumination intensity is necessary to elicit the full extent of structural change, showing illumination times of close to an hour for P3HT in d-ODCB, and from 2-5 hours for P3HT in d-styrene. This suggests that the structural change is a cumulative, but reversible, effect. Analyses of Figures 5.3 and 5.6 underline this point, where both samples exhibit a very gradual decrease in P3HT chain size which begins immediately upon illumination but which continues steadily until a final structure is attained. This is consistent with an underlying process which hinges not just on the number of excitons per chain, but is also sensitive to the total net number of excited species generated over a given time interval. Essentially each exciton generated contributes its own small "push" towards changing the solvent quality of the system, requiring a significant amount of total exposure time before the requisite amount of total species are generated to accomplish observable structural change. Further evidence of this relationship can be observed by comparing the two scattering curves of the d-styrene samples in Figures 5.4 and 5.5 studied under considerable differences in illumination intensity (50,000 lux vs.

9,000 lux), as the dependence on total generated excitons again becomes clear. By sharply increasing the amount of incident light and therefore similarly increasing the number of generated excitons, a notable acceleration in the rate of structure change is observed, further demonstrating the strong link between the total amount of exciton generation and the magnitude of change in polymer conformational changes.

The reproducibility experiments further demonstrate the time sensitive yet entirely non-destructive nature of this phenomenon. In the absence of any attempt to thermodynamically freeze the polymer-solvent system, removal of the illumination source will inevitably result in a withdrawal of the previously observed conformational shifts, evidenced by the complete reflex of observed scattering patterns seen in Figure 5.1. Once the light exposure ceases and exciton populations return to zero, the thermodynamic pressure is removed and the system is allowed to return to its previous equilibrium state. Additionally, this experiment identifies the non-destructive nature of the light/dark effects. Repeated applications of the light sources over the appropriate timeframe consistently result in identical effects, all of which return to the original ground state upon loss of illumination, indicating no permanent damage or irreversible disruption of the polymer system, a response which is consistent with the non-destructive nature of exciton generation.

Investigating the incident light wavelength dependence of these polymer chain conformational transformations further emphasizes the importance of

exciton formation. By separating the spectrum into distinct continuums inside and outside the prime P3HT absorbing region, it becomes clear that only absorbable light significantly influences the P3HT chains. Figures 5.7 and 5.8 emphasize that the samples that are measured in the dark and those that are illuminated with 610-1200 nm light are very similar, as are the samples that are measured in full illumination and those exposed to 410-590 nm light. Given that P3HT exhibits strong absorption across the 410-590 nm range, and very poor absorption above 600 nm, these results strongly suggest that the consistently observed changes in polymer structure are directly related to the total number of absorbed photons and subsequently generated excitons, and not the result of thermal effects or photo-degradation arising from persistent light exposure.[3,83] In the case of the samples exposed to 610-1200 nm light, by selectively limiting the wavelength range of light available to the P3HT chains, the generation of excitons can be effectively suppressed and consequently the fluctuations in polymer chain size are greatly diminished. This remains consistent with the behaviors observed in the accompanying experiments, where any alterations to experimental procedures that decrease the amount of excitons generated directly and predictably result in clear moderation of the observed light-induced structural changes.

This consistent and sensitive response of the change in conjugated polymer structure in solution by illumination by careful tuning of the illumination methodology presents expansive possibilities for application to device fabrication

procedures. Given the proven relationship between polymer conformation in solution and final solid-state device architecture, applying light-driven techniques directly from the onset of common fabrication methods will result in a powerful, tunable, and non-intrusive control of final device morphology. Knowledge of the precise levels of illumination necessary to achieve a targeted structure could allow measured dosages of light via a combination of light exposure time, illumination intensity, wavelength controls, and careful solvent choice to enable control of conjugated polymer conformation throughout the fabrication of a given optoelectronic device. Opportunities exist for expanded control over device patterning via illumination of select areas of a surface with a customizable range of light intensities, wavelengths, and exposure times. By carefully limiting the wavelength of incident light exposure, specific functional conjugated polymers could be targeted for precise structural alteration within a dispersion containing co-component materials, which would remain entirely unaffected. Clearly the availability of in-situ light exposure as a non-destructive control over conjugated polymer conformation and the resultant optoelectronic active layer morphology emphatically expands the versatility of conjugated polymeric materials and offers exciting new possibilities for further application.

Conclusion

Small angle neutron scattering has been utilized to study the effects of varying incident light intensity, exposure time, and wavelength on the changes to

conjugated polymer conformation in solution. These results further refine initial findings which demonstrate a consistent and powerful light-induced alteration of polymer structure of solvated conjugated polymers marked by a large and consistent decrease in polymer structural size upon exposure to white light, an effect believed to be driven by light induced deterioration of polymer-solvent interactions. By designing specific experiments to probe precise individual qualities of the relevant light exposure, the relationship between exciton density and the magnitude of subsequent conformational changes becomes clear. These studies reveal that the conformational effects occur gradually over a time period ranging on the order of hours, with their precise time sensitivity varying strongly as a function of initial solvent quality and total absorbable incident light intensity. The data suggests that increasing the number of excited species within the given conjugated polymer sample through prolonged light exposure times, increased light intensities, and targeted use of the ideal polymer absorption band consistently results in quicker realization and greater absolute magnitude of polymer structural changes. Thus by carefully managing the requisite light exposure methodology, conjugated polymer conformation in solution can be manipulated in-situ in a completely non-destructive manner, forming the basis for fabrication techniques permitting precisely controlled formation of device active layers. Further work exploring and refining these exciting new approaches to in-situ active layer manipulation opens the door to an array of possibilities centered around novel device fabrication and patterning methodologies.

Acknowledgements

The authors gratefully acknowledge the National Science Foundation (DMR-1409034) for support of this project. The SANS experiments of this research were completed at ORNL's High Flux Isotope Reactor, which was sponsored by the Scientific User Facilities Division, Office of Basic Energy Sciences, US Department of Energy. We also acknowledge the support of the National Institute of Standards and Technology, U.S. Department of Commerce, in providing additional SANS facilities used in this work, where these facilities are supported in part by the National Science Foundation under Agreement No. DMR-0944772.

CHAPTER SIX

THE EFFECT OF ILLUMINATION ON THE DEPTH PROFILE OF THERMALLY ANNEALED MEH-PPV:DPS BLENDS

Abstract

Due to its simplicity and cost-effectiveness, single solution casting of organic optoelectronics has grown in popularity for device fabrication methodologies geared towards producing technologies such as organic photovoltaics and thin film transistors. In order to more fully explore the structural evolution which occurs therein in a blend composed of polystyrene and the benchmark conjugated polymer MEH-PPV, we have performed a series of neutron reflectivity experiments focused on studying the film structure as it changes through the thermal annealing process both in the presence and absence of white light. Results indicate the formation of a semi-dispersed blend upon casting, which becomes stratified most effectively upon thermal annealing preformed under white light exposure. This data suggests in-situ illumination as a potential novel tool for manipulating the device-relevant morphologies of optoelectronic active layers throughout the fabrication process, offering a cheap non-destructive tool for effectively tuning desired structural parameters.

Introduction

One of the more recent novel applications for conjugated polymers has involved their incorporation into lightweight electronics such as thin film transistors and light emitting diodes via the emerging fabrication process known as self stratification or auto-layering. This methodology is based on the

thermodynamic process by which a film separates spontaneously into two continuous adherent functional layers during deposition, a concept introduced by Funke in 1976.[115] Self stratified coatings offer the dual advantages of affordability and significantly increased adhesion between the final layers, leading to better coating durability due to the lower risk of interlayer delamination, while allowing cost effective single solution casting initiated by simple drying or straightforward thermal annealing protocols.[116,117] Within the field of functional materials this method has been adopted to allow casting of both the active and dielectric layers of organic thin film transistors simultaneously from a single solution, resulting in a streamlined device fabrication system while substantially decreasing the undesirable inter-layer diffusion which plagues traditionally step-fabricated devices.[118,119,20,120] Through careful choice of active layer conjugated polymer, insulating dielectric polymer, and mutual solvent, the degree of phase separation and subsequent formation of layer architectures can be roughly controlled, leading to significant improvements in ultimate device efficiency. Variation of procedural tenants such as annealing type, time, and magnitude also have a powerful effect on the assembled depth profile, and therefore provide a convenient means for further tuning of a given polymer combination. Similarly, organic light emitting diodes (OLEDs), which harness the photonic effects of exciton recombination within a conjugated polymer active layer to produce high efficiency, low cost, and wavelength controllable light, can also be further refined through additional study of fabrication conditions and their subsequently

generated morphologies.[62,121,78] Thus, further exploration of both polymeric material choice and layer assembly conditions offers an enticing opportunity to continue rational device efficiency improvements to conjugated polymer based thin film transistors, increasing their relevance on an industrial scale.

However, despite the clear connection between thin film depth profiles and morphologies to device performance, many studies overlook this key aspect when assembling active layer materials. This disregard for the self-layering mechanisms assumes that initial casting of the optoelectronic materials immediately results in a completely homogenous blend with a uniform depth profile. Most organic electronic devices which can be fabricated from single solution conjugated polymer blends require preferred depth profiles, precisely ordered active layer domains and a specifically tailored domain interface, meaning that improper understanding of the relevant film depth profile can have far reaching effects. Regardless, even for well studied systems there often exists a serious lack of characterization information for the relevant blends in the z-dimension, leading to a fundamental misunderstanding of the relationship between basic film ordering and functionality. Through precise elucidation of vertical phase identity via appropriately generated scattering length density profiles, neutron reflectivity studies of these films provide a powerful tool to investigate this vital level of active layer structure and offer a window to better understand the performance-relevant structures developed over the course of the deposition and annealing procedures commonly used with these materials.

Towards this end, this chapter looks to investigate the layering morphologies for the benchmark conjugated polymer poly[2-methoxy-5-(2-ethylhexyloxy)-1,4-phenylenevinylene] (MEH-PPV), a material which has been successfully incorporated into a range of organic electronic devices such as thin film transistors and OLEDs. Previous work has identified that combining MEH-PPV with the ubiquitous non-conductive polymer polystyrene can result in an effective blend suitable for several device applications.[34,36,35] Specifically for the case of OLEDs, it has been found that the presence of polystyrene within the material substantially boosts electroluminescence efficiencies by suppressing detrimental MEH-PPV inter-chain interactions.[122,6] However the precise morphology and depth profile of the cast film and its individual component phases, as well as the exact structural effects of annealing procedures are rather poorly understood. As both the optoelectronic performance of the MEH-PPV active layer and the matrix isolation functionality of the inert polystyrene are clearly predicated on the phase dispersion of the materials throughout the blend, a more precise understanding of the structure and alignment of the formed layers both before and after the requisite annealing protocols becomes key to boosting device performance.

In addition to better understanding the morphologies of currently employed films and the processing techniques which modify them, increasing methods available for in-situ optoelectronic polymer structural manipulation is also desirable. In particular, exploratory studies that investigate the unobtrusive and

non-destructive properties of white light exposure on conjugated polymer structure and morphology have shown promise. This chapter also looks to build upon these experiments by introducing illumination methodologies to the MEHPPV/polystyrene film fabrication process while monitoring the relevant effects on layer composition and depth profile, hopefully moving towards the development of a novel non-destructive in-situ system for precisely manipulating polymer morphology during single solution film deposition processes.

Instrumental

Poly[2-methoxy-5-(2-ethylhexyloxy)-1,4-phenylenevinylene] (MEH-PPV) was purchased from Sigma Aldrich with a manufacturer reported number average molecular weight (M_n) between 150,000 and 250,000. Deuterated polystyrene (d8) with a number average molecular weight of 3600 and PDI of 1.7 was purchased from Polymer Source. The co-solvents tetrahydrofuran (THF), toluene, and cyclohexanone were purchased from Sigma Aldrich and pre-filtered with 0.45µ sieves. For the surface treatments poly(glycidyl methacrylate) (PGMA) with M_n 10,000-20,000 was purchased from Sigma Aldrich along with 2-butanone which was pre-filtered with 0.45µ sieves.

In order to create desirable surface conditions, UV-cleaned silicon wafers were either stripped with hydrofluoric acid treatments or coated with an ultrathin PGMA layer spin-cast at 1000 RPM for 30 seconds from a 0.02 wt% solution in 2-butanone, followed by a brief thermal annealing period at 100°C for 30

minutes. The MEH-PPV/dPS layers were subsequently spin-cast at1000 RPM for 30 seconds from a 0.1 wt% solution of 10:90 weight ratio MEH-PPV:dPS in a solvent cocktail made up of equal parts THF, toluene, and cyclohexanone. After casting, the films were allowed to dry and then stored under vacuum until the first set of reflectivity experiments could be performed. Thermal annealing procedures for the films involved heating to 125°C under vacuum for 15 minutes. "Dark" samples were blocked off from the 250 watt halogen light source while the "light" samples were directly exposed to the illumination throughout the annealing process.

Neutron reflectivity experiments were conducted on the NG7 Horizontal Neutron Reflectometer at the NIST Center for Neutron Research. Instrumental alignment and neutron wavelength of 4.8 Å allowed an effective Q range of 0.08-0.2 $Å^{-1}$, where $Q = 4\pi/\lambda\sin\theta$ (with λ being the neutron wavelength and θ the scattering angle). The programs from the reflpak suite were used for elements of the data reduction and analysis,[123] and relevant reflectivity curve fitting to allow acquisition of scattering length density profile curves was performed using the Motofit Igor macro.[124]

Results

In order to monitor the depth profile of an MEH-PPV/dPS blend cast from a single solution both before and after thermal annealing, as well as to determine the effect of white light exposure on the structures formed, a series of neutron

reflectivity experiments were completed. Deuterated polystyrene was employed due to the favorable contrast in neutron scattering length density which exists between MEH-PPV and dPS, the values for which are 9.95×10^{-7} $Å^{-2}$ and 6.42×10^{-6} $Å^{-2}$, respectively. Samples consisted of the MEH-PPV/dPS blend cast onto either an HF stripped bare silicon surface or a PGMA coated surface, in order to reduce dewetting effects and promote good adhesion to the wafer. Reflectivity measurements were taken on the as-cast samples initially, and again after the thermal annealing procedure. Two identical sets of samples were prepared, with one set kept completely in the dark throughout the annealing process (to be referred to as "dark" samples), while the other set was exposed to a halogen light source while annealing was occurring (to be referred to as "light" samples). Figures 6.1 and 6.2 display the raw reflectivity data for the as-cast samples on bare silicon and PGMA, respectively. The as-cast traces of the bare silicon data are identical for both light and dark, while the PGMA samples show only a small difference, due mostly to a small disparity in overall film thickness. This indicates that the samples offer a comparable baseline and are free of significant divergences in morphology and depth profile which would complicate the post-anneal comparison process.

Following the thermal annealing process in either the presence or absence of white light illumination, the samples are returned to the reflectometer and the reflectivity experiments are repeated. Figures 6.3 and 6.4 contain the post-annealing data for the thin films on the bare silicon and PGMA, respectively.

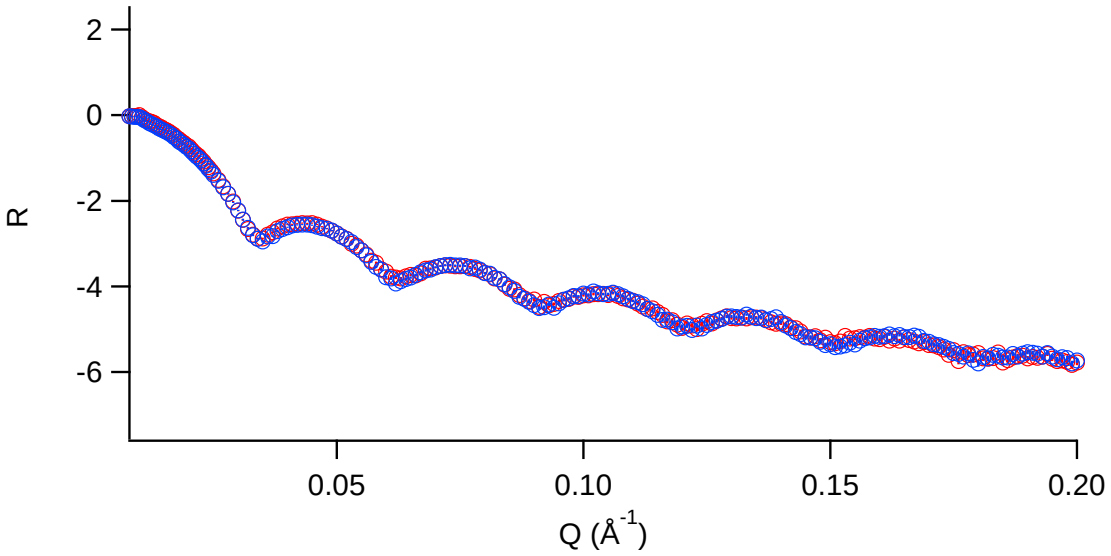


Figure 6.1: Reduced neutron reflectivity data for as-cast 10:90 MEH-PPV:dPS films cast on a bare silicon surface. Blue traces represent "dark" sample, red traces represent "light" sample.

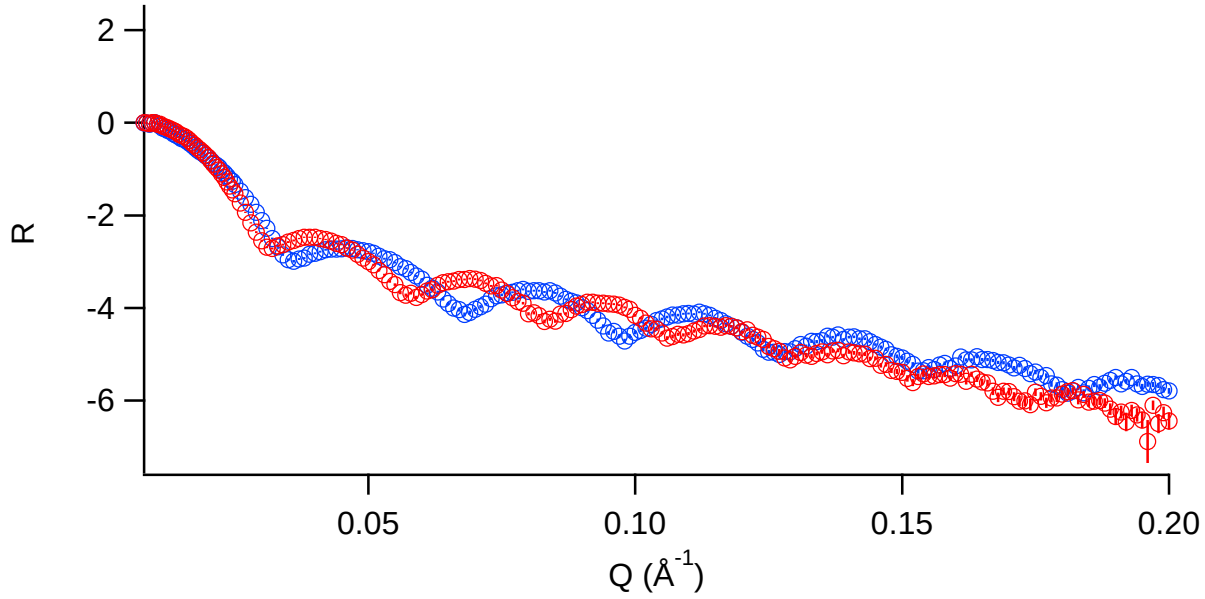


Figure 6.2: Reduced neutron reflectivity data for as-cast10:90 MEH-PPV:dPS films cast on a PGMA modified surface. Blue traces represent "dark" sample, red traces represent "light" sample.

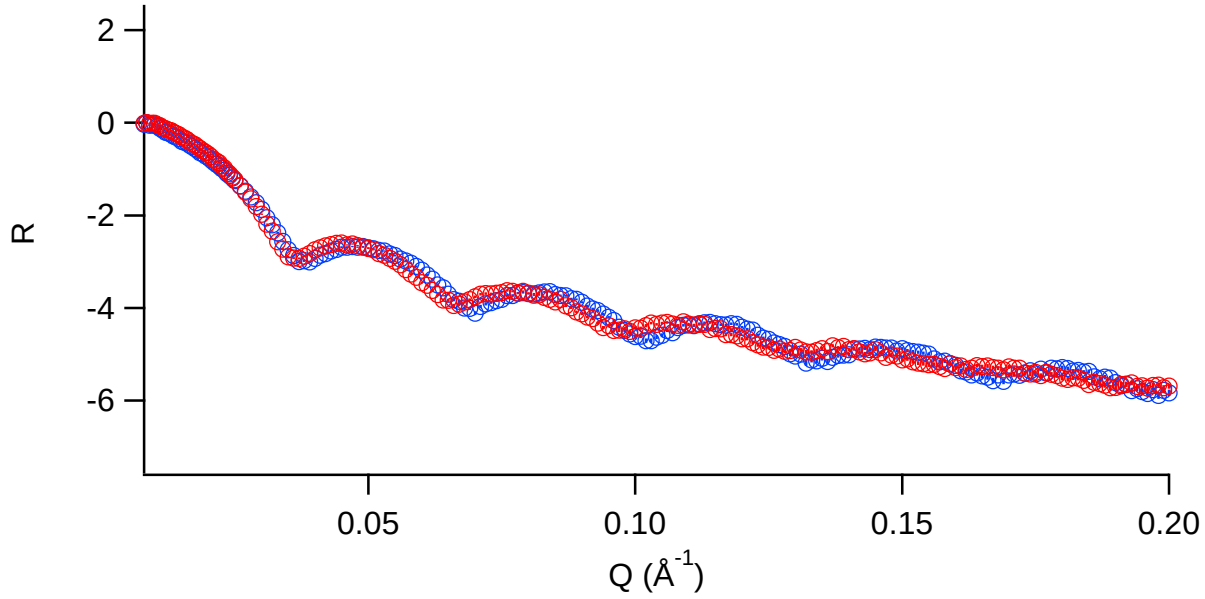


Figure 6.3: Reduced neutron reflectivity data for 10:90 MEH-PPV:dPS films cast on a bare silicon surface and thermally annealed for 15 minutes at 125°C. Blue traces represent the sample annealed in the dark and red traces represent the sample annealed under illumination.

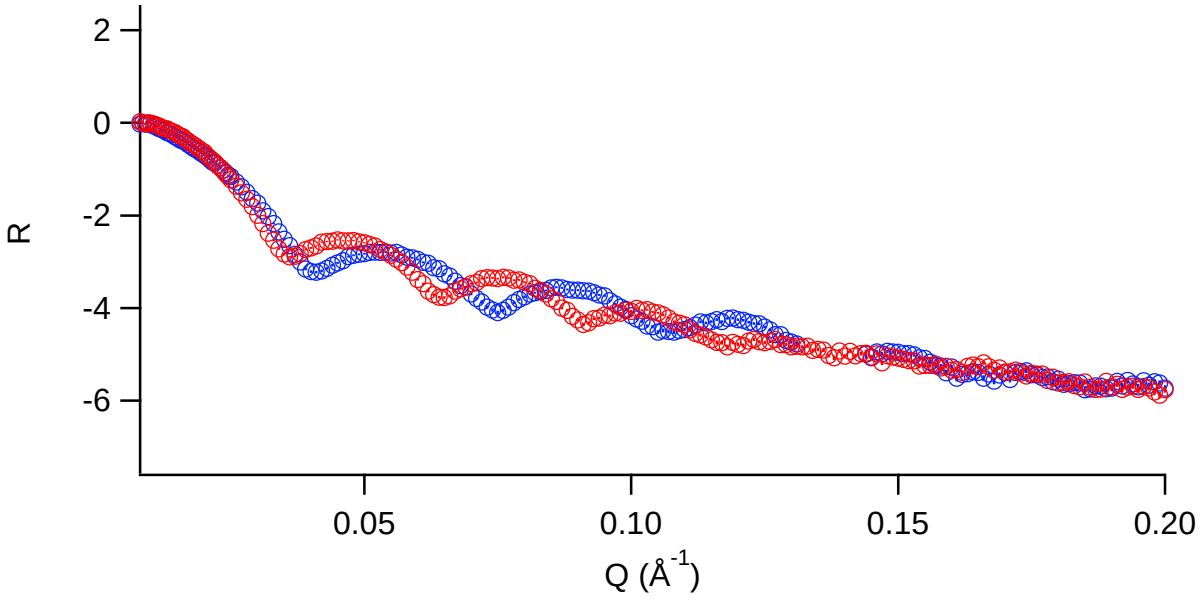


Figure 6.4: Reduced neutron reflectivity data for 10:90 MEH-PPV:dPS films cast on a PGMA modified surface and thermally annealed for 15 minutes at 125°C. Blue traces represent the sample annealed in the dark and red traces represent the sample annealed under illumination.

This post-anneal data predictably indicates a change in film structure brought on by the thermal annealing process for all samples.

To further explore and quantify these shifts, the relevant reflectivity data are fit with the Motofit analysis program to generate scattering length density profiles which describe the depth profile of the individual layers present in the films. Figure 6.5 displays an example fit to a data set. The samples cast on bare silicon were fit to a two layer model which assumed two primary bulk layers, while the samples cast on PGMA were fit to a three layer model which allowed for an extra layer representing the PGMA supporting layer. The dimensions of this PGMA domain were fixed and set using data obtained from reflectivity experiments performed on a PGMA only control film created using the same procedure as the surface treatments employed in the MEH-PPV:dPS films. The results of the fitting procedures provide the SLD profiles contained in Figures 6.6 and 6.7 for the films on the bare silicon and PGMA, respectively.

Focusing first on the as-cast samples, a consistent decrease in SLD is present in all samples from the air interface towards the substrate, indicative of a non uniform distribution of the blend upon casting with larger amounts of dPS closer to the air interface. Upon annealing, the depth profiles of all samples change. Most notably it becomes immediately clear that the presence of light during the annealing process substantially alters the layering of these films to a much greater extent than their non-illuminated counterparts.

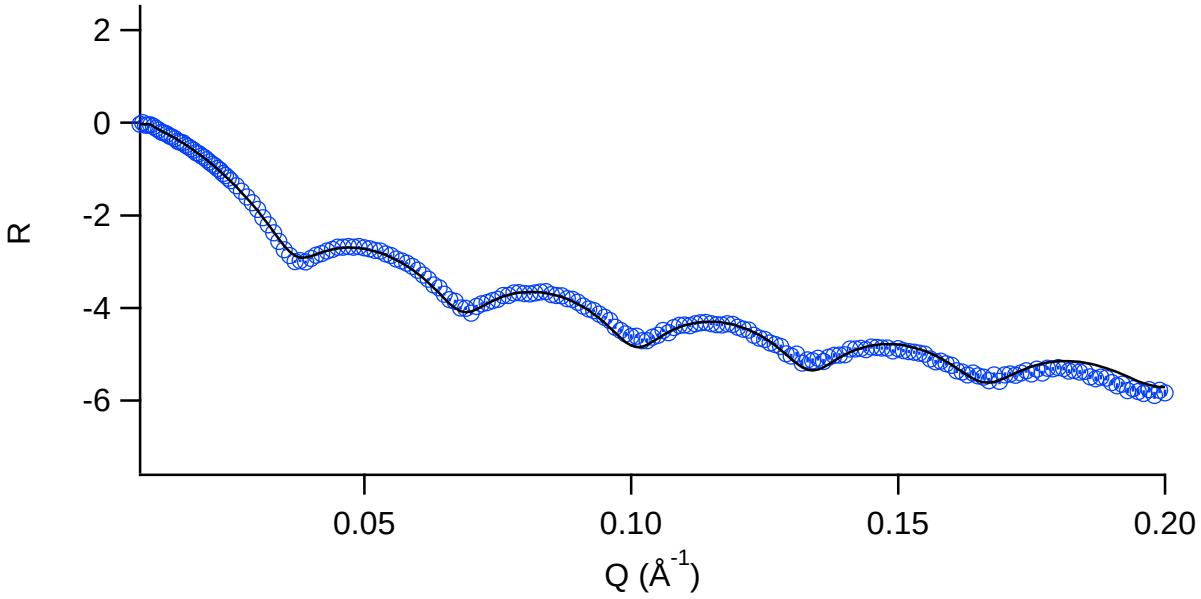


Figure 6.5: Example 2 layer curve fit (black trace) for 10:90 MEH-PPV:dPS film cast on a bare silicon surface and thermally annealed for 15 minutes at 125°C.

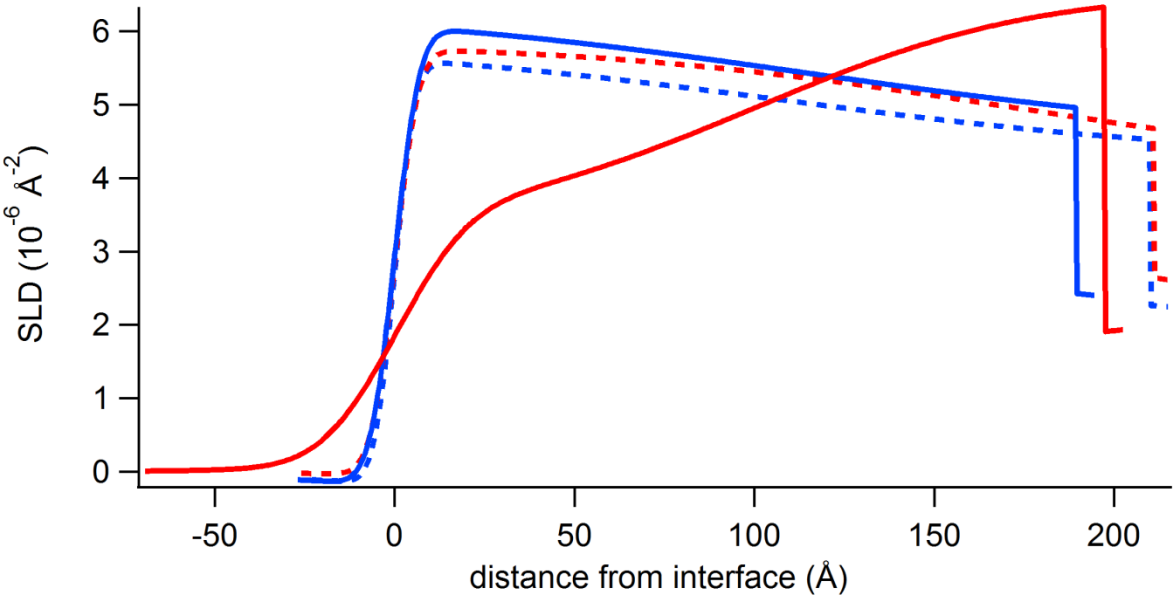


Figure 6.6: SLD profiles for 10:90 MEH-PPV:dPS films cast onto a bare silicon surface, where the distance from interface is defined from the polymer-air interface. Broken traces indicate as-cast samples (blue for dark, red for light) and solid traces indicate samples annealed for 15 minutes at 125°C (blue for dark, red for light).

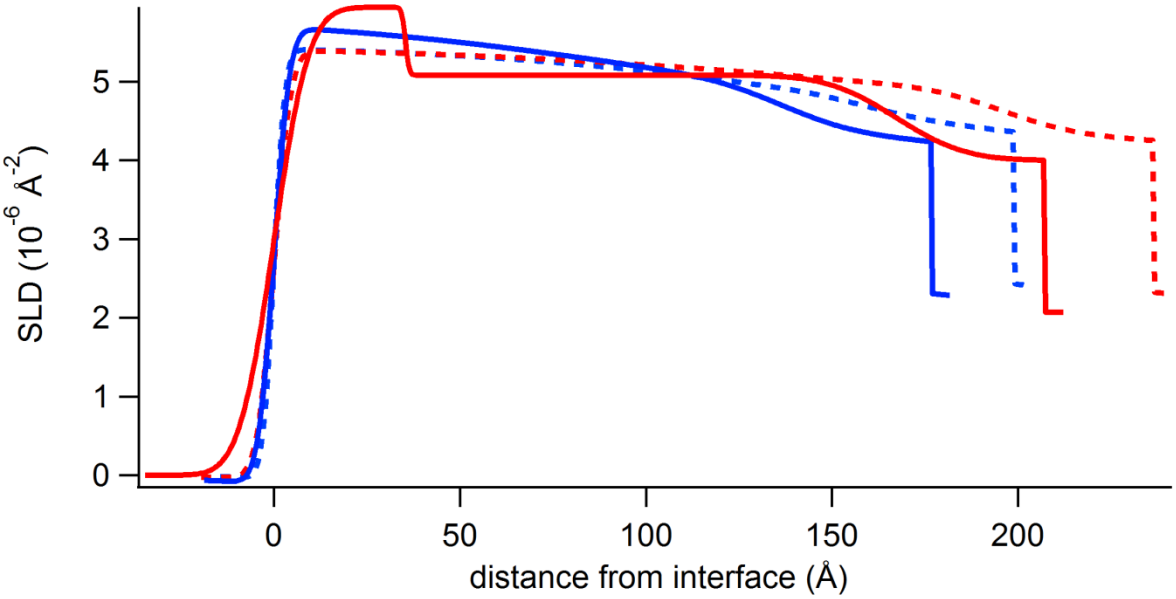


Figure 6.7: SLD profiles for 10:90 MEH-PPV:dPS films cast onto a PGMA treated surface, where the distance from interface is defined from the polymer-air interface. Broken traces indicate as-cast samples (blue for dark, red for light) and solid traces indicate samples annealed for 15 minutes at 125°C (blue for dark, red for light).

The scattering length density of dPS is much higher than that of MEH-PPV, and therefore a higher SLD indicates an excess of dPS. Therefore, for the bare silicon samples, the SLD profiles indicate a tremendous increase in the concentration of dPS closest to the substrate interface with annealing, along with an accompanying dip in dPS concentration at the air interface. Conversely, the annealed PGMA sample undergoes a comparatively small increase in dPS concentration at the air interface as a small but highly concentrated dPS domain is formed there while the remainder of the film is composed of a broad and significantly more mixed domain. These qualitative trends can be quantified by the structural characteristics of the layers present in the sample, as shown in Table 6.1.

All as-cast samples are primarily homogeneous throughout the bulk of the film, with slightly higher concentrations of dPS at the films air interface and increased MEH-PPV concentrations at the substrate surface. Upon annealing, the dark samples become slightly more uniform, but this trend remains. However, the films annealed in the light exhibit much more drastic changes. The silicon sample exhibits a dramatic shift in the concentration of MEH-PPV at the air interface, while a large assembly of MEH-PV at the substrate surface marks the PGMA sample. Thus, it is clear that the presence (or absence) of light significantly alters the depth profile of conjugated polymer blend thin films, and that the final morphology that emerges in the annealed sample is dependent on the chemical structure of the supporting surface.

Table 6.1: Parameters obtained from fit to neutron reflectivity data for MEHPPV/dPS films before and after thermal annealing on both bare silicon and PGMA surfaces.

Parameter	**PGMA Dark AsCast**	**PGMA Light AsCast**	**PGMA Dark Annealed**	**PGMA Light Annealed**	**Bare Dark AsCast**	**Bare Light AsCast**	**Bare Dark Annealed**	**Bare Light Annealed**
Layer 1 Thickness (Å)	154.2	172.0	106.7	35.3	107.9	172.8	120.3	99.7
Layer 1 SLD ($Å^{-2}$)	5.44	5.44	5.80	5.95	5.79	5.81	6.27	3.40
Layer 1 Roughness (Å)	2.3	3.6	3.4	7.4	4.5	5.2	5.2	16.1
Layer 2 Thickness (Å)	4.7	24.4	30.1	131.9	102.1	38.3	68.5	97.9
Layer 2 SLD ($Å^{-2}$)	4.17	4.45	4.47	5.08	4.33	4.10	4.32	6.49
Layer 2 Roughness (Å)	78.1	97.3	75.8	0.79	91.7	90.5	83.6	60.3
Layer 3 Thickness (Å)	40	40	40	40	-	-	-	-
Layer 3 SLD ($Å^{-2}$)	4	4	4	4	-	-	-	-
Layer 3 Roughness (Å)	12.5	14.2	14.3	14.6	-	-	-	-
Total Film Thickness (Å)	198.9	236.4	176.7	207.2	210.0	211.1	188.8	197.5

Discussion

In order to properly interpret the effect of substrate functionality and exposure of light to the depth profile of the MEH-PPV:dPS thin film blends, it becomes important to translate the scattering length density profiles to volume fraction depth profiles of the two components. This analysis is implemented by using a simple mass balance and knowledge of the scattering length densities of both polymer components to estimate the compositional depth profile of the as-cast and annealed films. Table 6.2 lists the volume fractions of each component in each layer within the film using this method, and Figures 6.8 and 6.9 display the volume fraction depth profiles for the samples on bare silicon and PGMA, respectively.

This data more intuitively quantifies previous conclusions, that the MEH-PPV prefers the substrate in the as-cast samples and annealing has little effect on the depth profile of the dark samples, whereas there are changes to the depth profile of the light samples with annealing. Moreover, the samples annealed in the light exhibit significant differences in the blend depth profile: the sample on the bare silicon sample shows that MEH-PPV migrates to the air interface during annealing, while the sample annealed on the PGMA surface contains a thin surface layer that is nearly entirely dPS, followed by a layer where the MEH-PPV is homogeneously distributed throughout the depth of the film.

Table 6.2: Volume fraction of each component in the layered thin films on bare silicon and PGMA treated samples in both the light and dark.

Sample	**Layer 1 ϕ_{dPS}**	**Layer 1 ϕ_{MEHPPV}**	**Layer 2 ϕ_{dPS}**	**Layer 2 ϕ_{MEHPPV}**
Bare as-cast dark	0.89	0.11	0.62	0.38
Bare annealed dark	0.97	0.03	0.61	0.39
Bare as-cast light	0.89	0.11	0.57	0.43
Bare annealed light	0.44	0.56	1	0
PGMA as-cast dark	0.82	0.18	0.59	0.41
PGMA annealed dark	0.89	0.11	0.64	0.36
PGMA as-cast light	0.82	0.18	0.64	0.36
PGMA annealed light	0.91	0.09	0.75	0.25

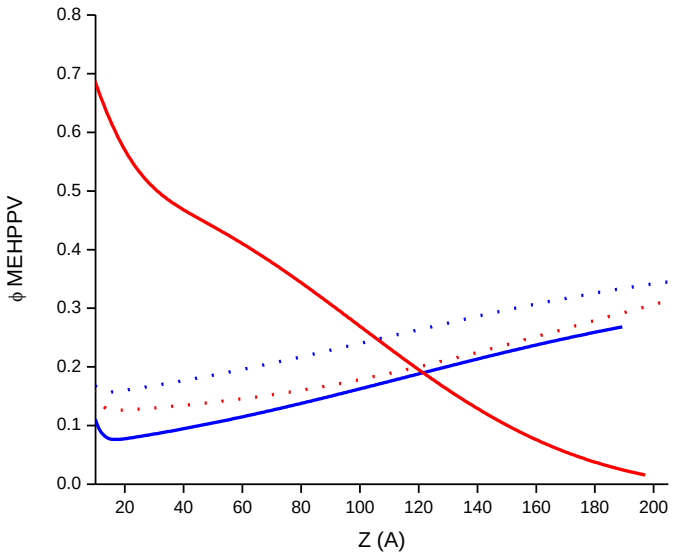


Figure 6.8: Volume fraction profile of MEH-PPV in the 10:90 MEH-PPV:dPS blend cast on HF stripped silicon, where Z is defined as the distance from the polymer-air interface. Broken traces indicate as-cast samples (blue for dark, red for light) and solid traces indicate samples annealed for 15 minutes at 125°C (blue for dark, red for light).

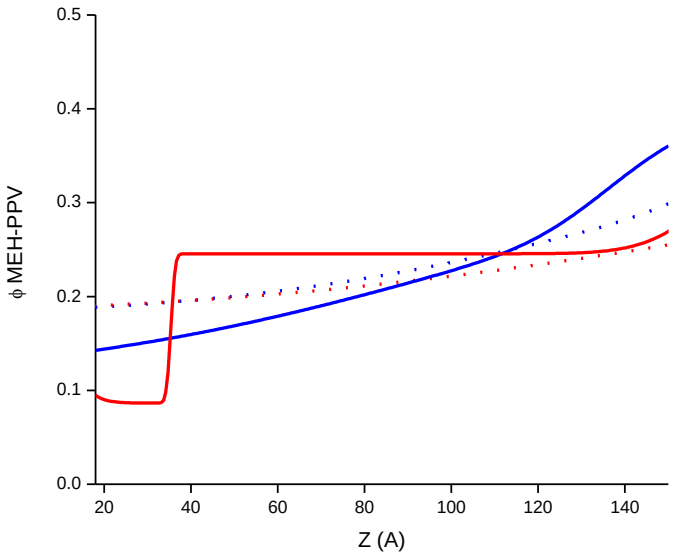


Figure 6.9: Volume fraction profile of MEH-PPV in the 10:90 MEH-PPV:dPS blend cast on a PGMA coated silicon wafer, where Z is defined as the distance from the polymer-air interface. Broken traces indicate as-cast samples (blue for dark, red for light) and solid traces indicate samples annealed for 15 minutes at 125°C (blue for dark, red for light).

Thus, a primary conclusion of these studies is that the presence of the illumination alters the evolution of the depth profile in conjugated polymer blend thin films, a factor that is often ignored in the implementation of such films in organic electronic devices. To provide insight into the thermodynamic driving forces that contribute to the evolution of the depth profile of these thin films with annealing, the entropy and enthalpy of these thin films must be considered. The surface energy of the supporting surfaces and the two polymeric components provides insight into the enthalpic interactions in a thin film. The surface energies for these materials (or their analogs) are listed in Table 6.3.

Poly(methyl methacrylate) is listed as it provides a useful analog to the expected surface energy of a PGMA coated surface, for which there exists little useful characterization.[125] Taking into consideration these surface energies offers a possible explanation for the layering behaviors observed in the films. All of the as-cast samples have MEH-PPV and dPS relatively well dispersed throughout depth of the film, due to the effects of the spin-casting process, which abruptly freezes film morphologies far from equilibrium. However, upon thermal annealing the blend shifts into a more thermodynamically stable morphology, an effect which occurs to varying extents across the samples investigated here. Most notably, the light exposed samples experience dramatic shifts in the depth profile as MEH-PPV shows a strong preference for the air or substrate interface in the bare silicon and PGMA coated samples, respectively.

Table 6.3: Total surface energies for relevant experimental materials

Material	**Surface Energy-γ (ergs/cm^2)**
MEH-PPV	25.61[126]
Poly(styrene)	41.3[127]
HF-stripped silicon	200[128]
Poly(methyl methacrylate)	40.2[127]

This behavior can be explained by considering the enthalpic and entropic forces at play and their contribution to the free energy of the film. The layering of the annealed film on bare silicon appears to be primarily dictated by the enthalpic surface energies, where the high surface energy dPS is found primarily at the silicon interface, minimizing the surface energy there while simultaneously allowing the low surface energy MEH-PPV to migrate to the air interface. The PGMA substrate film exhibits a clearly different depth profile with dPS dominating the air interface rather than the MEH-PPV. In this system, the surface energy of the substrate has been substantially decreased by the addition of the PGMA, mitigating much of the enthalpic impetus present in the bare silicon sample. In this case, entropic forces appear to dominate in determining the depth profile, wherein the considerably smaller dPS chains preferentially migrate to the air interface, limiting the entropic penalty of sequestering longer chains to the air surface.

However, a central question still remains: why do the annealed illuminated samples exhibit significantly different depth profiles than those annealed in the dark? Given that all samples were annealed simultaneously in the same thermostat-controlled vacuum oven, thermal contributions from the presence of the light source can be considered negligible. A potential route to better understanding this phenomenon may lie in the previous chapters, which have investigated the effects of illumination on the conformation of conjugated polymer chains in solution, in both dilute and concentrated. These works have shown that

the presence of excited states created via light absorption significantly alter the fundamental thermodynamic polymer-solvent interactions, resulting in varying degrees of change in polymer conformation.[95,114] Though the solution setting explored in these works is an emphatically different environment than the polymer melt experienced during thermal annealing by the films relevant to this work, the same thermodynamic properties remain pertinent in this thin film form. Considering the MEH-PPV loading has been set at a relatively low 10% by weight, the dPS can be thought of as a type of "solvent" for MEH-PPV. Light exposure in this state will still lead to absorption by the MEH-PPV and subsequent generation of excitons, which alters the thermodynamic interaction between the two species. Essentially the presence of these excited species appears to lead to a non-negligible shift in the surface energy of MEH-PPV. This effect appears to be similar to a chemical activation or functional group addition, which has repeatedly been shown to dramatically alter the surface energy of a given polymeric material. Though clearly less permanent and pronounced than established synthetic approaches, a sustained shift in the surface energy of MEH-PPV could provide sufficient enthalpic differences between MEH-PPV and dPS to disturb the partial miscibility observed in the as-cast samples and initiate a phase separation which results in the highly stratified films formed with illumination present during the annealing process.

The depth profile variation found in these studies also serves to highlight an important underlying theme: the presence of film stratification in these blends.

Despite the fact that many studies ignore or overlook the presence of stratification in organic electronic blends, the reality of its presence promises to have profound effects on layering architectures. Rather than existing as relatively homogonous intermixed blends, the formation of distinct layers rich in one particular component are noted throughout this work. Considering that many organic electronic devices such as thin film transistors and organic photovoltaics rely on concentrated active layer phases and distinct interfaces between domains, the presence of a natural or induced stratification effect in these films has powerful ramifications for layering procedures and device development.

Additionally, this work has identified a potentially powerful new tool for morphology control and stratification manipulation in conjugated polymer blends. By choosing the matrix polymer and substrate surface attributes carefully, device active layers could be generated with the desired layering pattern with an unprecedented degree of structural control. Due to the low cost, non-destructive nature, and in-situ capabilities of simple measured light exposure, incorporating it into existing fabrication methodologies should prove highly economical and straightforward, opening the door to an entirely new level of optoelectronic device architecture and efficiency focused morphology control.

Conclusion

Neutron reflectivity experiments have investigated the layering behavior of an MEH-PPV/dPS blend cast from a single solution as a function of substrate

structure, thermal annealing, and white light illumination. Analysis reveals the formation of a moderately homogeneous film upon spin-casting, where MEH-PPV shows a slight preference for the substrate, regardless of surface functionality. Upon thermal annealing, samples exposed to white light illumination demonstrate large changes in the layering of the sample and experience significant stratification compared to the films annealed in the dark, which show much reduced effects. This distinction indicates the presence of a light-induced effect on conjugated polymer thermodynamics in the melt, a phenomenon related to the effects previously observed in conjugated polymer solutions upon exposure to white light. Given the key role which domain size and layering plays in many organic electronic devices derived from similar blends such as thin film transistors and OLEDs, the identification of this stratification effect as well as a potential means for manipulating it has far reaching ramifications. If fully explored and properly harnessed, these effects could make possible an entirely new field of polymer blend morphology control and functional film manipulation, leading to a novel, non destructive in-situ methodology for preparing efficiency-focused organic optoelectronic devices.

Acknowledgments

The authors gratefully acknowledge the National Science Foundation (DMR-1409034) for support of this project. We also acknowledge the support of the National Institute of Standards and Technology, U.S. Department of

Commerce, in providing additional reflectivity facilities used in this work, where these facilities are supported in part by the National Science Foundation under Agreement No. DMR-0944772.

CHAPTER SEVEN
CONCLUSIONS AND FUTURE WORK

Conclusions

A series of robust neutron scattering and reflectivity experiments have studied the effects of illumination on the structural parameters of conjugated polymers in relatively dilute solution, in concentrated solution during the gelation process, and in the form of composite thin films. Careful analysis indicates that all systems respond in a significant manner on both a structural and thermodynamic basis to illumination. This data clearly points towards the presence of a universal effect within the field of conjugated polymers whereby the absorption of incident photons and subsequent generation of excited states fundamentally alters the relationship between the polymer and its surrounding matrix, leading directly to substantial changes to polymer conformation, assembly, and morphology. The ramifications of this phenomenon are far reaching and draw into special focus the importance of maintaining consistent illumination methodologies throughout all the relevant steps of the organic electronic device fabrication process in order to ensure consistent device architectures and ultimately, performance.

Illumination of Conjugated Polymer in Solution

Investigations of the evolution of conjugated polymer samples in a single chain solution environment clearly indicate that appropriate illumination consistently results in alterations to structural and thermodynamic parameters resulting in a shift in conformation of the chain. SANS experiments conducted on samples solvated in a relatively poor solvent reveal a sharp decrease of

structural size and deterioration of thermodynamic interaction parameters upon light exposure, indicative of a pseudo-chain collapse driven by a disruption of solubility caused by the generation and presence of excited states on the conjugated polymer chain. Further work on conjugated polymer samples in the dilute solution state highlights the key role which solvent quality has on the illumination driven alteration of polymer conformation. By studying the effects of illumination on conjugated polymers in a wide variety of solvents ranging from very suitable to very poor, it becomes clear that an initially unfavorable solvent environment results in larger observed changes to polymer structure, while higher quality solvents produce much reduced or even non-existent effects. This finding confirms the thermodynamic nature of the light driven conformation alterations, as polymer-solvent systems already close to their thermodynamic critical point require substantially less impetus to transition from the swollen to collapsed coil state. Further work studying the effects of varying the light exposure methodology in these experiments further clarify the underlying mechanism behind the conjugated polymer structural alterations. By limiting the number of absorbable photons to the conjugated polymer chain through changes to the total light exposure time, exposure intensity, or exposure wavelength, the number of excitons generated on the polymer backbone are significantly limited and thus the observed magnitude of shifts in polymer conformation are subsequently reduced. Similarly, decreasing the number of available absorbable photons increases the amount of total illumination time required to elicit the entire

possible change in polymer conformation for a given solvent system. All this data points towards the number of excitons generated as the key underlying driving force for the structural transformations which we consistently observe in these conjugated polymer systems. Clearly, illumination of conjugated polymer in the single chain dilute solution environment results in reproducible changes in polymer conformation and substantially alters the polymer chain's thermodynamic interaction with the surrounding solvent, an effect which varies in absolute magnitude as a function of both initial solvent quality and illumination methodology.

Illumination of Conjugated Polymer throughout Gelation

Small and ultra small angle neutron scattering experiments monitored the structural evolution of a highly concentrated conjugated polymer system as it proceeds through the gelation process as a function of controlled temperature change. Through use of SANS and a combined model fitting suite, structural parameters related to the dimensions of both nano-aggregates and free chains have been collected and compared for gelling systems studies in both the presence and absence of illumination. This information is complemented by USANS data which monitors the formation of micron scale aggregates formed in both the light and the dark. All data indicates that the size and number of nano-aggregates are significantly influenced by the presence of white light illumination, as are the sizes of the micro-structures which are formed through the aggregation of nanostructures. This analysis suggests that light exposure inhibits

the formation of nanometer and micron length scale structures, significantly altering the formation of the structural three dimensional networks formed throughout the gelation process.

Illumination of Conjugated Polymer Composite Thin Films during the Thermal Annealing Process

Conjugated polymer thin films composed of a blend of MEH-PPV and deuterated polystyrene were spin-cast from solution onto several substrates and annealed in the presence and absence of light. Analysis of the films with neutron reflectivity provides information of the depth profiles present in both as-cast and annealed samples under both illumination conditions. The as-cast films display a broad dispersion across the entire film thickness, with a preference of MEH-PPV for the substrate interface. Comparison of annealed samples highlights striking differences between samples based on illumination conditions, as illuminated samples display clear signs of phase separation compared to the relatively unchanged dark samples. Consideration of enthalpic and entropic forces at play in the films provides an understanding of the specific depth profiles that emerge in these samples annealed in the light. Ultimately the data indicates that the presence of illumination during the thermal annealing process alters the thermodynamics of the conjugated polymer, thus disrupting its partial miscibility in the deuterated polystyrene and increasing the phase separation and stratification of the materials.

Summary

The net result of these experiments has been to definitively illustrate that illumination substantively influences the conformation and morphology of conjugated polymers at multiple crucial points throughout a typical organic electronics fabrication process. The solutions which serve as the methodological starting point, the gelled state samples which effectively simulate the environment created during a typical fabrication solution casting process, and composite thin films subjected to a typical annealing process all show unmistakable signs of the influence of illumination on both structural and thermodynamic parameters of the relevant system. This being the case, it is undeniable that illumination can significantly alter the crucial architectures which make up the active layers key to the functionality of many organic electronic devices, thus altering the overall operational efficiency of these products. As a result, it becomes clear that illumination conditions must be kept consistent throughout the entirety of the device fabrication process in order to eliminate a previously overlooked variable and ensure both morphological and operational consistency of the devices fabricated.

However, this light-based phenomenon also offers potential advantages. Due to the obvious importance of active layer morphology within organic electronic devices, the expansion of methods capable of manipulating these morphologies becomes key. Light exposure as a tool for in-situ manipulation of conjugated polymer conformation fits this description very well, as it offers

advantages in ease of use, non-destructiveness, and affordability. Through careful control of ambient light intensity, illumination time, and wavelength along with proper selection of polymeric materials and solvent, active layer morphologies could be precisely manipulated and architectures shifted in a manner designed to boost the desired device efficiency metrics. The exact morphologies generated could be tuned based on the relevant device, for instance promoting well-defined bilayers in the case of thin film transistors or well separated but precisely sized micro-domains in the case of light emitting diodes. Due to its ubiquitous nature, illumination promises simple implementation as well as cost effective operation which offers a novel, low-risk option for fine tuning of these vital structural parameters in an unobtrusive and non-destructive manner easily run in line with a wide range of solution creation, casting, and film treatment methodologies employed during the fabrication of organic electronics.

Future Work

The experiments conducted previously have illustrated the powerful nature of illumination for manipulating conjugated polymer structure and thermodynamics, as well as clarifying some of the fundamental driving forces for this phenomenon. However, additional studies will further explore both the underlying mechanisms and expand the methods for applying these light induced effects.

Illumination of Conjugated Polymer in Solution

Employment of more advanced wavelength-tunable illumination sources will allow more robust investigation of the wavelength-dependant nature of the structural effects, allowing illumination intensity to be entirely removed from the equation by eliminating the unavoidable intensity loss inherent to the use of bandgap filters. The effect of solvent quality in these systems can be further investigated by both expanding the range of conjugated polymers and solvents surveyed and also introducing mixed solvent systems where the ratio of more favorable to less favorable solvents can be varied over a set range in order to identify the solvent quality domains where the major/minor structural effects come into play. Introduction of NMR experiments will be made possible by utilizing sample environments which allow for in-situ control of illumination environment, opening up an avenue to an otherwise unexplored method for light based conformational change analysis.

Illumination of Conjugated Polymer Gels

The experiments thus far have characterized the system extensively and have mostly concluded our analyses in this field. However additional work can be centered around analyzing the structural differences between fully gelled samples which have experienced the gelation process either under full illumination or entirely cut off from ambient light. This experiment is both simpler to conduct as a result of the removal of the temperature ramp and reduction of

analysis time required, while simultaneously allowing expanded analysis of the effects of illumination on the final gel structure.

Illumination of Conjugated Polymer Composite Thin Films during the Thermal Annealing Process

An enormous amount of potential exists for further investigations into the effects of illumination on conjugated polymers in the bulk. Building off of the initial experiments by exploring additional polymer loadings and substrate energies will allow further insight into the thermodynamic driving forces behind the phase separations. Exploring modified annealing protocols and extended annealing times will explore the stratification effects present as the films approach closer to true thermal equilibrium. A comprehensive series of contact angle measurements of all relevant polymeric materials and substrate surfaces will allow precise comparison of a wider variety of incorporated materials and their enthalpic interfacial contributions to the total system free energy. SANS experiments effectively designed to probe the shifts in chain conformation within the thin films between illuminated and non-illuminated annealing environments can provide insight into the driving forces behind the accelerated phase separation and possibly confirm the role of generated excitons in driving it. Finally, measurement of device relevant efficiency parameters such as power conversion efficiency of the devices fabricated from films annealed under differing illumination conditions will give important preliminary information about the ultimate effects which light

can have upon the functionality of the organic electronic devices fabricated in this manner.

LIST OF REFERENCES

(1) Strobl, G. *The Physics of Polymers*; Springer, 2007.
(2) Samuel, I. D. W.; Rumbles, G.; Collison, C. J. Efficient Interchain Photoluminescence in a High-Electron-Affinity Conjugated Polymer. *Phys. Rev. B* **1995**, *52* (16).
(3) Hotta, S.; Rughooputh, S. D. D. V; Heeger, A. J.; Wudl, F. Spectroscopic Studies of Soluble Poly (3-Alkylthienylenes). *Macromolecules* **1987**, *20*, 212–215.
(4) Rughooputh, S. D. D. V; Hotta, A.; Wudl, F. Chromism of Soluble Polythienylenes. *J. Polym. Sci. Part B Polym. Phys.* **1987**, *25*, 1071–1078.
(5) Haugeneder, A.; Neges, M.; Kallinger, C.; Spirkl, W.; Lemmer, U.; Feldmann, J.; Scherf, U.; Harth, E.; Gügel, A.; Müllen, K. Exciton Diffusion and Dissociation in Conjugated Polymer/fullerene Blends and Heterostructures. *Phys. Rev. B* **1999**, *59* (23), 15346–15351.
(6) Yan, M.; Rothberg, L. J.; Kwock, E. W.; Miller, T. M. Interchain Excitations in Conjugated Polymers. *Phys. Rev. Lett.* **1995**, *75* (10), 1992–1995.
(7) Liu, B. Q.; Liu, Z.; Zhang, X.; Yang, L.; Zhang, N.; Pan, G.; Yin, S.; Chen, Y.; Wei, J. Polymer Photovoltaic Cells Based on Solution-Processable Graphene and P3HT. *Adv. Funct. Mater.* **2009**, *19*, 894–904.
(8) Bassler, H. Non-Dispersive and Dispersive Transport in Random Organic Photoconductors. *Mol. Cryst. Liq. Cryst. Sci. Technol. Sect. A. Mol. Cryst. Liq. Cryst.* **1994**, *252* (1).
(9) Piris, J.; Dykstra, T. E.; Bakulin, A. A.; Van Loosdrecht, P. H. M.; Knulst, W.; Trinh, M. T.; Schins, J. M.; Siebbeles, L. D. A. Photogeneration and Ultrafast Dynamics of Excitons and Charges in P3HT/PCBM Blends. *J. Phys. Chem. C* **2009**, *113* (32), 14500–14506.
(10) Schwartz, B. J. Conjugated Polymers as Molecular Materials: How Chain Conformation and Film Morphology Influence Energy Transfer and Interchain Interactions. *Annu. Rev. Phys. Chem.* **2003**, *54* (3), 141–172.
(11) Li, L.; Lu, G.; Yang, X. Improving Performance of Polymer Photovoltaic Devices Using an Annealing-Free Approach via Construction of Ordered Aggregates in Solution. *J. Mater. Chem.* **2008**, *18*, 1984.
(12) Peet, J.; Heeger, A. J.; Bazan, G. C. “Plastic” solar Cells: Self-Assembly of Bulk Heterojunction Nanomaterials by Spontaneous Phase Separation. *Acc. Chem. Res.* **2009**, *42* (11), 1700–1708.
(13) Heremans, P.; Cheyns, D.; Rand, B. P. Strategies for Increasing the Efficiency of Heterojunction Organic Solar Cells: Material Selection and Device Architecture. *Acc. Chem. Res.* **2009**, *42* (11), 1740–1747.
(14) Huang, Y.; Cheng, H.; Han, C. C. Temperature Induced Structure Evolution of Regioregular Poly(3-Hexylthiophene) in Dilute Solution and Its Influence on Thin Film Morphology. *Macromolecules* **2010**, *43* (23), 10031–10037.
(15) Wang, H.; Xu, Y.; Yu, X.; Xing, R.; Liu, J.; Han, Y. Structure and Morphology Control in Thin Films of Conjugated Polymers for an Improved Charge Transport. *Polymers (Basel).* **2013**, *5* (4), 1272–1324.
(16) Prosa, T. J.; Prosa, T. J.; Winokur, M. J.; Winokur, M. J.; McCullough, R.

D.; McCullough, R. D. Evidence of a Novel Side Chain Structure in Regioregular Poly(3-Alkylthiophenes). *Macromolecules* **1996**, *29*, 3654–3656.
(17) Prosa, T. J.; Winokur, M. J.; Moulton, J.; Smith, P.; Heeger, a. J. X-Ray Structural Studies of Poly(3-Alkylthiophenes): An Example of An Inverse Comb. *Macromolecules* **1992**, *25* (17), 4364–4372.
(18) Samuelsen, E. J.; Mardalen, J.; Carlsen, P. H.; Gautun, O. R.; Le Guennec, P.; Travers, J. P.; Ressouche, E. Neutron Diffraction Studies of Deuterated and Hydrogenated Polyhexylthiophenes. *Synth. Met.* **1992**, *52* (3), 401–404.
(19) Dang, M. T.; Hirsch, L.; Wantz, G. P3HT:PCBM, Best Seller in Polymer Photovoltaic Research. *Adv. Mater.* **2011**, *23* (31), 3597–3602.
(20) Chang, J. F.; Sun, B.; Breiby, D. W.; Nielsen, M. M.; Sölling, T. I.; Giles, M.; McCulloch, I.; Sirringhaus, H. Enhanced Mobility of poly(3-Hexylthiophene) Transistors by Spin-Coating from High-Boiling-Point Solvents. *Chem. Mater.* **2004**, *16* (23), 4772–4776.
(21) Sirringhaus, H.; Brown, P. J.; Friend, R. H.; Nielsen, M. M.; Bechgaard, K.; Langeveld-Voss, B. M. W.; Spiering, a. J. H.; Janssen, R. a. J.; Meijer, E. W.; Herwig, P.; de Leeuw, D. M. Two-Dimensional Charge Transport in Self-Organized, High-Mobility Conjugated Polymers. *Nature* **1999**, *401* (6754), 685–688.
(22) Xiao, G.; Guo, Y.; Lin, Y.; Ma, X.; Su, Z.; Wang, Q. Controlled Evaporative Self-Assembly of Poly(3-Hexylthiophene) Monitored with Confocal Polarized Raman Spectroscopy. *Phys. Chem. Chem. Phys.* **2012**, *14*, 16286–16293.
(23) Yang, Y. Polymer Light-Emitting Logos Processed by Ink-Jet Printing Technology. *Proc. SPIE* **1998**, *3279* (1), 78–86.
(24) Zen, A.; Saphiannikova, M.; Neher, D.; Grenzer, J.; Grigorian, S.; Pietsch, U.; Asawapirom, U.; Janietz, S.; Scherf, U.; Lieberwirth, I.; Wegner, G. Effect of Molecular Weight on the Structure and Crystallinity of poly(3-Hexylthiophene). *Macromolecules* **2006**, *39* (6), 2162–2171.
(25) Dillard, C.; Singhal, R.; Kalra, V. Hierarchical Self-Assembly in Monoaxially Electrospun P3HT/PCBM Nanofibers. *Macromol. Mater. Eng.* **2015**, *300* (3), 320–327.
(26) Chan, K. H. K.; Yamao, T.; Kotaki, M.; Hotta, S. Unique Structural Features and Electrical Properties of Electrospun Conjugated Polymer poly(3-Hexylthiophene) (P3HT) Fibers. *Synth. Met.* **2010**, *160* (23-24), 2587–2595.
(27) Lee, C. S.; Yin, W.; Holt, A. P.; Sangoro, J. R.; Sokolov, A. P.; Dadmun, M. D. Rapid and Facile Formation of P3HT Organogels via Spin Coating: Tuning Functional Properties of Organic Electronic Thin Films. *Adv. Funct. Mater.* **2015**, *25* (36), 5848–5857.
(28) Yin, W.; Dadmun, M. A New Model for the Morphology of P3HT / PCBM Organic Photovoltaics from Small-Angle Neutron Scattering : Rivers and

Streams. *ACS Nano* **2011**, *5* (6), 4756–4768.
(29) Koppe, M.; Brabec, C. J.; Heiml, S.; Schausberger, A.; Duffy, W.; Heeney, M.; McCulloch, I. Influence of Molecular Weight Distribution on the Gelation of P3HT and Its Impact on the Photovoltaic Performance. *Macromolecules* **2009**, *42*, 4661–4666.
(30) Newbloom, G. M.; Weigandt, K. M.; Pozzo, D. C. Electrical, Mechanical, and Structural Characterization of Self-Assembly in poly(3-Hexylthiophene) Organogel Networks. *Macromolecules* **2012**, *45*, 3452–3462.
(31) Bearden, S. D.; Cannon, J. P.; Gold, S. a. Solvent Effects on Template Wetting Nanofabrication of MEH-PPV Nanotubules. *Macromolecules* **2011**, *44* (7), 2200–2205.
(32) Geens, W.; Shaheen, S. E.; Wessling, B.; Brabec, C. J.; Poortmans, J.; Sariciftci, N. S. Dependence of Field-Effect Hole Mobility of PPV-Based Polymer Films on the Spin-Casting Solvent. *Org. Electron. Physics, Mater. Appl.* **2002**, *3* (3-4), 105–110.
(33) Traiphol, R.; Charoenthai, N.; Srikhirin, T.; Kerdcharoen, T.; Osotchan, T.; Maturos, T. Chain Organization and Photophysics of Conjugated Polymer in Poor Solvents: Aggregates, Agglomerates and Collapsed Coils. *Polymer.* **2007**, *48* (3), 813–826.
(34) Nguyen, T.-Q.; Martini, I. B.; Liu, J.; Schwartz, B. J. Controlling Interchain Interactions in Conjugated Polymers: The Effects of Chain Morphology on Exciton−Exciton Annihilation and Aggregation in MEH−PPV Films. *J. Phys. Chem. B* **2000**, *104* (2), 237–255.
(35) Tessler, N. Efficient Near-Infrared Polymer Nanocrystal Light-Emitting Diodes. *Science (80-.).* **2002**, *295* (5559), 1506–1508.
(36) Harrison, M. G.; Grüner, J.; Spencer, G. C. W. Analysis of the Photocurrent Action Spectra of MEH-PPV Polymer Photodiodes. *Phys. Rev. B* **1997**, *55* (12), 7831–7849.
(37) Sariciftci, N.; Braun, D.; Zhang, C.; Srdanov, V.; Stucky, G.; Heeger, A.; Wudl, F. Polymer-Buckminsterfullerene Heterojunctions: *Appl. Phys. Lett.* **1993**, *62*.
(38) Adhikari, N.; Qiao, Q. Device and Morphological Engineering of Organic Solar Cells for Enhanced Charge Transport and Photovoltaic Performance. *J. Photonics Energy* **2015**, *5*, 57207, 1–17.
(39) Thévenot, J.; Oliveira, H.; Sandre, O.; Lecommandoux, S. Magnetic Responsive Polymer Composite Materials. *Chem. Soc. Rev.* **2013**, *42* (17), 7099–7116.
(40) Theato, P.; Sumerlin, B. S.; O'Reilly, R. K.; Epps, III, T. H. Stimuli Responsive Materials. *Chem. Soc. Rev.* **2013**, *42* (17), 7055.
(41) Rao, J. P.; Geckeler, K. E. Polymer Nanoparticles: Preparation Techniques and Size-Control Parameters. *Prog. Polym. Sci.* **2011**, *36* (7), 887–913.
(42) Irie, M.; Kunwatchakun, D. Reversible Photostimulated Dilation of Polyacrylamide Gels Having Triphenylmethane. *Macromolecules* **1986**, *19* (10), 2476–2480.

(43) Schmaljohann, D. Thermo- and pH-Responsive Polymers in Drug Delivery. *Adv. Drug Deliv. Rev.* **2006**, *58* (15), 1655–1670.
(44) Fouassier, J.; Rabek, J. *Radiation Curing in Polymer Science and Technology*; Springer, 1993.
(45) Decker, C. The Use of UV Irradiation in Polymerization. *Polym. Int.* **1998**, *45* (2), 133–141.
(46) Alvarez-lorenzo, C.; Bromberg, L.; Concheiro, A. Review: Light-Sensitive Intelligent Drug Delivery Systems. *Photochem. Photobiol.* **2009**, *85*, 848–860.
(47) Volodkin, D.; Skirtach, A.; Möhwald, H. Bioapplications of Light-Sensitive Polymer Films and Capsules Assembled Using the Layer-by-Layer Technique. *Polym. Int.* **2012**, *61* (5), 673–679.
(48) Yu, Y.; Nakano, M.; Ikeda, T. Directed Bending of a Polymer Film by Light. *Nature* **2003**, *425* (6954), 145–145.
(49) Kumar, J.; Li, L.; Jiang, X.; Kim, D.; Lee, T.; Tripathy, S. Gradient Force: The Mechanism for Surface Relief Grating Formation in Azobenzene Functionalized Polymers. *Appl. Phys. Lett.* **1998**, *72* (17), 2096.
(50) Tretiak, S.; Saxena, A.; Martin, R.; Bishop, A. Conformational Dynamics of Photoexcited Conjugated Molecules. *Phys. Rev. Lett.* **2002**, *89* (9), 097402.
(51) Botiz, I.; Freyberg, P.; Stingelin, N.; Yang, A. C.-M.; Reiter, G. Reversibly Slowing Dewetting of Conjugated Polymers by Light. *Macromolecules* **2013**, *46*, 2352–2356.
(52) Botiz, I.; Freyberg, P.; Leordean, C.; Gabudean, A.; Astilean, S.; Yang, A. C.; Stingelin, N. Enhancing the Photoluminescence Emission of Conjugated MEH-PPV by Light Processing. *ACS Appl. Mater. Interfaces* **2014**, *6* (7), 4974–4979.
(53) Virkar, A.; Mannsfeld, S.; Bao, Z.; Stingelin, N. Organic Semiconductor Growth and Morphology Considerations for Organic Thin-Film Transistors. *Adv. Mater.* **2010**, *22*, 3857–3875.
(54) Xu, W.; Tang, H.; Lv, H.; Li, J.; Zhao, X.; Li, H.; Wang, N.; Yang, X. Sol–gel Transition of poly(3-Hexylthiophene) Revealed by Capillary Measurements: Phase Behaviors, Gelation Kinetics and the Formation Mechanism. *Soft Matter* **2012**, *8*, 726.
(55) Guo, R. H.; Hsu, C. H.; Hua, C. C.; Chen, S. a. Colloidal Aggregate and Gel Incubated by Amorphous Conjugated Polymer in Hybrid-Solvent Medium. *J. Phys. Chem. B* **2015**, *119* (7), 3320–3331.
(56) Alcazar, D.; Wang, F.; Swager, T. M.; Thomas, E. L. Gel Processing for Highly Oriented Conjugated Polymer Films. *Macromolecules* **2008**, *41* (24), 9863–9868.
(57) Chang, R.; Hsu, J.; Fann, W.; Yu, J.; Lin, S.; Lee, Y.; Chen, S. Aggregated States of Luminescent Conjugated Polymers in Solutions. *Chem. Phys. Lett.* **2000**, *317*, 153–158.
(58) Heunt, S.; Mahrtt, R.; Greinert, A.; Lemmeri, U.; Bssleri, H.; Halliday, D.;

Bradley, D.; Bums, P.; Holmes, A. Selective Fluorescence Conformational Effects in Poly (P-Phenylene viny1ene) S Revealed by Low-Temperature Site-Selective Fluorescence. *J. Phys. Condens. Mtr.* **1993**, *5*, 247–260.
(59) Yu, J.; Hu, D.; Barbara, P. Unmasking Electronic Energy Transfer of Conjugated Polymers by Suppression of O2 Quenching. *Science (80-.).* **2000**, *289*, 1327–1330.
(60) Schwartz, B. J. Conjugated Polymers as Molecular Materials: How Chain Conformation and Film Morphology Influence Energy Transfer and Interchain Interactions. *Annu. Rev. Phys. Chem.* **2003**, *54*, 141–172.
(61) Brinkmann, M. Structure and Morphology Control in Thin Films of Regioregular poly(3-Hexylthiophene). *J. Polym. Sci. Part B Polym. Phys.* **2011**, *49*, 1218–1233.
(62) Kulkarni, A.; Tonzola, C.; Babel, A.; Jenekhe, S. Electron Transport Materials for Organic Light-Emitting Diodes. *Chem. Mater.* **2004**, *16* (23), 4556–4573.
(63) Segalman, R.; McCulloch, B.; Kirmayer, S.; Urban, J. Block Copolymers for Organic Optoelectronics. *Macromolecules* **2009**, *42* (23), 9205–9216.
(64) Tammer, M.; Horsburgh, L.; Monkman, A.; Brown, W.; Burrows, H. Effect of Chain Rigidity and Effective Conjugation Length on the Structural and Photophysical Properties of Pyridine-Based Luminescent Polymers. *Adv. Funct. Mater.* **2002**, *12* (6-7), 447–454.
(65) Shimoboji, T.; Larenas, E.; Fowler, T.; Kulkarni, S.; Hoffman, A.; Stayton, P. Photoresponsive Polymer-Enzyme Switches. *PNAS* **2002**, *99* (26), 16592–16596.
(66) Takemoto, K. *Functional Monomers and Polymers*; Taylor and Francis, 1997.
(67) Irie, M.; Hirano, Y.; Hashimoto, S.; Hayashi, K. Reversible Solution Viscosity Change of Polyamides Having Azobenzene Residues in the Main Chain. *Macromolecules* **1981**, *14* (2), 262–267.
(68) Zhu, M.; Zhu, L.; Han, J.; Wu, W.; Hurst, J.; Li, A. Spiropyran-Based Photochromic Polymer Nanoparticles with Optically Switchable Luminescence. *J. Am. Chem. Soc.* **2006**, *128* (13), 4303–4309.
(69) Rosario, R.; Gust, D.; Hayes, M.; Jahnke, F.; Springer, J.; Garcia, A. A. Photon-Modulated Wettability Changes on Spiropyran-Coated Surfaces. *Langmuir* **2002**, *18* (21), 8062–8069.
(70) Ciardelli, F.; Pieroni, O.; Fissi, A.; Carlini, C. Photoresponsive Optically Active Polymers-A Review. *Br. Polym. J.* **1989**, *21*, 97–106.
(71) Irie, M.; Menju, A.; Hayashi, K. Photoresponsive Polymers. Reversible Solution Viscosity Change of Poly (Methyl Methacrylate) Having Spirobenzopyran Side Groups. *Macromolecules* **1979**, *12* (6), 1176–1180.
(72) Pedersen, J. S.; Schurtenberger, P. Scattering Functions of Semiflexible Polymers with and without Excluded Volume Effects. *Macromolecules* **1996**, *29* (23), 7602–7612.
(73) Chen, W.; Butler, P.; Magid, L. Incorporating Intermicellar Interactions in

the Fitting of SANS Data from Cationic Wormlike Micelles. *Langmuir* **2006**, *22* (15), 6539–6548.
(74) https://www.ncnr.nist.gov/resources/activation (accessed Feb 1, 2013).
(75) https://www.ncnr.nist.gov/programs/sans/data/red_anal.html (accessed Feb 1, 2013).
(76) Justice, R.; Wang, D.; Tan, L.; Schaefer, D. Simplified Tube Form Factor for Analysis of Small-Angle Scattering Data from Carbon Nanotube Filled Systems. *J. Appl. Crystallogr.* **2007**, *40*, s88–s92.
(77) Chang, M.; Lee, J.; Kleinhenz, N.; Fu, B.; Reichmanis, E. Photoinduced Anisotropic Supramolecular Assembly and Enhanced Charge Transport of Poly(3-Hexylthiophene) Thin Films. *Adv. Funct. Mater.* **2014**, *24* (28), 4457–4465.
(78) Friend, R. H.; Gymer, R. W.; Holmes, A. B.; Burroughes, J. H.; Marks, R. N.; Taliani, C.; Bradley, D. D. C.; Lo, M.; Salaneck, W. R.; Santos, D. A. Dos; Bre, J. L. Electroluminescence in Conjugated Polymers. *Nature* **1999**, *397*, 121–128.
(79) Solids, O.; Barbara, S.; Barbara, S. Polarons and Bipolarons on a Conducting Polymer in Solution. *Macromolecules* **1987**, *20*, 965–968.
(80) Greenham, N. C.; Samuel, I. D. W.; Hayes, G. R.; Phillips, R. T.; Holmes, A. B.; Friend, R. H. Measurement of Absolute Photoluminescence Quantum Efficiencies in Conjugated Polymers. *Chem. Phys. Lett.* **1995**, *241*, 89–96.
(81) Galvin, M. E.; Miller, T. M.; Laboratories, A. T. B.; Hill, M. Spatially Indirect Excitons as Primary Photoexcitations in Conjugated Polymers. *Phys. Rev. Lett.* **1994**, *72* (7), 1104–1107.
(82) Cook, S.; Furube, A.; Katoh, R. Analysis of the Excited States of Regioregular Polythiophene P3HT. *Energy Environ. Sci.* **2008**, *1*, 294–299.
(83) Li, Y.; Vamvounis, G.; Holdcroft, S. Tuning Optical Properties and Enhancing Solid-State Emission of Poly (Thiophene) S by Molecular Control : A Postfunctionalization Approach. *Macromolecules* **2002**, *35*, 6900–6906.
(84) Jiang, H.; Kelch, S.; Lendlein, A. Polymers Move in Response to Light. *Adv. Mater.* **2006**, *18* (11), 1471–1475.
(85) Delaire, J.; Nakatani, K. Linear and Nonlinear Optical Properties of Photochromic Molecules and Materials. *Chem. Rev.* **2000**, *100* (5), 1817–1846.
(86) Lendlein, A.; Jiang, H.; Junger, O.; Langer, R. Light-Induced Shape-Memory Polymers ¨. *Nature* **2005**, *434*, 695–697.
(87) Al-Ibrahim, M.; Ambacher, O.; Sensfuss, S.; Gobsch, G. Effects of Solvent and Annealing on the Improved Performance of Solar Cells Based on poly(3-Hexylthiophene): Fullerene. *Appl. Phys. Lett.* **2005**, *86*, 201120.
(88) Bu, L.; Pentzer, E.; Bokel, F. A.; Emrick, T.; Hayward, R. C. Growth of Polythiophene / Perylene Tetracarboxydiimide Donor / Acceptor Shish-Kebab Nanostructures by Coupled Crystal Modi Fi Cation. *ACS Nano*

2012, *6* (12), 10924–10929.
(89) Yang, C. Y.; Heeger, a. J.; Cao, Y. Microstructure of Gel-Processed Blends of Conjugated Polymer and Ultrahigh Molecular Weight Polyethylene. *Polymer (Guildf).* **2000**, *41*, 4113–4118.
(90) Wicklein, A.; Ghosh, S.; Sommer, M.; Würthner, F.; Thelakkat, M. Self-Assembly of Semiconductor Organogelator Nanowires for Photoinduced Charge Separation. *ACS Nano* **2009**, *3* (5), 1107–1114.
(91) Terech, P.; Weiss, R. G. Low Molecular Mass Gelators of Organic Liquids and the Properties of Their Gels. **1997**, *2665* (97).
(92) Herrmann, H.; Landau, D.; Stauffer, D. New Universality Class for Kinetic Gelation. *Phys. Rev. Lett.* **1982**, *49* (6), 412–415.
(93) Zaccarelli, E. Colloidal Gels: Equilibrium and Non-Equilibrium Routes. *J. Phys. Condens. Matter* **2007**, *19*, 323101, 1–50.
(94) Newbloom, G. M.; Kim, F. S.; Jenekhe, S. a.; Pozzo, D. C. Mesoscale Morphology and Charge Transport in Colloidal Networks of Poly(3-Hexylthiophene). *Macromolecules* **2011**, *44*, 3801–3809.
(95) Morgan, B.; Dadmun, M. D. Illumination of Conjugated Polymer in Solution Alters Its Conformation and Thermodynamics. *Macromolecules* **2016**, *49* (9), 3490–3496.
(96) Schulz, G. *Z. Phys. Chem.* **1935**, *43*, 25.
(97) Mittelbach; Porod. *Acta Phys. Austriaca* **1961**, *14*, 185–211.
(98) Guinier, A.; Fournet, G. *Small-Angle Scattering of X-Rays*; Wiley: New York, 1955.
(99) Park, M. S.; Aiyar, A.; Park, J. O.; Reichmanis, E.; Srinivasarao, M. Drain Current in Poly(3-Hexylthiophene) Solutions during Film Formation: Correlations to Structural Changes. *ChemNanoMat* **2015**, *1* (1), 32–38.
(100) Yu, J.; Wang, Z.; Chu, B. Kinetic Study of Coil-to-Globule Transition. *Macromolecules* **1992**, *25*, 1618–1620.
(101) Tanaka, T. Collapse of Gels and the Critical Endpoint. *Phys. Rev. Lett.* **1978**, *40* (12), 820–823.
(102) Nishio, I.; Sun, S.; Swislow, G.; Tanaka, T. First Observation of Chain-Globule Transition. *Nature* **1979**, *281*, 208–209.
(103) Ilavsk, M. Phase Transition in Swollen Gels. 2. Effect of Charge Concentration on the Collapse and Mechanical Behavior of Polyacrylamide Networks. *Macromolecules* **1982**, *15*, 782–788.
(104) Wu, C.; Zhou, S. Laser Light Scattering Study of the Phase Transition of Poly(N-Isopropylacrylamide) in Water. 1. Single Chain. *Macromolecules* **1995**, *28*, 8381–8387.
(105) Barker, J. G.; Glinka, C. J.; Moyer, J. J.; Kim, M. H.; Drews, A. R.; Agamalian, M. Design and Performance of a Thermal-Neutron Double-Crystal Diffractometer for USANS at NIST. *J. Appl. Crystallogr.* **2005**, *38* (6), 1004–1011.
(106) Kline, S. R. Reduction and Analysis of SANS and USANS Data Using IGOR Pro. *J. Appl. Crystallogr.* **2006**, *39* (6), 895–900.

(107) Lee, C.; Pao, C. Nanomorphology Evolution of P3HT/PCBM Blends during Solution- Processing from Coarse-Grained Molecular Simulations. *J. Phys. Chem. C* **2014**, *118*, 11224–11233.
(108) Choi, W. T.; Song, J.; Ko, J.; Jang, Y.; Kim, T. H.; Han, Y. S.; Lim, J.; Lee, C.; Char, K. Effect of Solvent Additives on Bulk Heterojunction Morphology of Organic Photovoltaics and Their Impact on Device Performance. *J. Polym. Sci. Part B Polym. Phys.* **2015**, *54*, 128–134.
(109) Li, L.; Tang, H.; Wu, H.; Lu, G.; Yang, X. Effects of Fullerene Solubility on the Crystallization of poly(3-Hexylthiophene) and Performance of Photovoltaic Devices. *Org. Electron. physics, Mater. Appl.* **2009**, *10* (7), 1334–1344.
(110) Hammouda, B. SANS from Homogeneous Polymer Mixtures - A Unified Overview. *Adv. Polym. Sci.* **1993**, *106*, 87–133.
(111) Wen, Y. H.; Lin, P. C.; Hua, C. C.; Chen, S. a. Dynamic Structure Factor for Large Aggregate Clusters with Internal Motions: A Self-Consistent Light-Scattering Study on Conjugated Polymer Solutions. *J. Phys. Chem. B* **2011**, *115* (49), 14369–14380.
(112) Li, Y. C.; Chen, K. B.; Chen, H. L.; Hsu, C. S.; Tsao, C. S.; Chen, J. H.; Chen, S. A. Fractal Aggregates of Conjugated Polymer in Solution State. *Langmuir* **2006**, *22* (26), 11009–11015.
(113) Teixeira, J. Small-Angle Scattering by Fractal Systems. *J. Appl. Crystallogr.* **1988**, *21* (6), 781–785.
(114) Morgan, B.; Dadmun, M. D. Illumination Alters the Structure of Gels Formed from the Optoelectronic Material P3HT. *In Preperation* **2016**.
(115) Funke, W. *J. Oil Colour Chem. Assoc.* **1976**, *59*, 398.
(116) Walbridge, D. J. Self-Stratifying Coatings - An Overview of a European Community Research Project. *Prog. Org. Coatings* **1996**, *28* (3 SPEC. ISS.), 155–159.
(117) Ogle, K.; Morel, S.; Meddahi, N. An Electrochemical Study of the Delamination of Polymer Coatings on Galvanized Steel. *Corros. Sci.* **2005**, *47* (8), 2034–2052.
(118) Chua, L. L.; Ho, P. K. H.; Sirringhaus, H.; Friend, R. H. Observation of Field-Effect Transistor Behavior at Self-Organized Interfaces. *Adv. Mater.* **2004**, *16* (18), 1609–1615.
(119) Qiu, L.; Lim, J. A.; Wang, X.; Lee, W. H.; Hwang, M.; Cho, K. Versatile Use of Vertical-Phase-Separation-Induced Bilayer Structures in Organic Thin-Film Transistors. *Adv. Mater.* **2008**, *20* (6), 1141–1145.
(120) Wang, X.; Lee, W. H.; Zhang, G.; Wang, X.; Kang, B.; Lu, H.; Qiu, L.; Cho, K. Self-Stratified Semiconductor/dielectric Polymer Blends: Vertical Phase Separation for Facile Fabrication of Organic Transistors. *J. Mater. Chem. C* **2013**, *1* (25), 3989.
(121) Burroughes, J. H.; Bradley, D. D. C.; Brown, A. R.; Marks, R. N.; Mackay, K.; Friend, R. H.; Burns, P. L.; Holmes, A. B. Light-Emitting Diodes Based on Conjugated Polymers. *Letters to Nature*. 1990, pp 539–541.

(122) He, G.; Li, Y.; Liu, J.; Yang, Y. Enhanced Electroluminescence Using Polystyrene as a Matrix. *Appl. Phys. Lett.* **2002**, *80* (22), 4247–4249.
(123) Kienzle, P. A.; O'Donovan, K. V.; Ankner, J. F.; Berk, N. F.; Majkrzak, C. F. NIST Reflectivity Accredidation.
(124) Nelson, A. Co-Refinement of Multiple-Contrast neutron/X-Ray Reflectivity Data Using MOTOFIT. *J. Appl. Crystallogr.* **2006**, *39* (2), 273–276.
(125) Iyer, K. S.; Zdyrko, B.; Malz, H.; Pionteck, J.; Luzinov, I. Polystyrene Layers Grafted to Macromolecular Anchoring Layer. *Macromolecules* **2003**, *36* (17), 6519–6526.
(126) Ma, K.-X.; Ho, C.-H.; Zhu, F.; Chung, T.-S. Investigation of Surface Energy for Organic Light Emitting Polymers and Indium Tin Oxide. *Thin Solid Films* **2000**, *371* (1), 140–147.
(127) Owens, D. K.; Wendt, R. C. Estimation of the Surface Free Energy of Polymers. *J. Appl. Polym. Sci.* **1969**, *13* (8), 1741–1747.
(128) Gosele, U.; Stenzel, H.; Martini, T.; Steinkirchner, J.; Conrad, D.; Scheerschmidt, K. Self-Propagating Room-Temperature Silicon Wafer Bonding in Ultrahigh Vacuum. *Appl. Phys. Lett.* **1995**, *67* (1995), 3614–3616.

APPENDIX

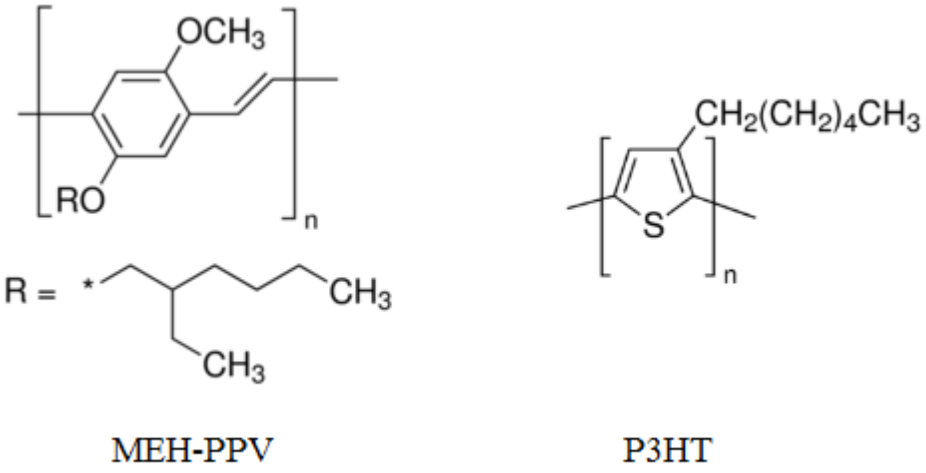


Figure 0.1: Molecular structure of benchmark conjugated polymers poly[2-methoxy-5-(2-ethylhexyloxy)-1,4-phenylenevinylene] (left), and poly(3-hexylthiophene-2,5-diyl) (right).

VITA

Brian Frank Morgan was born June 12, 1989 in Rochester New York. He graduated from the College of the Holy Cross with a B.A. in Chemistry in May 2011. He joined the University of Tennessee, Knoxville in August 2011 to pursue his Ph.D. in Polymer Chemistry.